EFFECTS OF 5′-TRIPHOSPHATE METABOLITES OF SPECIFIC ANTIVIRAL DRUGS ON CTP SYNTHASE ACTIVITY

by

Thomas D. Gillis

Submitted in partial fulfilment of the requirements
for the degree of Master of Science

at

Dalhousie University
Halifax, Nova Scotia
December 2021

TABLE OF CONTENTS

LIST OF TABLES

LIST OF FIGURES

LIST OF SCHEMES

ABSTRACT

Cytidine-5′-triphosphate (CTP) synthase (CTPS) catalyzes the biosynthesis of CTP from UTP using either L-glutamine or free NH_3 as a substrate. CTP is an essential precursor for viral replication; thus, its production has been targeted for the development of antiviral agents. With the advent of SARS-CoV-2, one approach for identifying therapies for COVID-19 is through the repurposing of existing antiviral drugs. To better understand potential off-target effects of repurposed antiviral agents, I analyzed the effects of vidarabine-5′-triphosphate (araATP), ribavirin-5′-triphosphate (RBVNTP), sofosbuvir-5′-triphosphate (STP), and N^4-OH-CTP on *Escherichia coli* CTPS (*ec*CTPS) activity and filament formation. AraATP and STP were modest substrates for *ec*CTPS, while RBVNTP and N^4-OH-CTP activated and inhibited *ec*CTPS, respectively. N^4-OH-CTP induced filament formation by *ec*CTPS while STP prevented filament assembly. ATPγS was a substrate for *ec*CTPS and gemcitabine-5′-triphosphate inhibited both the wild-type and C268A *ec*CTPS variants to the same extent. Hence, repurposed antiviral drugs could affect intracellular CTP production.

LIST OF ABBREVIATIONS USED

ADP	adenosine-5′-diphosphate
ADPNP	adenosine-5′-[β, γ-imido]triphosphate
AMPPCP	adenosine-5′-[(β,γ)-methyleno]triphosphate
araATP	adenine-arabinofuranoside-5′-triphosphate
ATP	adenosine 5′-triphosphate
ATPγS	adenosine-5′-(3-thio)-triphosphate
CDP	cytidine 5′-diphosphate
CPEC-TP	cyclopentenylcytosine-5′-triphosphate
CTP	cytidine-5′-triphosphate
CTPS	cytidine-5′-triphosphate synthase
Da	Dalton
ddhCTP	3-deoxy-3,4-didehydro-CTP
dF-dCTP	gemcitabine-5′-triphosphate
*dm*CTPS	cytidine-5′-triphosphate synthase from *Drosophila melanogaster*
DNA	deoxyribonucleic acid
DON	6-diazo-5-oxo-L-norleucine
*ec*CTPS	cytidine-5′-triphosphate synthase from *Escherichia coli*
EGTA	ethylene glycol tetraacetic acid
ESI-MS	electrospray ionization mass spectrometry
Gln	glutamine
GMP	guanidine-5′-monophosphate
GTP	guanidine-5′-triphosphate
hCTPS	cytidine-5′-triphosphate synthase from *Homo sapiens*
HCV	hepatitis C virus
HEPES	2-[4-(2-hydroxyethyl) piperazin-1-yl] ethanesulfonic acid
His_6	hexahistidine
HPLC	high performance liquid chromatography
IMPDH	inosine-5′-monophosphate dehydrogenase
IPTG	isopropyl β-D-1-thiogalactopyranoside
K_A	dissociation constant for the enzyme·GTP complex
k_{act}	activation constant
k_{cat}	turnover number
k_{inhib}	inhibition constant

K_m	Michaelis constant
LB	Luria Bertani
mantATP	*N*-methyl-anthraniloyl-ATP
mCTPS	cytidine-5′-triphosphate synthase from *Mus musculus*
MERS	middle east respiratory syndrome
n	Hill number
N^4-OH-CDP	β-D-N^4-hydroxycytidine-5′-diphosphate
N^4-OH-CMP	β-D-N^4-hydroxycytidine-5′-monohosphate
N^4-OH-CTP	β-D-N^4-hydroxycytidine-5′-triphosphate
NHC	β-D-N^4-hydroxycytidine
NMR	nuclear magnetic resonance
NSP	nonstructural protein
NTP	nucleotide-5′-triphosphate
NTPase	nucleoside-triphosphatase
OD_{600}	optical density at 600 nm
RBVNMP	ribavirin-5′-monophosphate
RBVNTP	ribavirin-5′-triphosphate
RdRp	RNA-dependent RNA polymerase
RNA	ribonucleic acid
RSV	respiratory syncytial virus
$[S]_{0.5}$	concentration of substrate at half-maximum activity
SARS-CoV-2	severe acute respiratory syndrome coronavirus 2
SDS	sodium dodecyl sulfate
STP	sofosbuvir-5′-triphosphate
TEM	transmission electron microscopy
TNP-AMP	2′,3′-*O*-trinitrophenyl-adenosine-5′-monophosphate
Tris	tris(hydroxymethyl)aminomethane
UDP	uridine-5′-diphosphate
UMP	uridine-5′-monophosphate
UTP	uridine-5′-triphosphate
UV-SPEC	ultraviolet–visible spectroscopy
v_i	initial velocity
V_{max}	maximal velocity
v_o	initial velocity in absence of inhibitor
+ssRNA	positive-sense single stranded RNA

ε	molar extinction coefficient

ACKNOWLEDGMENTS

I would like to extend my deepest gratitude to Dr. Stephen Bearne for not only supervising my project throughout my Masters, but also mentoring and shaping me as a student and researcher. I feel very fortunate to have had this opportunity to learn from someone so passionate and dedicated to their work. Thank you for your patience and guidance.

I would like to pay regards to my cancer care team at the QEII Cancer Centre. A special thanks to the oncology nurses for our long conversations and motivation through many hours on the ward. I must also thank those involved in assisting with my transition back to lab after an extended period off. I would also like to thank my family for their endless care. I am extremely grateful to have the support system that they provide for me.

I would like to sincerely thank my supervisory committee members Dr. Vanya Ewart and Dr. David Langelaan for their time and care in guiding me through my MSc. Many thanks to the members of the Bearne lab during my time here: Oliver, Amar, Noa, Krishna, Josh, Laura, Meg, and Amanda - all of whom have given insightful discussions, support, and fun times whilst working in the lab. Special thanks to Oliver for showing me the ropes and helping me troubleshoot many issues along the way.

I am extremely grateful to those organizations who helped to fund my studies. I would like to thank MITACS and NSERC-CREATE BioActives for providing me with support and exposure to many more opportunities along the way.

I would also like to thank my dear friend and fellow scientist Joey Stewart, who has been my sounding board throughout this degree. Thank you for keeping me sane and

being a friend. Finally, I thank everyone, those mentioned and unmentioned above, for making this journey possible.

CHAPTER 1: INTRODUCTION

1.1 CTPS IS A UNIVERSALLY CONSERVED ENZYME

Enzymes are biological macro-molecules that act as catalysts in living organisms. All metabolic processes in the cell require enzymatic catalysis to support basic life. They regulate the rate of chemical reactions by lowering the activation energy barrier associated with conversion between the reactants and products through favoured binding at the transition state. The resulting reduction in the energy of the transition state species causes the reaction to proceed at much increased rates compared to the uncatalyzed reaction. Enzymes are highly specific; often, they will catalyze reactions of only a single substrate or a few closely related substrates. The function of the enzyme is determined by its structure and active site architecture.

Cytidine-5′-triphosphate (CTP) synthase (CTPS, EC 6.3.4.2), also known as UTP-ammonia ligase, is a universally conserved enzyme that catalyzes the *de novo* biosynthesis of CTP. CTP can be incorporated directly into RNA via RNA polymerases, or DNA following ribonucleotide reductase-catalyzed conversion to 2′-deoxyCTP (dCTP) (Abeles & Beck, 1967). Consequently, all forms of life require CTP and CTPS.

The *de novo* biosynthesis of CTP was first described experimentally using an extract of *Escherichia coli* (*E. coli*), in which CTP was generated from ATP, UTP, Mg^{2+}, and NH_3 (Lieberman, 1956). Since CTPS was first isolated from *E. coli* and characterized by Long and Pardee (Long & Pardee, 1967), it has been studied further by many groups due to its important role in pyrimidine biosynthesis. CTPS has been purified from other organisms including *Anoxybacillus gonensis G2* (Sandalli *et al*., 2013), *Caulobacter crescentus* (Ingerson-Mahar *et al.*, 2010), *Chlamydia trachomatis* (Wylie, Berry, *et al*.,

1996), *Drosophila melanogaster (*Strochlic *et al.*, 2014*)*, *Lactococcus lactis* (Jørgensen *et al*., 2003), *Plasmodium falciparum* (Yuan *et al*., 2005), *Saccharolobus solfataricus* (Lauritsen *et al*., 2011), *Saccharomyces cerevisiae* (Yang *et al*., 1994), *Thermus thermophilus* (Goto *et al*., 2003), *Trypanosoma Brucei* (Hofer *et al.*, 2001), *Mus musculus* (Kizaki *et al*., 1985), *Bos taurus* (Weinfeld *et al*., 1978), and *Homo sapiens* (Kursula *et al.*, 2006), though the *E. coli* enzyme (*ec*CTPS) remains the most thoroughly studied to date. CTPS amino acid sequences are conserved between species and isoforms (Tatusov *et al*., 2001). Indeed, the *ec*CTPS amino acid sequence shares 40% identity and 60% similarity with human CTPS (hCTPS1) and X-ray crystal structures show conservation of structurally and functionally important residues (Endrizzi *et al*., 2004; Kursula *et al*., 2006; Yamauchi *et al*., 1990).

1.2 METABOLIC ROLE OF CTPS

CTPS catalyzes the final step in the *de novo* pathway of pyrimidine nucleotide biosynthesis (**Figure 1.1**). The conversion of UTP to CTP is the rate-limiting step in the formation of cytosine nucleotides and is therefore an important regulatory control point in pyrimidine biosynthesis (Evans & Guy, 2004). CTP plays a critical role in cellular metabolism, serving as precursors for the biosynthesis of RNA, DNA, and CDP-diacylglycerol (Chang & Carman, 2008), which is necessary for the assembly of cell membranes.

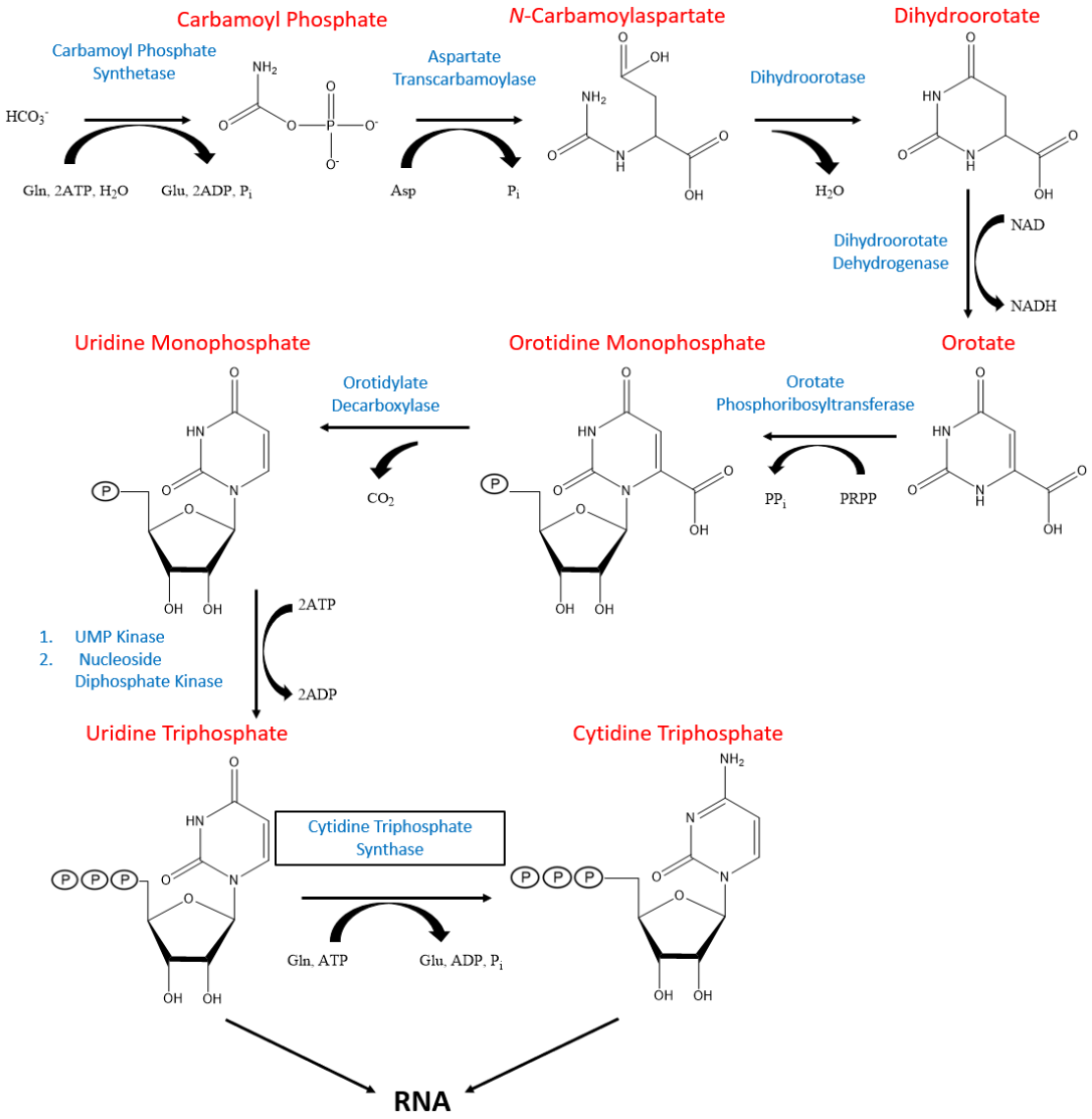

Figure 1.1. Schematic overview of *de novo* pyrimidine biosynthesis of UTP and CTP.

CTPS is subject to multiple forms of allosteric regulation, which control the rate of conversion of UTP to CTP and indirectly, the rate at which CTP is incorporated into RNA (Lunn *et al*., 2008). Guanosine-5′-triphosphate (GTP) is a purine nucleotide that acts as an allosteric activator to strongly promote the hydrolysis of L-glutamine (Gln), but also inhibits Gln-dependent CTP formation at high concentrations (Lunn *et al*., 2008); thus, GTP acts as a modulator of pyrimidine nucleotide levels. The reaction product, CTP, also acts as an inhibitor, since the CTP-binding site overlaps with the UTP-binding site with the 5′-triphosphate binding site being common to both ligands (Endrizzi *et al*., 2005).

The activity of *ec*CTPS is also regulated through cooperative binding of its substrates. ATP, UTP, and GTP bind cooperatively to CTPS in a concentration-dependent manner (Long & Pardee, 1967); high GTP concentrations inhibit CTP formation through the uncoupling of Gln hydrolysis and CTP synthesis (Lunn *et al*., 2008; MacDonnell *et al*., 2004). Interestingly, despite GTP's activating role when Gln is the substrate, it offers little catalytic advantage when ammonia is the substrate (Levitzki & Koshland, 1972b). In contrast, mammalian CTPS does not exhibit cooperativity for any of its ligands, however, GTP is still a positive allosteric effector of the glutaminase reaction (Savage & Weinfeld, 1970). Despite differences in the effects of allosteric regulators on CTPS from bacteria and mammalian sources, CTPS plays a critical role in the biosynthesis of pyrimidines in all forms of life.

1.3 CLINICAL SIGNIFICANCE

The disorders associated with pyrimidine metabolism are unusual in their variety of clinical presentations; the inherited defects often manifest as hematologic, neurological, and developmental disorders (Nyhan, 2005). Symptoms such as seizures may present shortly after birth, particularly when an individual is homozygous null for a critical enzyme in the pathway (Micheli *et al*., 2011). Although multiple systems are affected by pyrimidine metabolism disorders, diagnosis of such cases can be challenging.

Upregulated CTPS activity has been observed in various solid tumours including kidney and liver in both humans and rodents (Kizaki *et al*., 1980). In a Chinese hamster ovary cell model of leukemia, mutations in CTPS have resulted in resistance to cytotoxic drugs such as cytosine arabinoside (Whelan *et al*., 1994). Interestingly, such mutations were not found in human patients with cytosine arabinoside resistance (Whelan *et al*., 1994), indicating that the mutation at these sites in the human CTPS gene (*PyrG*) is not a major mechanism for cytosine arabinoside resistance in patients with acute leukemia and alternative mechanisms to resistance are possible.

CTPS is a recognized target for the development of antiviral agents (De Clercq, 1993; Kang *et al*., 1989). The RNA-dependent replication and transcription in severe acute respiratory syndrome coronavirus 2 (SARS-CoV-2) utilizes a critical set of pyrimidine-related metabolic pathways to access the pool of nucleotide-5′-triphosphates (Lucas-Hourani *et al*., 2013). CTP is the least abundant nucleotide in cells (Traut, 1994), thus, replication is dependent on the anabolism of cytosine-containing nucleotides, especially CTP (Cluzel *et al*., 2020; Danchin & Marlière, 2020; Ou *et al*., 2020). As a result, the integrity of the viral genome is highly sensitive to intracellular CTP pool levels. Reduction in the CTP pools can be achieved by inhibiting CTPS, which catalyzes

the rate-limiting step in the de novo biosynthesis of CTP in human host cells (van Moorsel *et al*., 2000).

Several accounts of CTPS inhibition by use of nucleotide and Gln analogues have been shown to potentiate the action of anti-HIV-1 drugs lamivudine (Dereuddre-Bosquet *et al*., 2004) and 2′,3′-dideoxycytidine (Gao *et al*., 2000) in activated peripheral blood mononuclear cells. The ability of nucleotide-based CTPS inhibitors to act as antiviral agents and augment the effects of other antiviral agents suggests that such inhibitors may be valuable drug candidates for the treatment of SARS-CoV-2. The inhibition of CTPS may potentiate the effect of other antiviral therapies targeting COVID-19 infections by reducing intracellular CTP pools.

CTPS has been observed to aggregate into macromolecular filamentous structures also known as cytoophidia (Chang *et al*., 2017). The presence of such filaments have been reported in various human cancer tissues including colon, liver, and prostate cancers (Sun & Liu, 2019). Given the observations of upregulated CTPS and filamentous structures in various cancers, this enzyme is a clinically significant target for drug development. Studies on the structure and mechanism of CTPS may provide novel ways to disrupt its function or regulation, which would be beneficial in the design of new anticancer and immunosuppressive drugs.

1.4 STRUCTURE

1.4.1 General Structure

The X-ray crystal structure of *ec*CTPS (PDB: 1S1M) was determined in 2004 and provided considerable information regarding the structure and function of the enzyme

(Endrizzi *et al*., 2004). Wild-type *ec*CTPS consists of a single polypeptide chain of 545 amino acids with a calculated weight of 60,374 Da. It consists of two major domains: the C-terminal glutaminase domain (residues 287-544) and the N-terminal synthase domain (residues 1-266). The domains are connected by a ~25-Å gated tunnel (residues 267–286) that functions to transport ammonia from the glutaminase domain to the synthase domain (Endrizzi *et al*., 2004; McCluskey & Bearne, 2018b). The binding sites for substrates (Gln, ATP, and UTP) and products (CTP and ADP), were evident in the structure, however the binding site for the allosteric activator (GTP) was not observed (Barry *et al*., 2014; Levitzki & Koshland, 1972b).

In the absence of ligands, apoCTPS exists as a homodimer under physiological conditions (Koshland & Levitzki 1974). While dimers maintain some glutaminase activity, tetramerization is required for CTP production (Levitzki & Koshland, 1972a). ATP and UTP act synergistically to induce tetramerization, though high concentrations of either NTP substrate alone can induce oligomerization in the absence of the other (Levitzki & Koshland, 1972a). The glutaminase domains are located away from the interfaces and are not affected by the oligomeric state (**Figure 1.2**) (Lauritsen *et al*., 2011). The ATP-binding site and CTP-binding site in the synthase domain are located at the tetramer interface; it is for this reason that ATP and UTP are required for tetramerization (Lauritsen *et al*., 2011).

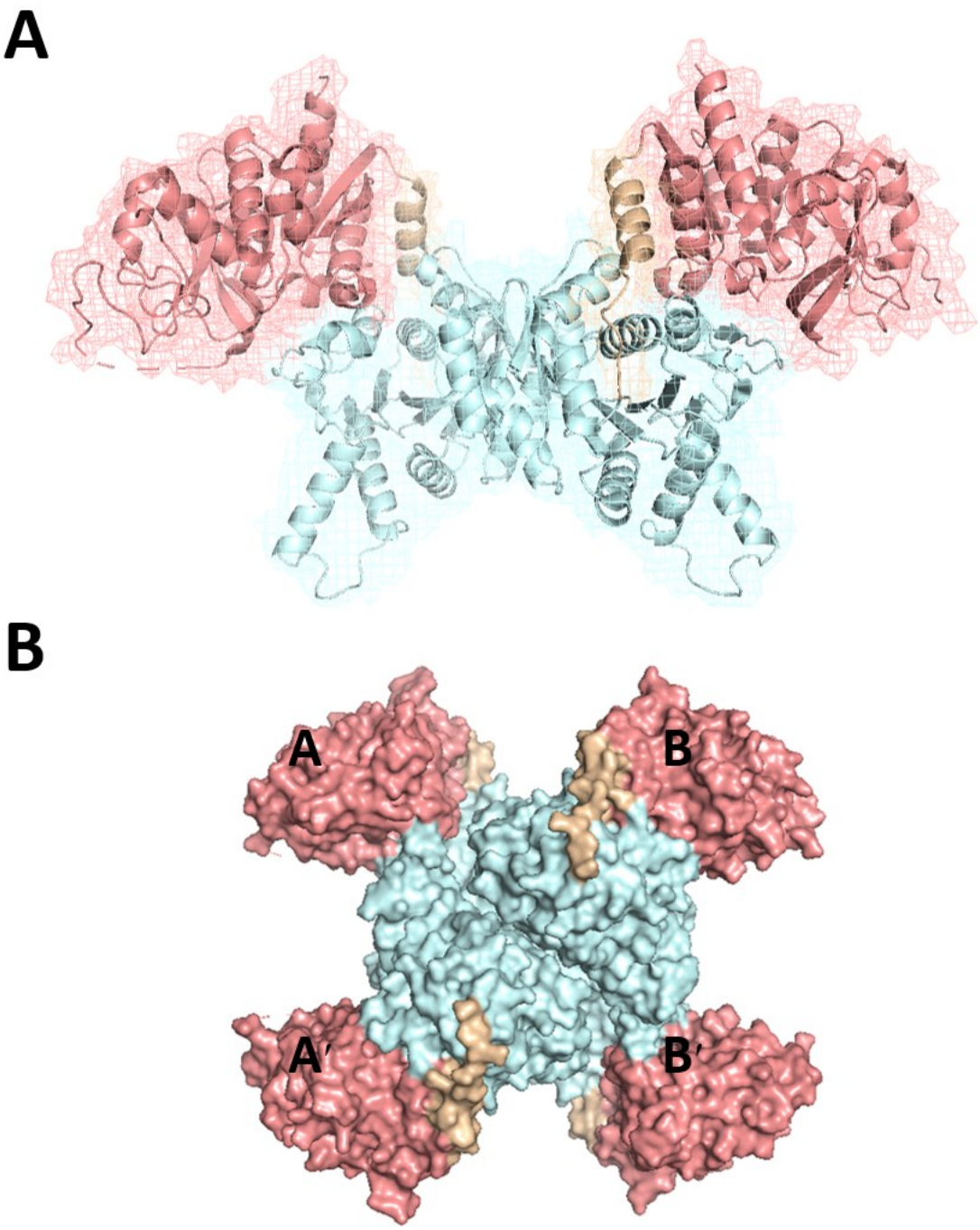

Figure 1.2. Crystal structure of the *ec*CTPS homodimer and homotetramer. In the *ec*CTPS dimer, the two protomers interact via contacts in the synthase domains (pale cyan) of the A and B subunits (**A**). Linker domains (wheat) connect the synthase domain to the glutaminase domain (salmon). The homotetramer consists of four subunits (A, B, A′, and B′) (**B**). (PDB: 2AD5). Images were rendered using PyMOL v. 2.3.2.

1.4.2 GTP-binding site

Rudimentary modelling of GTP into the *ec*CTPS crystal structure revealed a putative GTP-binding site over the top of a 'vestibule' near the opening of the NH_3 tunnel in the glutaminase domain (Endrizzi *et al*., 2004), although bound GTP has never been directly observed in any CTPS X-ray crystallographic or cryo-EM study until recently. Liu and colleagues (X. Zhou *et al*., 2021) presented the structural confirmation of the location of the GTP-binding site in CTPS from *Drosophila melanogaster* (*dm*CTPS) using 6-diazo-5-oxo-L-norleucine (DON) as a Gln substitute. Although CTPS isoforms from various organisms differ slightly in structure and function, the GTP-interacting residues in *dm*CTPS are conserved in *ec*CTPS (X. Zhou *et al*., 2021). The GTP-binding site in *dm*CTPS is located at a cleft between the glutaminase and synthase domain (S. Zhou *et al*., 2021), similar to the predicted GTP-binding position in *ec*CTPS (Endrizzi *et al*., 2004).

hCTPS1 resembles a 'open' state when bound to CTP (Lynch *et al*., 2017; Lynch & Kollman, 2020). Interestingly, Pasca *et al*. (Mori *et al*., 2015) solved the structure of *Mycobacterium tuberculosis* CTPS with two UTP-bound molecules; one at the UTP-binding site and the other at the ATP-binding site. Similar to CTP-bound hCTPS1, this structure assembled a similar 'open' state (Mori *et al*., 2015). Given the position of bound GTP in *dm*CTPS (X. Zhou *et al*., 2021), and the binding of two UTP molecules in *Mycobacterium tuberculosis* CTPS (Mori *et al*., 2015), it was suggested that the open-to-closed structural transition is likely due to binding of ligands at the synthase domain, as previously suggested by Kollman and colleagues (Lynch *et al*., 2017; Lynch & Kollman, 2020). Liu *et al*. (X. Zhou *et al*., 2021) found that the distance between both sides of the

cleft, in which GTP binds *dm*CTPS, varies greatly in closed and open states of CTPS, likely due to binding of ligands at the synthase domain. In *dm*CTPS, the binding of ATP and/or UTP triggers the open-to-closed transition and thereby alters the conformation of the cleft to create the GTP-binding site (X. Zhou *et al*., 2021). Conversely, while *dm*CTPS returns to the open state, the GTP can no longer bind with *dm*CTPS.

At the proposed *dm*CTPS GTP-binding site, the guanine base of GTP interacts with Leu 444 of the binding monomer and Leu 107 of an adjacent monomer (X. Zhou *et al*., 2021) (**Figure 1.3**). The oxygen of the guanine base interacts with the ε-nitrogen of Arg 481 through a hydrogen bond. Additionally, a π–π interaction between the guanine ring and Phe 373 is apparent (X. Zhou *et al*., 2021). The binding of DON stabilizes Phe 373, suggesting that the presence of Gln or Gln analogs at the binding site is a prerequisite for the observation of bound GTP (X. Zhou *et al*., 2021). The ribose ring of GTP interacts with Arg 479 and Phe 50 of an adjacent monomer through hydrogen bonds between the O2 and O3 and the amino acids, respectively (X. Zhou *et al*., 2021). The triphosphate moiety also forms three hydrogen bonds with Lys 306, Tyr 307, and Arg 376 (X. Zhou *et al*., 2021). Point mutations at Arg 359 of *Lactococcus lactis* CTPS (Willemoës *et al*., 2005) and Leu 109 of *ec*CTPS greatly impede the Gln-dependent CTP synthesis in the presence of GTP (Lunn & Bearne, 2004). The corresponding residues of these two points of *dm*CTPS are Arg 376 and Leu 107, both of which were shown to directly interact with GTP (X. Zhou *et al*., 2021).

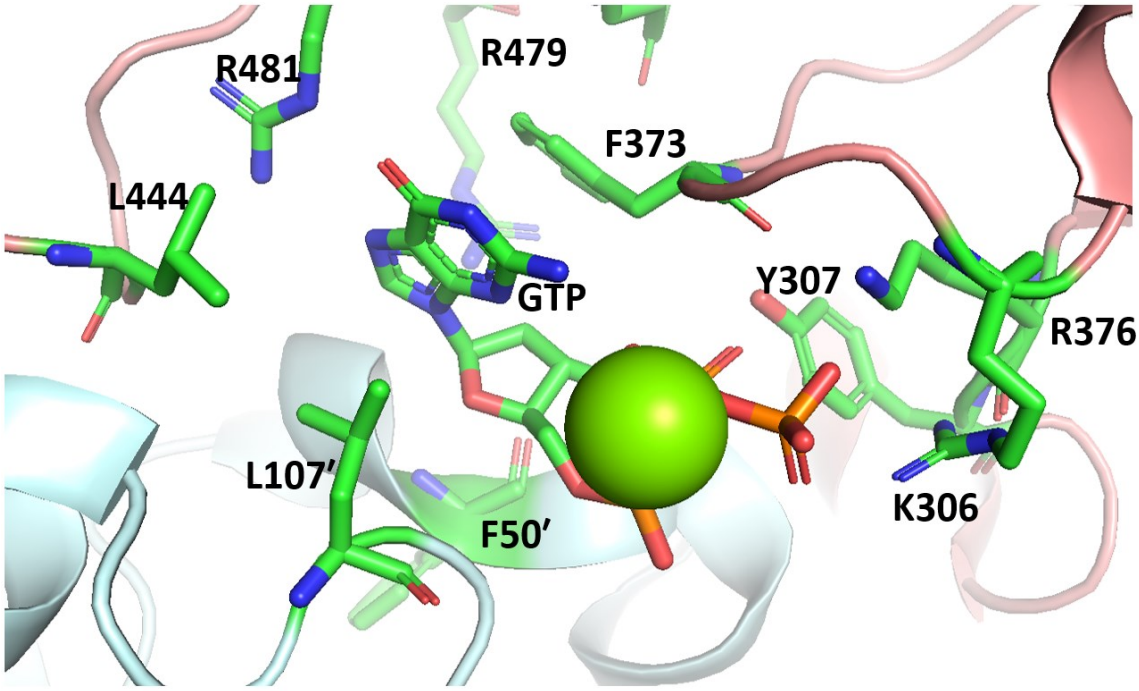

Figure 1.3. The GTP-binding site in *dm*CTPS is located on a cleft between the synthase and glutaminase domains. Residues in the glutaminase domain (salmon) make up most contacts with GTP. The synthase domain (light cyan) contains L107 which is proposed to interact with the guanine base. Atoms are colored as green (carbons), red (oxygen), blue (nitrogen), orange (phosphorous), and green (magnesium). (PDB: 7DPT). Image was rendered using PyMOL v. 2.3.2.

1.4.3 ATP-binding site

The synthase active site, in which UTP phosphorylation and displacement by ammonia occurs, resides in a large crevice, of which the walls are contributed by three different subunits (**Figure 1.4.A**) (Endrizzi *et al*., 2004). Subunit A provides most of the ATP- and UTP-binding determinants with subunits B and A′ providing a few additional nucleotide-binding determinants (Endrizzi *et al*., 2004). The ADP ribose ring observed in the structure of the product complex is sandwiched between the Ile 20 side chain and Ala 182 from the B subunit (Endrizzi *et al*., 2005). This direct contact, combined with the extensive interactions with loop residues 176–187 from the adjacent subunit, are consistent with the role of ATP in inducing tetramer formation (Endrizzi *et al*., 2005). Interestingly, when the enzyme is in its filament form, such inferences are disputed as all active sites are solvent accessible, and UTP, ATP, and Gln can freely diffuse to and from their binding sites (Barry *et al*., 2014). Additionally, CTP alone is capable of inducing filaments of stacked tetramers, indicating that ATP and UTP are not essential for the transition of dimer to tetramer. More specifically, with respect to bound ADP, the ribose O4′ atom is bound via a water-mediated hydrogen bond to Ser 15 and Arg 211, whereas the 2′- and 3′-hydroxyl groups have no direct protein contacts. The diphosphate moiety is bound via a network of main chain and side chain hydrogen bonds (Endrizzi *et al*., 2005). The β-phosphate forms H-bonds with the backbone amides of residues Ser 15, Gly 17, and Lys 18, while the α-phosphate forms H-bonds with the backbone amides of Gly 19 and Ile 20 (**Figure 1.4.B**) (Endrizzi *et al*., 2005).

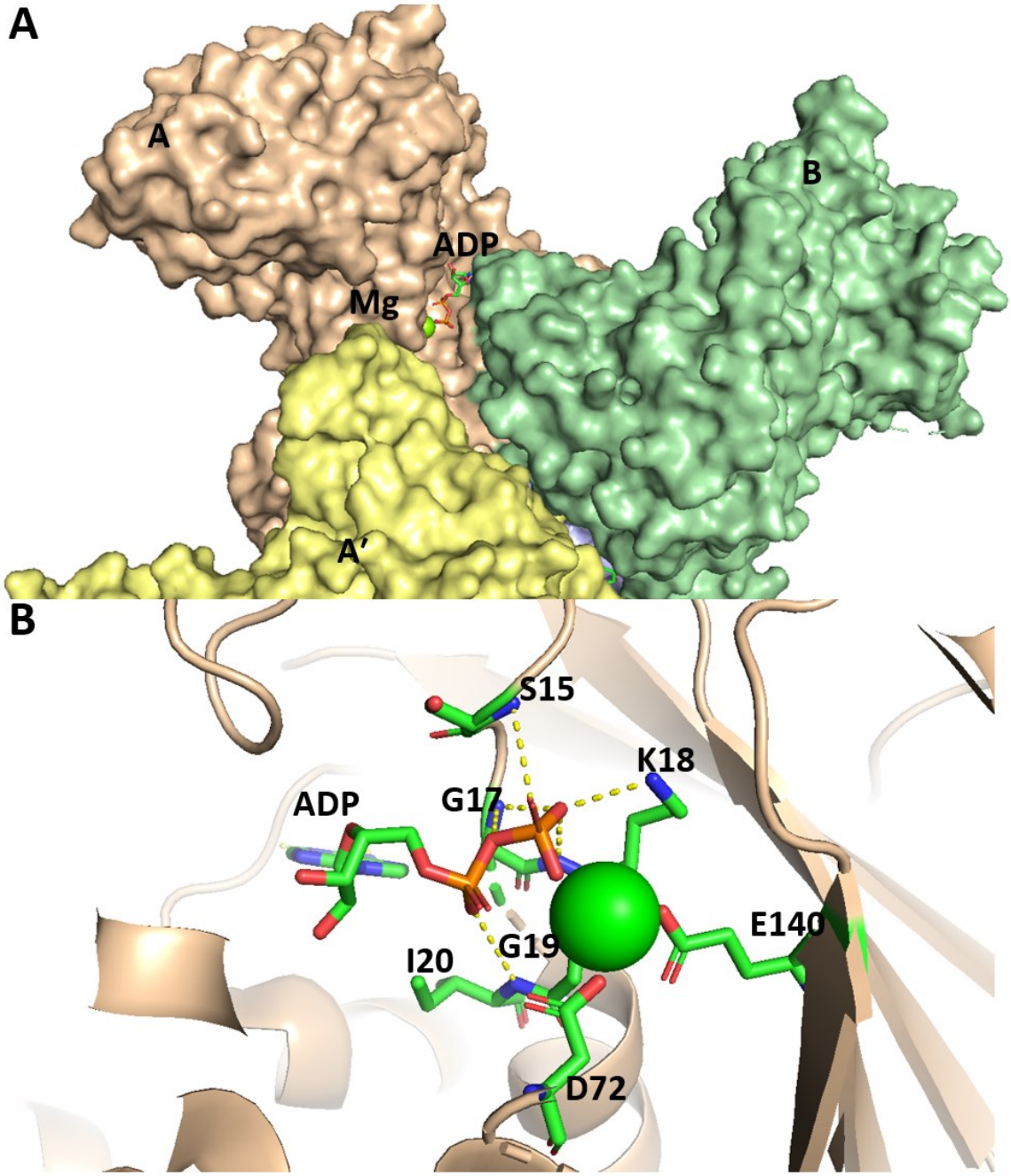

Figure 1.4. ATP/ADP-binding site in *ec*CTPS. ADP, and magnesium are bound in a crevice comprised of three subunits of the tetramer: A (wheat), B (pale green), and A′ (yellow) (**A**). Specific binding interactions of the ADP phosphate moiety (S15, G17, K18, G19, and I20) and proposed catalytic residues of the ATP γ-phosphate (E140 and D72) are shown (**B**). (PDB: 2AD5). Images were rendered using PyMOL v. 2.3.2.

The magnesium ion that activates the ATP γ-phosphate for transfer to O4 of UTP bridges the β-phosphate and the proposed catalytic residues Glu 140 and Asp 72 (**Figure 1.4.B**) (Endrizzi *et al*., 2004, 2005).

Though the ADP/ATP-binding site in *ec*CTPS was well-characterized by Baldwin and colleagues (Endrizzi *et al*., 2004, 2005), there was still merit in probing this site, especially considering that ATP-binding likely induces changes in conformation. Bearne and co-workers (MacLeod *et al.*, 2006) investigated the specific interactions in the ATP-binding site of *ec*CTPS with the affinity label 2′,3′-dialdehyde adenosine 5′-triphosphate (oATP). *ec*CTPS was labeled using [2,8-^{3}H]oATP and subsequently subjected to trypsin-catalyzed proteolysis. Tryptic peptides were separated and analyzed using N-terminal sequencing. Lys 306 in the glutaminase domain was found to be modified by oATP, supporting structural data that demonstrates close proximity of Lys 306 to the 2′- and 3′-hydroxyl groups (Endrizzi *et al*., 2005). Kinetic investigations indicated that Lys 306 is not essential for ATP-binding but plays a role in the conformational changes that mediate interactions between the ATP-binding site and the glutaminase domain (MacLeod *et al*., 2006).

1.4.4 CTP-binding site – Cytosine Ring

The CTP-binding site has been well characterized by Baldwin and colleagues (**Figure 1.5**) (Endrizzi *et al*., 2004, 2005). The cytosine and ribose moieties are accommodated by an “induced fit” protein rearrangement that involves an inward rotation of the side chains of Asp 147, Ile 148, and Glu 149 rotate and an inward shift of Ile 116 (B′) from an adjacent subunit (Endrizzi *et al*., 2005). This creates the cytosine

ring-binding pocket, while the Gln 114 side chain from subunit B′ is rotated to both provide space and pack against the ribose ring (Endrizzi *et al*., 2005). Main chain amides from α-helical loop residues Ile 148 and Glu 149 donate hydrogen bonds that recognize the O2 and N3 acceptors in the cytosine ring, while the Asp 147 carboxylate provides favorable stacking interactions for the electron-deficient pyrimidine ring (Endrizzi *et al*., 2005). The N^4 exocyclic atom is not directly contacted by the enzyme, however, a water-mediated hydrogen bond to the Gly 146 carbonyl oxygen provides potential recognition of N^4 (Endrizzi *et al*., 2005). The cytosine C5 and C6 atoms are proximal to Phe 227 from subunit A′ (Endrizzi *et al*., 2005), which has an apparent role in the polymerization of *ec*CTPS tetramers (Lynch *et al*., 2017; McCluskey & Bearne, 2018a) (*vide infra*). The CTP ribose packs against Glu 149 and residues 114–116 from subunit B′, whereas the triphosphate moiety makes extensive protein contacts via a network of polar interactions, provided primarily by the noncrystallographically-related “dissociable” subunit (Endrizzi *et al*., 2005).

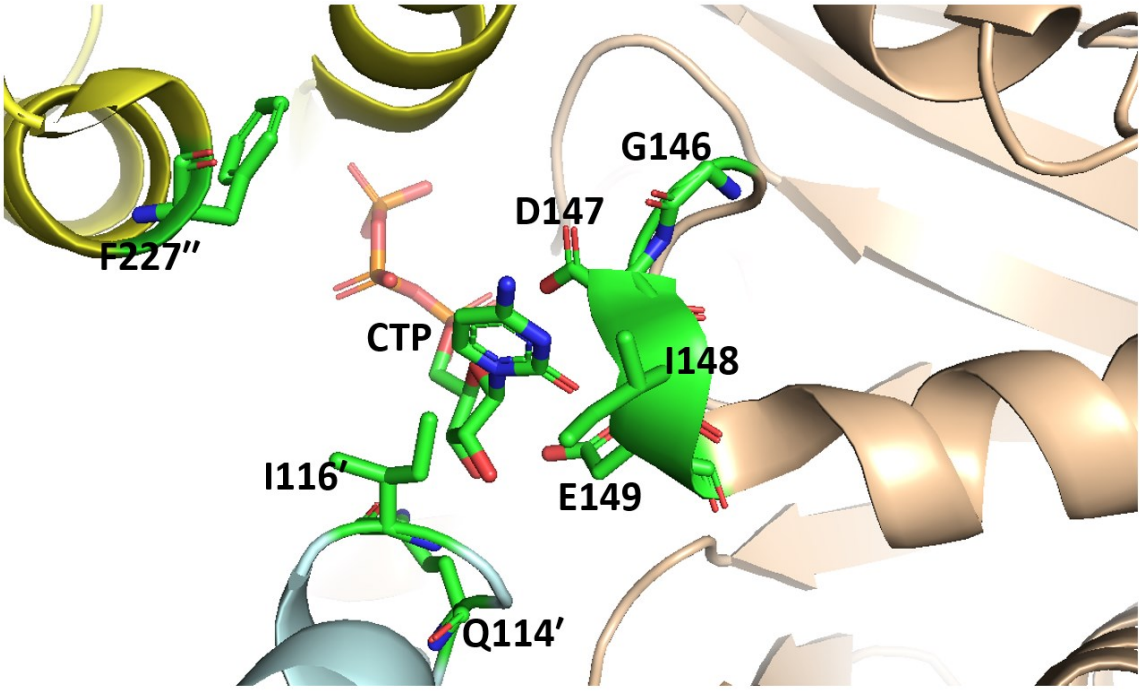

Figure 1.5. *ec*CTPS residues interacting with the cytosine ring of CTP. CTP is bound in a crevice comprised of three subunits of the tetramer: A (wheat), A′ (yellow), and B′ (pale cyan). Residues identified as forming interactions with the cytosine ring are indicated and atoms are colored as green (carbons), red (oxygen), blue (nitrogen), and orange (phosphorous). Residues identified as forming interactions with the ribose ring and/or triphosphate moiety are not indicated for clarity. (PDB: 2AD5). Image was rendered using PyMOL v. 2.3.2.

1.4.5 UTP-binding site

CTP competitively inhibits UTP binding (Long & Pardee, 1967) and is isosteric to UTP. However, drug resistance mutations that reduce CTP binding in *Saccharomyces cerevisiae* CTPS do not interfere with UTP binding, but actually increase the catalytic efficiency (Ostrander *et al*., 1998), and are located away from the predicted catalytic site where the uracil ring is located (Endrizzi *et al*., 2004). The mechanism by which *ec*CTPS can differentiate between CTP and UTP has been characterized by probing the active site of *ec*CTPS variants (Simard *et al*., 2003), analysis of substrate specificity (Scheit & Linke, 1982), and analysis of crystal structures (Endrizzi *et al.*, 2004, 2005).

There are structural data available for UTP-bound hCTPS1 (PDB: 7MGZ, 7MIF, and 7MIG), hCTPS2 (PDB: 7MII and 7MIH), mCTPS1 (PDB: 7MIP), mCTPS2 (PDB: 7MIU) (Lynch *et al*., 2021), and *Mycobacterium tuberculosis* CTPS (PDB: 4ZDK and 4ZDJ) (Mori *et al*., 2015). Although *ec*CTPS has not yet been crystalized with UTP as a ligand, Baldwin and colleagues (Endrizzi *et al*., 2004) inferred the location of the UTP-binding site by residue conservation with other CTPSs, steric restrictions, the location of the interfacial anion-binding site that is well-placed to interact with the UTP γ-phosphate, and structural analogy to the diaminoperlargonic acid (DAPA) substrate location in dethiobiotin synthetase (DTBS), a structural homologue of the CTPS N-terminal domain.

Conserved residues Pro 43, Tyr 44, and His 57 line the pocket binding uracil (Endrizzi *et al*., 2004). A P-loop-like structure, composed of conserved residues Lys 187, Thr 188, and Lys 189, is reasonably placed to interact with the UTP γ-phosphate (Endrizzi *et al*., 2004). Consistent with this, Lys 187 is protected from proteolysis in the presence of UTP and the K187A substituted enzyme does not synthesize CTP (Simard *et*

al., 2003). The putative location of the β-phosphate is proximal to side chains of Asp 147, Lys 189, Gln 192, and Lys 223 (Endrizzi *et al*., 2004). Gln 149 and Thr 112 and Gln 114 from an adjacent subunit (A′) appear to be positioned to recognize the ribose moiety. The side chain of His 118 from subunit A′ helps position the Thr 112 and Gln 114 positions through main chain hydrogen bonds (Endrizzi *et al.*, 2004).

1.5 MECHANISM AND FUNCTION

Glutamine amidotransferases are a family of enzymes that catalyze the hydrolysis of Gln as a nitrogen source and subsequently transfer the ammonia to another substrate, thus creating a new carbon-nitrogen bond. Glutamine amidotransferases can exist either as single polypeptides or as domains in much larger multifunctional synthase proteins. Class-I glutamine amidotransferases are defined by a conserved catalytic triad for the hydrolysis of Gln, consisting of cysteine, histidine, and glutamate (Weng & Zalkin, 1987) (**Figure 1.6**).

CTPS catalyzes the hydrolysis of Gln and uses the nascent ammonia for catalyzing the amination of UTP to yield CTP. The enzyme's mechanism can be partitioned into two half-reactions occurring in two domains: the amide hydrolysis in the glutaminase domain, and the amination of UTP in the synthase domain. Ammonia travels from the glutaminase domain to the synthase domain via a ~25-Å gated tunnel (Endrizzi *et al*., 2004; McCluskey & Bearne, 2018b). Alternatively, exogenous ammonia can be used as a substrate and is proposed to enter the enzyme near the gated tunnel in the glutaminase domain and subsequently react with UTP in a similar manner as Gln-derived ammonia.

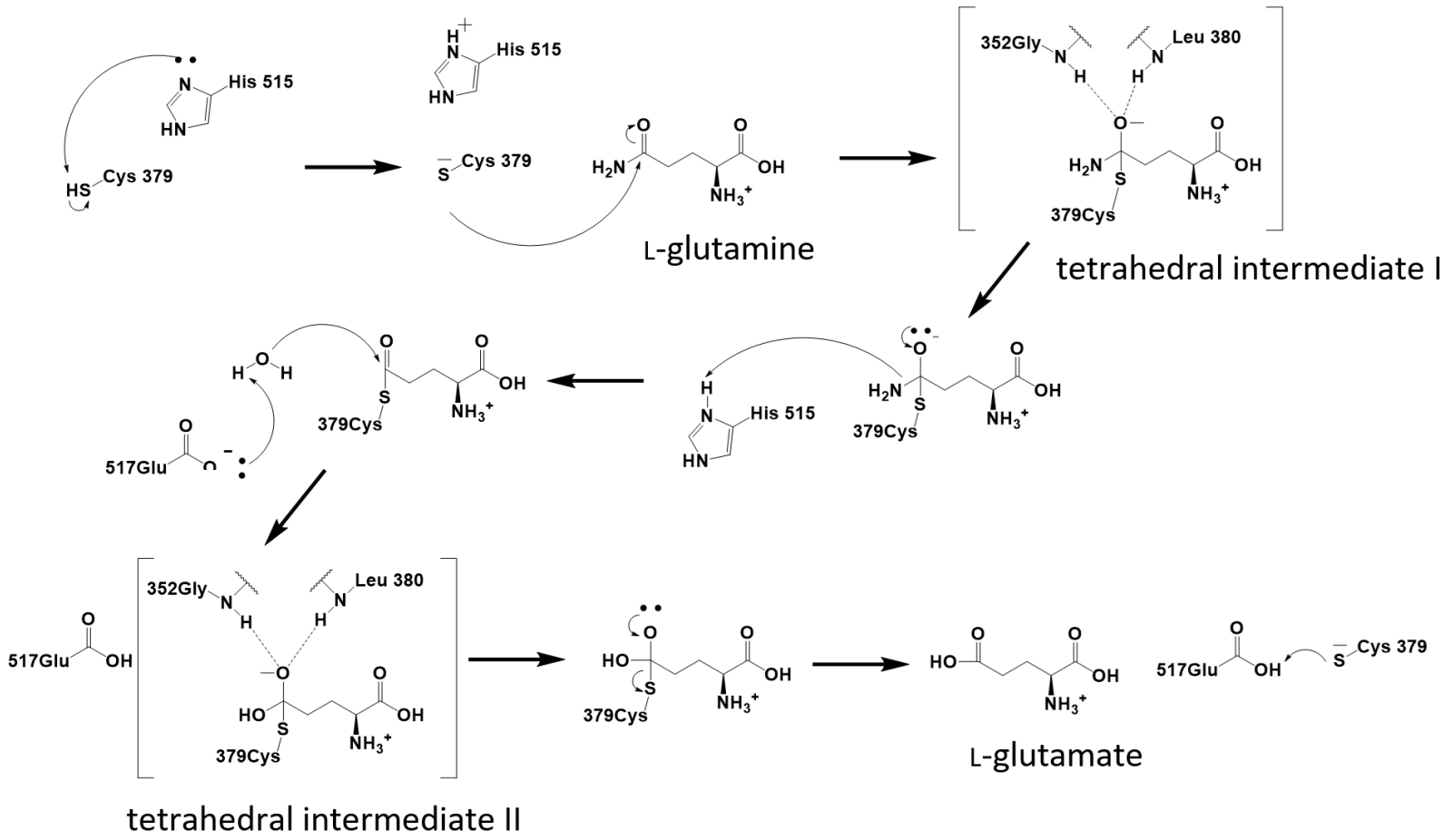

Figure 1.6. Proposed mechanism of the CTPS-catalyzed glutaminase reaction. CTPS utilizes a class-I glutaminase domain to generate L-glutamate through the formation of two tetrahedral intermediates (Endrizzi *et al*., 2004; Goto *et al.*, 2004).

Ammonia derived from Gln travels through a gated-tunnel to the synthase domain (**Figure 1.7**). The tunnel has a constriction formed by Pro 54, His 57, and Val 60 in *ec*CTPS (Endrizzi *et al*., 2004). McCluskey and Bearne (McCluskey & Bearne, 2018b) described the effects of "pinching" the tunnel by substituting various residues for the gate using site-directed mutagenesis. They showed that upon substitution of Val 60 by a bulkier residue (V60F), the passage of ammonia was impeded. Catalytic activity of the Gln-dependent CTP formation was reduced slightly, however, the variant was not able to catalyze CTP formation with exogenous ammonia as a substrate (McCluskey & Bearne, 2018b). Furthermore, GTP was required for the utilization of exogenous NH_3 by the V60F variant even though GTP normally inhibits NH_3-dependent CTP formation (Lunn *et al*., 2008; McCluskey & Bearne, 2018b). The requirement for GTP, and the alleged proximity of its binding site to Val 60, suggested that GTP could induce a conformational change in the vicinity of the gate to facilitate NH_3 transport (McCluskey & Bearne, 2018b).

His 57, near the end of this tunnel, plays a key role in regulating the diffusion of ammonia through to the synthase domain. In the crystal structure, the His 57 side chain has two distinct conformations: one in which the residue's side chain is adjacent to the UTP-binding site to allow for exit of ammonia from the tunnel (Endrizzi *et al*., 2004). The other arrangement blocks the tunnel, thus, preventing ammonia molecules from entering the synthase domain (Endrizzi *et al*., 2004). This suggested that His 57 acts as a gate for the ammonia tunnel.

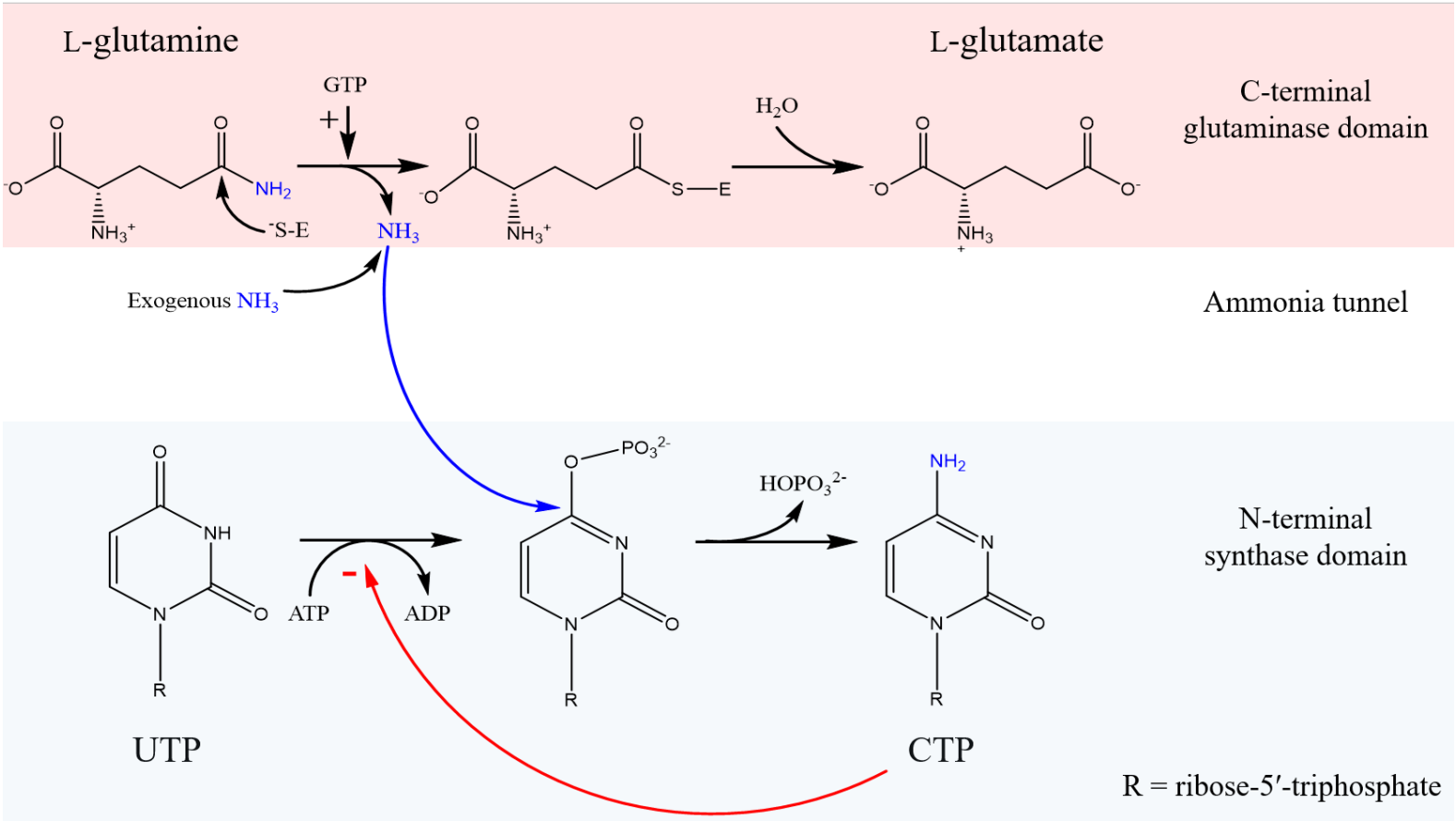

Figure 1.7. Mechanism of CTPS with either L-glutamine or exogenous ammonia as a substrate. GTP-dependent hydrolysis of L-glutamine occurs in the C-terminal glutaminase domain (salmon). Ammonia travels through the NH_3 tunnel to the N-terminal synthase domain (light cyan), where it reacts with ATP-activated UTP to form CTP. Exogenous ammonia (dark blue) is illustrated as an alternative substrate where it is proposed to enter the enzyme near the NH_3 tunnel in the glutaminase domain and react with the activated UTP in a similar manner to Gln-derived ammonia. CTPS is susceptible to feedback inhibition in the synthase reaction.

During catalysis of the initial phosphorylation reaction in the tetramer, the magnesium ion activates ATP's γ-phosphate for transfer to the O4 of UTP; thus, the metal ion is essential for the catalytic efficiency of CTPS. Although Mg^{2+} is the most efficient metal ion at supporting catalysis, Co^{2+} and Mn^{2+} can be substituted at concentrations below 1.0 mM (Robertson & Villafranca, 1993).

After ammonia travels through the tunnel, it reacts with UTP that has been activated by ATP-dependent phosphorylation in the synthase domain (**Figure 1.7**). ATP binds in a cleft such that the γ-phosphate is positioned at the exit of the NH_3 tunnel (Endrizzi *et al*., 2004; Lynch *et al*., 2017). The reaction involves the activation of the O4 of UTP through phosphorylation from ATP to produce a 4-phospho-UTP intermediate compound (von der Saal *et al*., 1985). This intermediate undergoes nucleophilic attack by ammonia, to yield the final product, CTP. The *E. coli* enzyme is highly specific for the substrate UTP and has been observed to utilize only a few other UTP analogues chemically modified at the uracil, ribose, or 5′-triphosphate moieties as substrates (McCluskey *et al*., 2016; Pappas *et al*., 1999; Scheit & Linke, 1982).

1.6 FILAMENT FORMATION BY *ec*CTPS

The oligomerization of non-cytoskeletal enzymes into filaments has been a known phenomenon for years; however, only recently has the discovery of the enzyme self-regulation by filaments become appreciated (Park & Horton, 2019). As protein crystallography became a more routine tool in enzymology, analysis of filament formation was essentially suspended. However, in 2009, the discovery of enzymes with fluorescent proteins or antibodies self-assembling into filaments in cells when viewed

using confocal microscopy regenerated the interest of many researchers (Park & Horton, 2019). These membrane-less, reversibly forming subcellular structures have been observed to respond to cellular stress, as well as activators and inhibitors that typically inhibit the enzyme (Park & Horton, 2019). Filament formation by CTPS is of interest because of its contribution to regulation of the conversion of UTP to CTP and pyrimidine metabolism overall.

Filament formation by bacterial CTPS is thought to sequester the enzyme into repeating units of reversibly inactivated tetramers (**Figure 1.8.A**). Due to the overlapping UTP- and CTP-binding sites, upon increased levels of UTP, filaments disassemble to accommodate the metabolic needs of the cell (McCluskey & Bearne, 2018a). The activity of CTPS filaments differs slightly amongst various organisms. CTPS filaments arising from bacterial sources bind CTP and form an inactive enzyme filament (Lynch *et al*., 2017). Interestingly, the two human isoforms, hCTPS1 and hCTPS2 behave differently from one another, and from bacterial CTPS: filaments of hCTPS1 maintain an active, substrate-bound state, whereas filaments of hCTPS2 dynamically switch between substrate- and product-bound states in response to the metabolic requirements (Lynch *et al*., 2017). All CTPS filaments are formed by the stacking of tetramers, but differences arise in the conformation of the tetramers and, therefore, the interfaces between tetramers (Park & Horton, 2019). *ec*CTPS tetramers can self-assemble and this process is promoted by the CTP analogue dF-dCTP (McCluskey & Bearne, 2018a), which suggests that nucleotide analogues employed as chemotherapeutic agents may affect the filamentous states of enzymes and potentially alter their regulation *in vivo*.

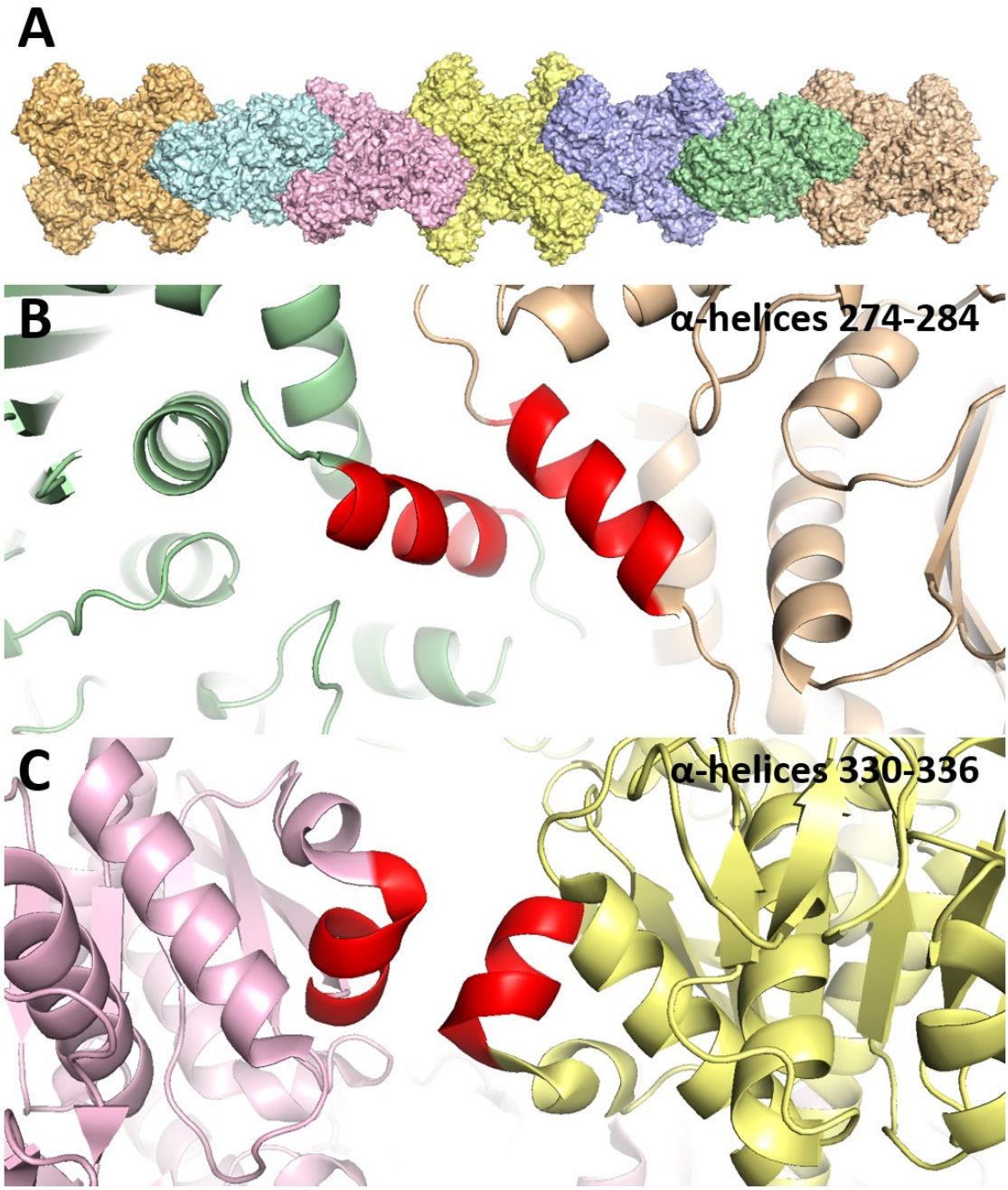

Figure 1.8. *ec*CTPS tetramers polymerize into filaments. *ec*CTPS tetramers (various colours) interact with one another to form filaments of ≥ 30 nm in length (**A**). Interactions of the α-helices 274–284 of the interdomain linker (**B**), and 330–336 of the glutaminase domain (**C**) are highlighted in red. (PDB: 5U3C). Images were rendered using PyMOL v. 2.3.2

Transition from the apo-state of *ec*CTPS to the filamentous form reorganizes the tetramer interface, compacting the *ec*CTPS subunits around the bound CTP (Lynch *et al*., 2017). The conformational changes are mostly rigid-body motions except for the shift of helix 218–228 3.6 Å closer to the bound CTP such that Phe 227 packs against the CTP base (Lynch *et al*., 2017). This shift also repositions Asn 229 at the base of helix 218–228, creating a new hydrogen-bond network with Arg 158 and Glu 155 across the tetramer interface, likely stabilizing the filament conformation (Lynch *et al*., 2017). Two discrete segments constitute the filament assembly contacts: the linker region α-helix 274–284 (**Figure 1.8.B**) and the α-helix 330–336 of the glutaminase domain (**Figure 1.8.C**) (Barry *et al*., 2014). The E155K variant cannot assemble filaments (Barry *et al*., 2014), likely through resistance to feedback inhibition (i.e., its inability to bind CTP) (Trudel *et al*., 1984). The E277R variant also cannot form filaments (Barry *et al*., 2014). Furthermore, the E149D variant cannot form filaments in the presence of CTP or dF-dCTP (McCluskey & Bearne, 2018a), emphasizing the importance of ligand-binding at the CTP-binding site for filament formation. The F227A variant can not form filaments, whereas the F227L variant can (McCluskey & Bearne, 2018a), indicating that a bulky hydrophobic residue at the 227-position is sufficient for filament formation.

1.7 INHIBITION OF CTPS

CTPS is a target of interest for drug design due to its essential role in the *de novo* biosynthesis of pyrimidines. As mentioned previously, CTPS is allosterically regulated by the activator GTP and product CTP. Elevated concentrations of GTP inhibit CTP formation through the uncoupling of Gln hydrolysis (Lunn *et al*., 2008; MacDonnell *et*

al., 2004). The CTP-binding site overlaps with the UTP-binding site, thus, the product CTP acts as an inhibitor of CTPS (Endrizzi *et al*., 2005). These forms of allosteric regulation occur inevitably, however the enzyme can be inhibited by other means including but not limited to nucleoside analogues and Gln analogues (Barry *et al*., 2014; Lunn *et al*., 2008; McCluskey *et al*., 2016; Narvaez-Ortiz *et al*., 2018).

Many studies have sought to determine the requirements for designing a potent inhibitor of *ec*CTPS. Bearne and colleagues (Lunn *et al*., 2008) investigated guanine-based inhibitors and found that the ribose 5′-triphosphate moiety is unnecessary for inhibition. The ribose moiety, however, increased the solubility of the inhibitor (Lunn *et al*., 2008). This finding simplified the future of the design of guanine-based inhibitors by limiting them to nucleosides or soluble purine bases (Lunn *et al.*, 2008). It is absolutely necessary to have an amino group at the 2-position of the purine ring for activation and the substituent at the 6-position should not be an H-bond acceptor as it can allow for triphosphorylation *in vivo* and could generate an activator (Lunn *et al*., 2008).

dF-dCTP induces cell death through a variety of mechanisms and is therefore utilized as a chemotherapeutic agent for the treatment of several solid tumors (McCluskey *et al*., 2016). Bearne and colleagues (McCluskey *et al*., 2016) showed that dF-dCTP is a potent competitive inhibitor of *ec*CTPS with respect to UTP and that its binding affinity exceeds that of CTP by ~75-fold. McCluskey and Bearne (McCluskey & Bearne, 2018a) also demonstrated the ability of dF-dCTP to induce filament formation in solution with lengths up to 30 nm by dynamic light scattering. Gemcitabine is employed as a first line treatment of pancreatic cancer, and the active metabolite depleted

intracellular CTP levels, potentially limiting the amount of competing intracellular CTP (Heinemann *et al*., 1995)

DON is a nonstandard amino acid that is used as an inhibitor to study CTPS and other glutaminases. The structure of DON is very similar to Gln, thus, it can bind at the Gln-binding site of these enzymes and inhibit them through covalent modification (Pinkus, 1977). Gitai and colleagues (Barry *et al*., 2014) performed filament formation studies of *ec*CTPS with DON and found that DON abolishes both CTP production and CTPS polymerization. DON-treated CTPS can still polymerize when CTP is added to the solution (Barry *et al*., 2014), indicating that the enzyme is not able to catalyze the conversion of UTP to CTP but can still interact with other tetramers.

1.8 OVERVIEW OF THIS WORK

In this thesis, investigations focus on (i) how the 5′-triphosphate metabolites of specific antiviral agents affect *ec*CTPS activity and filament assembly, (ii) the role of ATPγS as a ligand, and (iii) the inhibition of the C268A variant of *ec*CTPS by dF-dCTP to further our understanding of how dF-dCTP inhibits *ec*CTPS activity. We determined that adenine-arabinofuranoside-5′-triphosphate (araATP or vidarabine-5′-triphosphate) and ribavirin-5′-triphosphate (RBVNTP) act as a substrate and allosteric activator, respectively, affording a possible mechanism by which CTPS can remain active when intracellular pools of substrates are diminished as well as assist in maintaining intracellular pools of CTP. Sofosbuvir-5′-triphosphate (STP), an analogue of UTP, was also found to be a substrate of *ec*CTPS, which was aminated to 4-NH_2-STP, an additional antiviral metabolite. Like UTP, STP demonstrates the ability to prevent filament

assembly, thus, affording a mechanism by which CTPS can remain active in the presence of STP. Furthermore, β-D-N^4-hydroxycytidine-5′-triphosphate (N^4-OH-CTP) was found to be a competitive inhibitor of *ec*CTPS with respect to UTP, though the binding affinity was reduced ~ 3.5-fold relative to CTP.

ATPγS was found to be a potent, competitive inhibitor of *ec*CTPS with respect to ATP, and demonstrated no apparent effects on filament assembly. Finally, the kinetics of a C268A *ec*CTPS variant were determined to investigate the mechanism by which dF-dCTP exhibits potent inhibition of *ec*CTPS. The nearly identical k_{cat}, K_m, and IC_{50} values for inhibition of wild-type and C268A variants by CTP and dF-dCTP indicate that conformational changes alone do not account for the tight-binding exhibited by dF-dCTP.

CHAPTER 2: EFFECTS OF THE 5′-TRIPHOSPHATES OF SPECIFIC ANTIVIRAL AGENTS ON CTP SYNTHASE ACTIVITY

2.1 INTRODUCTION

2.1.1 Targeting CTPS for the Synergistic Treatment of COVID-19

Severe acute respiratory syndrome coronavirus 2 (SARS-CoV-2), a novel coronavirus, was first identified in December 2019 as the cause of a respiratory illness designated coronavirus disease 2019, or COVID-19 (Helmy *et al*., 2020). Rapid transmission of COVID-19 has led to a pandemic, causing a dramatic loss of human life worldwide and presenting an unprecedented challenge to public health. Coronaviruses are enveloped, single-stranded RNA viruses known to mutate rapidly and cross species barriers (Decaro *et al*., 2010; Romano *et al*., 2020). RNA viruses a have particularly complex replication machinery (Lucas-Hourani *et al*., 2013; Romano *et al*., 2020), which greatly complicates the design of broad-spectrum antiviral agents. Despite the evaluation of several therapeutic agents for the treatment of COVID-19, there have been limited antiviral agents shown to be effective (Beigel *et al*., 2020). It has become clear that there is an urgent need to develop broad spectrum therapeutic approaches to combat the present and future pandemics (Li *et al*., 2020).

The use of small molecule antiviral agents offers a promising approach to relieve the pressure on the health care system by reducing hospitalizations and mortality rates. Drug repurposing is the process of identifying new uses for approved or investigational drugs. Examining known antiviral agents presents an effective strategy for identifying new uses of approved drugs in a cost-effective and timely manner (Singh *et al*., 2020). Hence, efforts have focused on exploring the efficacy of known antiviral compounds,

such as remdesivir, favipiravir, ribavirin, lopinavir, and ritonavir, with remdesivir (GS-5734) being the most promising (Cao *et al*., 2020; Joshi *et al*., 2020; Siegel *et al*., 2017; Tong *et al*., 2020; Wang *et al*., 2020). This nucleotide analogue is delivered as a prodrug and subsequently metabolized to its respective 5′-triphosphate by the action of intracellular kinases. Remdesivir-5′-triphosphate directly inhibits the coronavirus RNA-dependent RNA polymerase (RdRp) (Gordon *et al*., 2020) and was shown to decrease the median recovery time of patients with COVID-19 infections (Beigel *et al*., 2020). Nucleoside-5′-triphosphate analogues compete with endogenous nucleotide substrates for the viral RdRp, which then incorporates the analogues into the nascent viral RNA, leading to chain-termination. In addition to the direct inhibition of the RdRp of SARS-CoV-2, synergistic approaches to antiviral therapies are also being considered. One such approach is to limit the nucleotide pools available for viral replication, thus starving the viral replication machinery.

SARS-CoV-2 RNA-dependent replication and transcription utilizes a critical set of pyrimidine-related metabolic pathways to access the pool of nucleoside-5′-triphosphates (Lucas-Hourani *et al*., 2013). Replication is dependent on the anabolism of cytosine-containing nucleotides, especially CTP (Cluzel *et al*., 2020; Danchin & Marlière, 2020; Ou *et al*., 2020), thus, the integrity of the viral genome is highly sensitive to the levels of intracellular CTP. Reduction in the CTP pools can be achieved by inhibiting CTPS (van Moorsel *et al*., 2000). Despite acknowledgment of the crucial role of pyrimidine-related metabolic pathways, the specific role of CTP in RNA-dependent replication and transcription has been overlooked until recently (Ou *et al*., 2020).

CTP plays an integral role in four independent processes, all of which are essential for the construction of functional SARS-CoV-2 viral particles (Ou *et al*., 2020). In addition to being one of the four nucleotide precursors required for construction of the viral genome, CTP is required for synthesis of the liponucleotide precursors of the viral envelope (Bakovic *et al*., 2007; Danchin & Marlière, 2020; Ostrander *et al*., 1998). The double layer of phospholipids that forms most membranes is derived from cytosine-based liponucleotides. Although the membrane lipid composition differs in the three domains of life, the general organization of pathways is similar, in which CTP-dependent enzymes catalyze the formation of lipid constituents of the lipid bilayer, which control its shape (Cornell & Ridgway, 2015). CTP is also involved in the biosynthesis of active human tRNAs via a CTP-dependent nucleotidyltransferase (CCAse) (Wellner *et al*., 2018). The sole function of the CCA-adding enzyme is to maintain and repair the CCA termini in the tRNA pool (Lizano *et al*., 2008). Finally, CTP plays a role in post-translational glycosylation of viral proteins (e.g., the spike protein) via the endoplasmic reticulum (Shridas & Waechter, 2006). This requires dolichyl-phosphate formed through the action of a CTP-dependent dolichol kinase (Shridas & Waechter, 2006). The addition of a carbohydrate moiety to the spike protein helps the pathogen evade recognition by the host immune system (Grant *et al*., 2020). Finally, CTP is converted into the natural antiviral agent 3-deoxy-3,4-didehydro-CTP (ddhCTP) by the enzyme viperin as part of the innate immune response (Rivera-Serrano *et al*., 2020). Incorporation of ddhCTP causes premature termination of RNA synthesis by the RdRp in some viruses (Rivera-Serrano *et al*., 2020). Evidently, survival and replication of SARS-CoV-2 is highly sensitive to the cell's CTP synthesis and regulation.

CTPS is a recognized target for the development of antiviral agents (De Clercq, 1993; Kang *et al*., 1989). For example, the CTPS inhibitor cyclopentenylcytosine (CPEC)-5′-triphosphate (CPEC-TP) exhibits antiviral activity against a wide range of viruses including influenza, rhinovirus, parainfluenza, measles, and herpes (De Clercq, 1993; Kang *et al*., 1989). Specifically, CPEC-TP leads to a depletion in CTP pools, which is closely correlated with the cytocidal activity of CPEC (De Clercq, 1993). Despite its antiviral activity, this drug displayed pronounced cardiotoxicity in a phase I clinical trial in patients with solid tumours (Schimmel *et al*., 2007). The inhibition of CTPS activity by nucleotide and Gln analogues has been shown to potentiate the action of the anti-HIV-1 drugs lamivudine (Dereuddre-Bosquet *et al*., 2004) and 2′,3′-dideoxycytidine (Gao *et al*., 2000) in activated peripheral blood mononuclear cells. The ability of nucleotide-based CTPS inhibitors to act as antiviral agents and augment the effects of other antiviral agents suggests that such inhibitors may be valuable drug candidates for a combination therapy for the treatment of SARS-CoV-2. The inhibition of CTPS may potentiate the effect of other antiviral therapies targeting COVID-19 infections by reducing intracellular CTP pools.

This chapter explores the effects of the nucleotide analogues adenine-arabinofuranoside-5′-triphosphate (araATP or vidarabine-5′-triphosphate), ribavirin-5′-triphosphate (RBVNTP), sofosbuvir-5′-triphosphate (STP), and β-D-N^4-hydroxycytidine-5′-triphosphate (N^4-OH-CTP) on the activity of *ec*CTPS, as well as their effects on filament formation by *ec*CTPS.

2.1.2 Vidarabine-5′-triphosphate (araATP)

9-β-D-Arabinofuranosyladenine (araA or Vidarabine) is an analogue of adenosine in which the D-ribose is replaced by D-arabinose (**Figure 2.1**). It was first isolated by Bergmann and colleagues (Bergmann & Feeny, 1951) in the 1950s from the Caribbean sponge *Tethya crypta* (*Tethylidae*). Vidarabine is the prodrug of araATP, which was first synthesized in 1960 by the Bernard Randall Baker lab at the Stanford Research Institute (Lee *et al*., 1960). The molecule was originally intended as an anti-cancer drug; however, antiviral activity against herpes simplex virus and vaccina virus in cell culture was discovered shortly after its preparation (Privat de Garilhe & De Rudder, 1964; Schabel, 1968). Schabel (Schabel, 1968) discovered that araATP has activity against a number of other DNA and RNA viruses in cell culture including varicella and herpes marmoset. A series of patient studies in 1976 demonstrated that araATP acts as an antiviral agent with few toxicity issues (Ch'ien *et al*., 1976). Because of its anticipated interactions with various viral proteins (Min *et al*., 2020; Mongia *et al*., 2021; Prajapat *et al.*, 2020; Zhang *et al*., 2020), AraATP has since been of interest as a potential SARS-CoV-2 inhibitor.

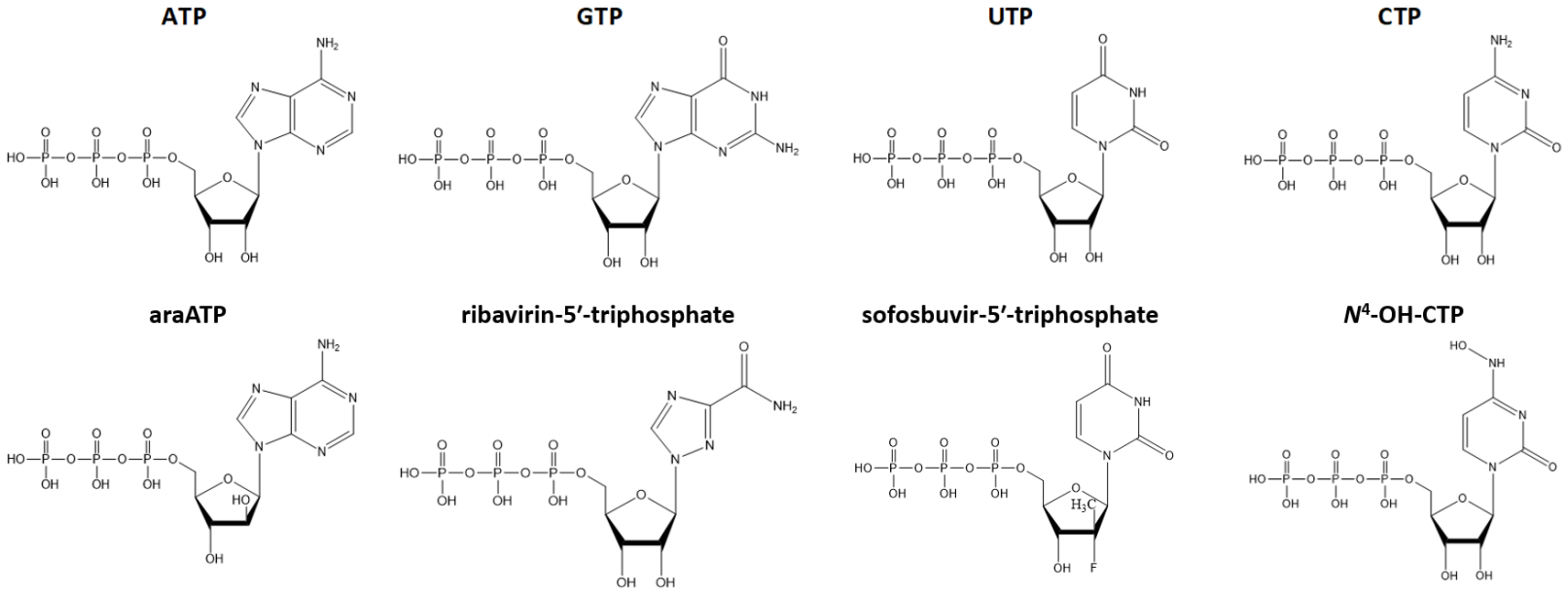

Figure 2.1. Structures for small-molecule CTPS substrates, activators, or inhibitors.

Using large datasets of previously established SARS inhibitors, one can use algorithms to predict potential binding of compounds to various proteins of SARS-CoV-2. Vidarabine was identified as a potential drug to target the 3C-like protease of SARS-CoV-2 (Zhang *et al*., 2020). Similarly, molecular dynamics studies predicted vidarabine as a top candidate as an inhibitor of the interaction between the SARS-CoV-2 spike protein S1 receptor binding domain and the angiotensin-converting enzyme 2 receptor (Prajapat *et al*., 2020). Despite the proposed RNA antiviral activity, in a cell-based reporter assay for Middle East respiratory syndrome (MERS)-CoV RdRp activity, araATP did not directly inhibit RNA replication in cells (Min *et al*., 2020). However, because vidarabine was identified as a drug candidate targeting other SARS-CoV-2 proteins, we examined the effect of its 5′-triphosphate metabolite on *ec*CTPS activity.

2.1.3 Ribavirin-5′-triphosphate (RBVNTP)

Ribavirin (1-β-D-ribofuranosyl-1,2,4-triazole-3-carboxamide) is a purine nucleoside analogue with an incomplete purine ring (**Figure 2.1**). The carboxamide moiety of the pseudobase serves as a structural mimic of guanosine and inosine (Prusiner & Sundaralingam, 1973). Ribavirin is the prodrug of RBVNTP, which displays broad spectrum antiviral activity (De Clercq, 1993; Sidwell *et al*., 1972). The molecule was originally approved for treatment of severe respiratory syncytial virus (RSV) infection in children but has since been used for the treatment of several other infections including hepatitis C virus (HCV), Middle East respiratory syndrome coronavirus (MERS-CoV), and SARS-CoV-2 (Tam *et al*., 2001).

HCV, MERS-CoV, and SARS-CoV-2 are all positive-sense single-stranded RNA (+ssRNA) viruses that evoke similar immune responses (Alothaid *et al*., 2020). The amino acid sequence at the active site is highly conserved among their RdRps, suggesting that nucleotide analogues used to treat HCV infections might also be effective against COVID-19 (Elfiky, 2020a, 2020b; Ju *et al*., 2020). An understanding of the effects of ribavirin on other +ssRNA viruses may contribute to a better understanding of those observed with SARS-CoV-2. MERS-CoV has been shown to be sensitive to combination therapy with interferon-α2b and ribavirin in rhesus monkeys (Falzarano, de Wit, Martellaro, *et al.,* 2013; Falzarano, de Wit, Rasmussen, *et al.,* 2013). It reduces viral replication, promotes repair of damaged tissue, and improves clinical outcomes (Falzarano, de Wit, Martellaro, *et al*., 2013; Falzarano, de Wit, Rasmussen, *et al*., 2013). Additionally, chronic HCV patients demonstrated higher virologic responses (the absence of detectable viral RNA in blood 6 months after the completion of antiviral therapy) when treated with a combination therapy of ribavirin and interferon-α2b versus interferon-α2b alone (McHutchison *et al*., 1998). The exact mechanism responsible for the improved response that occurs when ribavirin is combined with interferon is unknown. Despite success in combination therapy, a cell-based reporter assay for the MERS-CoV RdRp showed ribavirin does not inhibit the RNA replication *in cellulo* (Min *et al*., 2020). Additionally, when administered to patients with chronic HCV alone, ribavirin decreases serum aminotransferase concentrations but has no antiviral effect (Bodenheimer *et al*., 1997; Di Bisceglie *et al*., 1995; Dusheiko *et al*., 1996).

Similarly to araATP, *in silico* docking studies suggested that RBVNTP could bind the SARS-CoV-2 RdRp, thus, disrupting the polymerase function (Elfiky, 2020b). With

respect to COVID-19 infections, ribavirin exhibits antiviral activity when in a triple combination therapy by alleviating symptoms and shortening the duration of viral shedding (Hung *et al*., 2020). When administered in combination therapy with lopinavir/ritnovir and/or interferon-β1b against COVID-19 infection, the median time to a negative nasopharyngeal swab test in patients with mild to moderate COVID-19 was significantly reduced (Hung *et al*., 2020; Khalili *et al*., 2020).

Interestingly, a retrospective study on patients with severe COVID-19 revealed that ribavirin therapy alone was not associated with an improved negative conversion time for a SARS-CoV-2 test or an improved mortality rate (Tong *et al*., 2020). Other studies have shown no benefit in patient outcome with administration of a combination therapy of ribavirin and interferon-α over either drug individually (Li *et al*., 2021). In fact, in one study (Li *et al*., 2021), ribavirin treated patients had a higher probability of having a hospital stay greater than 15 days. As a caveat, studies have suggested that adverse outcomes including anemia, hypomagnesemia, and bradycardia may be associated with the use of ribavirin to treat SARS (Muller *et al*., 2007). Additional studies have found that ribavirin antiviral activity and mutagenesis are present only in the face of significant cellular toxicity (S. Zhou *et al*., 2021).

Ribavirin's antiviral effects can arise through several mechanisms, including inhibition of RNA capping activity, immunomodulatory effects, inhibition of viral polymerases, and increased mutational frequency due its incorporation into the RNA genome during viral replication (Graci & Cameron, 2006). *In vivo*, phosphorylation leads to the 5′-monophosphate (RBVNMP), 5′-diphosphate, and 5′-triphosphate, with the latter often being the major metabolite (Page & Connor, 1990; Zimmerman & Deeprose, 1978).

RBVNMP acts as a competitive inhibitor of human inosine-5′-monophosphate dehydrogenase (IMPDH) with respect to GMP (Hager *et al*., 1995; Markland *et al*., 2000), leading to depletion of the intracellular pools of GTP, which contributes indirectly to ribavirin's antiviral activity (Graci & Cameron, 2006). Interestingly, the intracellular CTP and UTP pools typically increase with ribavirin treatment (Müller *et al*., 1977; Zimmerman & Deeprose, 1978). The concomitant elevation of the CTP pools is unexpected considering that GTP is an allosteric activator of CTPS-catalyzed Gln-dependent CTP formation. Consequently, we assessed the direct effect of RBVNTP on CTPS activity.

Ribavirin promotes the rapid polymerization of the IMPDH protein into cytoplasmic filamentous structures termed rods and rings (Carcamo *et al*., 2011; Ji *et al*., 2006). Other drugs that target enzymes upstream or downstream of IMPDH to block guanidine-5′-monophosphate (GMP) synthesis induce formation of similar structures (Calise *et al*., 2016; Carcamo *et al*., 2014). IMPDH and CTPS can assemble into shared filamentous structures, constituting mostly independent adjacent segments of the structures (Chang *et al*., 2015; Keppeke *et al*., 2015). DON and dF-dCTP have been reported to induce filament formation by *ec*CTPS *in vitro* (Barry *et al.*, 2014; McCluskey & Bearne, 2018a). In DON-treated HeLa and COS-7 cells, antibodies detected both hCTPS1-based and IMPDH2-based filamentous structures, while ribavirin-treated cells only showed the presence of IMPDH2-based structures (Keppeke *et al*., 2015).

Despite the existence of several drugs that can induce rods and rings *in vitro*, interferon/ribavirin-treated HCV patients are the only patients to date who developed antibodies targeting these structures (Calise *et al*., 2015). Because of the ability of

ribavirin to induce copolymerization of IMPDH2 and CTPS1 in cells, as well as observed filament formation of *ec*CTPS with Gln and nucleotide analogues, we examined the effect of RBVNTP on filament formation by *ec*CTPS.

2.1.4 Sofosbuvir-5′-triphosphate (STP)

Sofosbuvir was approved by the Food and Drug Administration in 2013 as a UTP analogue for the treatment of chronic HCV infection as part of a combination therapy with several other antiviral agents (Bhatia *et al*., 2014). The standard of care for HCV patients up until this point was a combination of protease inhibitors, interferons, and ribavirin for up to 48 weeks, which proved unsatisfactory in many cases due to a lack of efficacy or adverse effects (Bhatia *et al*., 2014). In combination with ledipasvir, a direct acting antiviral, sofosbuvir demonstrated superior sustained virologic response rates and did not require the coadministration of interferons and/or ribavirin (Gritsenko & Hughes, 2015). Sofosbuvir is metabolized into its active form, (2′*R*)-2′-deoxy-2′-fluoro-2′-methyl-uridine-5′-triphosphate (STP) by the action of kinases. Against HCV, STP has been shown to mimic the natural substrate of the NS5B polymerase and become incorporated into the growing RNA, inducing a chain termination event (Sofia *et al*., 2010).

Because of the highly conserved RdRps among +ssRNA viruses, nucleotide analogues used to treat HCV infections such as sofosbuvir might also be effective against COVID-19 (Elfiky, 2020a, 2020b; Ju *et al*., 2020). *In silico* docking studies with the SARS-CoV-2 RdRp identified sofosbuvir as a potent drug (Elfiky, 2020a). A structural superposition of the SARS-CoV-2 NSP12 polymerase (which possesses an architecture common to all viral polymerases (Kirchdoerfer & Ward, 2019)) with sofosbuvir-bound

HCV NSP5B demonstrated that the inhibitor can be modeled into active site of the SARS-CoV-2 NSP12 without any steric hindrance (Jácome *et al*., 2020). A multiple alignment of several SARS-CoV-2, SARS and MERS-related coronaviruses RdRps showed that the sofosbuvir binding residues are conserved in all these viral enzymes (Jácome *et al*., 2020).

STP is incorporated into RNA by the highly error-prone SARS-CoV-2 RdRp, but not by the high-fidelity host DNA polymerase, terminating extension (Chien *et al*., 2020; Ju *et al*., 2020). In fact, sofosbuvir-terminated RNA resists removal by the viral exonuclease proof-reading complex to a greater extent than RNA terminated by the antiviral drug Remdesivir (Jockusch *et al*., 2020). One trial with SARS-CoV-2 infected patients showed that administration of sofosbuvir in addition to the standard care significantly reduced the duration of hospital stays but did not have any statistically significant benefit on mortality (Sadeghi *et al*., 2020). Some doubts regarding the effects of sofosbuvir have been raised since others (Zandi *et al*., 2020) have found that STP does not inhibit SARS-CoV-2 RdRp in a panel of different cell lines, including human peripheral blood mononuclear cells. These findings are consistent with the observation that sofosbuvir did not inhibit the activity of MERS-CoV RdRp in a cell-based reporter assay (Min *et al*., 2020), and is consistent with the similarity of RdRps from SARS-CoV-2, SARS and MERS-related coronaviruses based on amino acid sequence alignment data (Jácome *et al*., 2020).

With the exception of dUTP (Pappas *et al*., 1999) and dF-dUTP (McCluskey *et al*., 2016) CTPS is specific for UTP and will not utilize other UTP analogues as substrates (Scheit & Linke, 1982). However, such analogues have demonstrated potential

as CTPS inhibitors (Scheit & Linke, 1982). To date, the effects of STP on CTPS have not yet been explored, however, given the attention focused on sofosbuvir as an antiviral drug, we explored the effect of STP on *ec*CTPS activity and filament formation by *ec*CTPS.

2.1.5 N^4-OH-CTP

*ec*CTPS is regulated by product inhibition due to an overlapping binding site for UTP and CTP (Endrizzi *et al*., 2004). When CTP is bound, the enzyme is unable to bind UTP and catalyze its conversion to CTP. Thus, CTP analogues, such as CPEC-TP (Kang *et al*., 1989), and dF-dCTP (McCluskey *et al*., 2016) have been utilized as inhibitors of *ec*CTPS activity. Unfortunately, mutations in CTPS led to the loss of feedback inhibition by CTP and resistance to the cytotoxic effects of CPEC (Blaney *et al*., 1993; Wylie, Wang, *et al*., 1996; Zhang *et al*., 1993). Additionally, CPEC treatment has been associated with cardiotoxic side effects (Schimmel *et al*., 2007). dF-dCTP is a potent competitive inhibitor of *ec*CTPS with respect to UTP, exhibiting a binding affinity that exceeds that of CTP by ~ 75-fold (McCluskey *et al*., 2016). CTP, along with dF-dCTP, have been reported to induce filament formation by *ec*CTPS in solution (Barry *et al.*, 2014; McCluskey & Bearne, 2018a). Although potent inhibition of *ec*CTPS by CTP analogues modified at the ribose moiety have been reported (e.g., dF-dCTP), CTP analogues modified at the cytosine base have not yet been identified as potent inhibitors.

β-D-N^4-Hydroxycytidine (NHC) is unique when compared with other cytidine analogues (Kang *et al*., 1989; McCluskey *et al*., 2016; Scheit & Linke, 1982) because it bears an oxime at the 4-position of the nucleobase (**Figure 2.1**). The nucleoside is

phosphorylated in cells to the active 5′-triphosphate, which is incorporated into the genome of new virions, resulting in the accumulation of inactivating mutations (Painter *et al*., 2019; Urakova *et al*., 2018). Using cryogenic electron microscopy structures of apo, RNA-bound, and inhibitor-bound SARS-CoV-2 RdRp, NHC was identified as a potential nucleoside analogue that binds at the active site of the RdRp (Prussia & Chennamadhavuni, 2021). NHC is known to be mutagenic (Negishi *et al*., 1983; Stuyver *et al*., 2003), it exhibits antiviral activity against multiple coronaviruses, including SARS-CoV-2 (Sheahan *et al*., 2020; Zandi *et al*., 2020).

NHC was found to be >100-fold more active than ribavirin or favipiravir against SARS-CoV-2 in cells, with antiviral activity correlated to the level of mutagenesis in the viral RNA (S. Zhou *et al*., 2021). It also inhibits proofreading by coronavirus RdRp (Agostini *et al*., 2019). Mutagenic nucleoside analogues, such as ribavirin have been described as ineffective at inhibiting wild-type coronaviruses due to the proofreading activity of the viral 3′-5′ exoribonuclease (Smith *et al*., 2013). NHC, however, inhibited murine coronavirus lacking exoribonuclease proofreading activity similarly to its inhibition of wild-type exoribonuclease, suggesting an ability to evade or overcome exoribonuclease activity (Agostini *et al*., 2019).

NHC exhibited synergistic antiviral effects with nelfinavir, an antiretroviral protease inhibitor, against SARS-CoV-2 in Calu-3 cells (Ianevski *et al*., 2020). Therapeutic and prophylactic administration of the isopropylester prodrug of NHC (EIDD-2801, molnupiravir), inhibited SARS-CoV-2 replication in human lung-only mice (Wahl *et al*., 2021). It was shown to reduce the SARS-CoV-2 load in the upper respiratory tract of ferrets and completely suppressed the spread of the virus to untreated

contact animals (Cox *et al*., 2021). Molnupiravir also inhibited SARS-CoV-2 proliferation in a concentration-dependent manner in primary human airway epithelial cells (Sheahan *et al*., 2020). However, based on the stability studies in human and monkey whole blood, NHC might not persist long enough in plasma at a physiological pH and temperature to deliver significant antiviral levels of NHC into HCV-infected liver cells (Hernandez-Santiago *et al*., 2004). NHC may be converted to uridine and cytidine, which is then deaminated to uridine (Hernandez-Santiago *et al*., 2004).

The N^4 exocyclic nitrogen atom of CTP does not directly interact with *ec*CTPS. Instead, a water-mediated hydrogen bond to the backbone carbonyl oxygen of Gly 146 provides a potential recognition site (Endrizzi *et al*., 2005). Preliminary modeling studies using the published structure of *ec*CTPS with bound CTP (Endrizzi *et al*., 2004) suggested and that an enhanced interaction may arise from H-bonding between the N^4-hydroxyl group and Lys 196 (**Figure 2.2**) (Bearne, S.L., personal communication). Tighter binding of N^4-OH-CTP to *ec*CTPS may play a role in the antiviral activity exhibited in cells. Because of the potent inhibition of *ec*CTPS exhibited by other CTP analogues, the antiviral activity of NHC, and the proposed enhanced interaction of N^4-hydroxyl group, we explored the effects of N^4-OH-CTP on *ec*CTPS activity and filament formation.

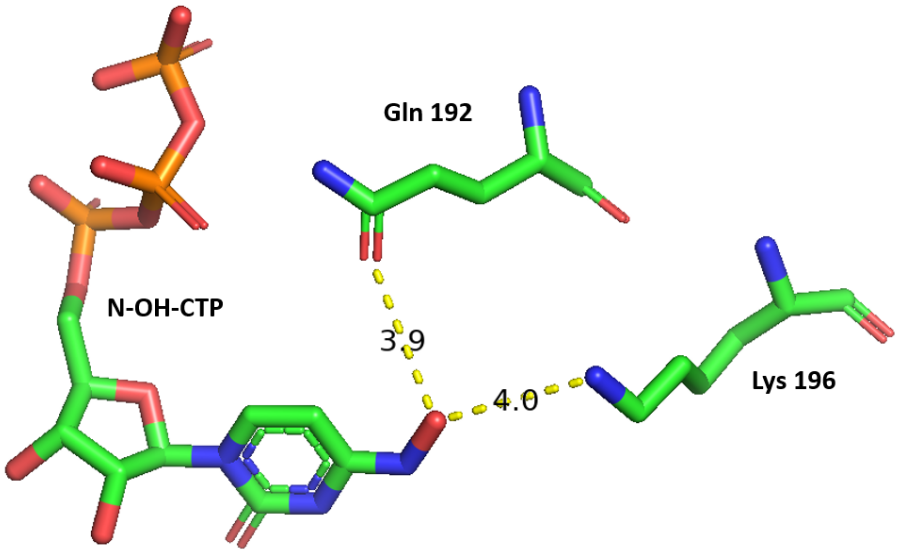

Figure 2.2. Anticipated additional interaction of N^4-OH CTP in active site of *ec*CTPS. This structure is based on a model (Bearne, S.L., personal communication). Atoms are colored as green (carbons), red (oxygen), blue (nitrogen), and orange (phosphorous). Proposed H-bond distances are displayed in angstroms. Image was rendered using PyMOL v. 2.3.2.

2.2 MATERIALS AND METHODS

All materials are described in **Chapter 5.1**. All methods follow those described in **Chapter 5** unless otherwise stated.

2.2.1 Assay with Sofosbuvir-5′-triphosphate (STP) as the Substrate

Kinetic parameters for *ec*CTPS-catalyzed turnover of STP were determined using UV spectrophotometry, by following the change in absorbance at 282 nm ($\Delta\varepsilon = 4036\ M^{-1}\ cm^{-1}$). The extinction coefficient was estimated using β-D-2′-deoxy-2′-α-F-2′-β-C-methyluridine (PSI-6206, SynInnova, Edmonton, AB) ($\varepsilon = 1858\ M^{-1}\ cm^{-1}$) and β-D-2′-deoxy-2′-α-F-2′-β-C-methylcytidine (PSI-6130, Toronto Research Chemicals, Toronto) ($\varepsilon = 5894\ M^{-1}\ cm^{-1}$) at pH 8.0. Samples were prepared at various concentrations (50, 75, 100, and 150 μM in assay buffer). The Beer–Lambert law (eqn. 1) was used to solve for the extinction coefficients of the individual compounds and the Δε was determined, where b is the light-path length and c is the concentration of the species.

$$A = \varepsilon \cdot b \cdot c \tag{1}$$

Gln-dependent amination of STP was measured using saturating conditions of Gln (6.0 mM) and ATP (1.0 mM), and varying amounts of STP (0.025 – 1.000 mM). GTP was maintained at a fixed saturating concentration of 0.25 mM in all assays with varying concentrations of STP. Additionally, Gln-dependent amination of STP was measured at fixed concentrations of STP (1.0 mM) and ATP (1.0 mM), and varying amounts of Gln (0.05 – 10.00 mM). Eqn. 3 was fitted to the initial velocity data when STP was the

variable substrate, and eqn. 2 was fitted to the initial velocity data when Gln was the variable substrate. Non-linear regression analysis was used to determine values of k_{cat}, K_m, $[S]_{0.5}$, and n. The reported errors are the standard deviations from three trials.

2.2.2 Analysis of (2′*R*)-2′-deoxy-2′-fluoro-2′-methylcytidine-5′-triphosphate (4-NH_2-STP) Formation Catalyzed by *ec*CTPS

A product analysis was conducted to show that STP was a substrate for *ec*CTPS-catalyzed amination. STP (2.0 mM) was incubated at 37 °C in assay buffer containing *ec*CTPS (0.5 μM) in the presence of ATP (1.0 mM) and NH_4Cl (150 mM) in a total volume of 1 mL. NH_4Cl was used as the substrate rather than Gln to avoid the presence of an added nucleotide (i.e., GTP) in the analysis. At 5, 15, 30, 60, 120, and 180 min, the absorbance at 291 nm was measured and aliquots (100 μL) were removed, and the enzyme was removed by centrifugation through a 10-kDa MWCO spin-filter (Millipore). The flow-through was submitted for ESI-MS analysis. ESI-MS spectra were collected using a Bruker microTOF Focus orthogonal ESI-TOF mass spectrometer operating in negative ion mode. The peaks corresponding to substrate and product at each time point were integrated using the program Compass Data Analysis software. The intensity and area of the peaks were plotted against the time of incubation.

2.2.3 Synthesis and Purification of N^4-OH-CTP

Triethylammonium bicarbonate (TEAB) buffer (1 M, pH 8.0) was prepared by carbonating a solution of triethylammonium (1 M) with CO_2 gas at 10 psi for 5 h. N^4-OH-CTP was obtained by reacting CTP with hydroxylamine (pH 5.0) as described by Painter

et al. (Painter *et al*., 2016). The reaction mixture was heated with stirring at 55 ℃ for 5 h and then cooled to room temperature prior to addition of TEAB (100 mM, 2 mL). The reaction mixture was then subjected to anion-exchange chromatography on DEAE-Sephadex A-25 (2.5 cm i.d., × 42 cm) and the various nucleotides were eluted using a TEAB stepwise gradient (0.1-1.0 M), total volume 2.2 L. Fractions (12 mL) were collected using a Retriever II Fraction Collector (ISCO Manufacturing Solutions, Bend, OR, USA) and the absorbance of each fraction at 260 nm of each fraction was subsequently measured using a HP 8453 UV-visible spectrophotometer. Fractions exhibiting elevated absorbance readings at 260 nm were pooled and the solvent was removed using rotary evaporation (temperature ≤ 37 ℃). Samples were then suspended in water and lyophilized several times until a consistent mass was obtained. Finally, the samples were dissolved in water and decolourized by elution through a C_{18} column (Varian, Bond ElutC18) using acetonitrile, followed by elution with water. ESI-MS were collected using a Bruker microTOF Focus orthogonal ESI-TOF mass spectrometer instrument operating in negative mode.

For HPLC analysis, a Waters 510 pump and a controller were used for solvent delivery. Injections were made using a Rheodyne 7725i sample injector fitted with a 20-μL injection loop, and a Waters 486 absorbance detector was used to detect nucleotides at 260 nm. Samples were separated on a 250 × 4.6 mm (5μm) Kinetix C_{18} column (Phenomenex, Torrance, CA, USA) and eluted under isocratic conditions using degassed 50 mM $NH_4CO_3^-$ buffer, pH 7.0; containing 2 μM tributylamine and 10% acetonitrile at a flow rate of 1.0 mL/min.

^{1}H NMR spectra of samples in D_2O were obtained using a Bruker AV 500 MHz spectrometer at the Dalhousie University Nuclear Magnetic Resonance Research Resource Centre (NMR-3). The concentration of N^4-OH-CTP was determined using ^{1}H NMR with integration of the H6-proton (δ 7.17, 7.19 ppm) compared to the integral for an internal pyrazine standard at (5.00 mM, δ 8.61 ppm).

The presence of the hydroxamic acid group was determined during the synthesis by adding a dilute ferric chloride solution to a small amount of sample dissolved in water. The formation of a blue, violet, purple, or red-brown color indicates the presence of phenols or hydroxamic acids (Reeve, 1958).

2.3 RESULTS AND DISCUSSION

2.3.1 Effects of araATP on *ec*CTPS Activity

Though there have been studies investigating UTP analogues as substrates or inhibitors of *ec*CTPS (Kang *et al*., 1989; McCluskey *et al*., 2016; Taylor *et al*., 2008), ATP analogues have largely remained understudied with respect to *ec*CTPS. We discovered that araATP is recognized as a substrate in the *ec*CTPS-catalyzed conversion of UTP to CTP. *ec*CTPS activity was assayed at various concentrations of araATP (0.05 – 3.00 mM) and ATP (0.05 – 2.00 mM) with Gln and NH_3 as the nitrogen sources (**Figure 2.3**). All other substrates were fixed at saturating conditions in accord with **Table 5.1**.

Comparison of the kinetic parameters (**Table 2.1**) revealed that the $[S]_{0.5}$ values for ATP and araATP are similar (Gln: $[S]_{0.5}^{ATP}$ = 0.21 mM and $[S]_{0.5}^{araATP}$ = 0.14 mM and NH_3: $[S]_{0.5}^{ATP}$ = 0.57 mM and $[S]_{0.5}^{araATP}$ = 0.60 mM). The k_{cat} values (**Table 2.1**), however,

differed substantially (Gln: k_{cat}^{ATP} = 11.6 s^{-1} and k_{cat}^{araATP} = 3.1 s^{-1}, and NH_3: k_{cat}^{ATP} = 8.0 s^{-1} and k_{cat}^{araATP}= 1.5 s^{-1}). Values of catalytic efficiency were significantly decreased when araATP was employed as substrate in both Gln- and NH_3-dependent reactions (i.e., ~2.5- and 5-fold relative to ATP, respectively) (**Table 2.1**). These results indicate that, although *ec*CTPS is capable of binding araATP and ATP with similar affinity, the enzyme exhibits markedly reduced turnover and efficiency with araATP as a substrate (**Figure 2.3**).

Table 2.1. Kinetic characterization of intrinsic and antiviral nucleoside-5′-triphosphates as substrates and activators of *ec*CTPS

	Gln-dependent *ec*CTPS activity				NH_3-dependent *ec*CTPS activity			
varied ligand	**K_m or $[S]_{0.5}$[a] or K_A[b] (mM)**	**k_{cat} or k_{act}[c] (s^{-1})**	**k_{cat}/K_m, $k_{cat}/[S]_{0.5}$ or k_{act}/K_A (s^{-1} mM^{-1})**	***n***	**K_m or $[S]_{0.5}$[a] (mM)**	**k_{cat} (s^{-1})**	**k_{cat}/K_m or $k_{cat}/[S]_{0.5}$ (s^{-1} mM^{-1})**	***n***
Gln[d]	0.25 ± 0.04	10.6 ± 1.1	42.4 ± 8.1	-	-	-	-	-
Gln[e]	0.32 ± 0.03	1.21 ± 0.03	3.78 ± 0.37	-	-	-	-	-
NH_3	-	-	-	-	1.72 ± 0.25	10.8 ± 1.7	6.30 ± 1.35	-
ATP	0.21 ± 0.02[a]	11.6 ± 0.6	55.2 ± 6.0	1.18 ± 0.01	0.57 ± 0.03[a]	8.0 ± 0.1	14.0 ± 0.8	3.0 ± 0.5
GTP[d]	0.068 ± 0.019[b] k_{inhib} = 0.547 ± 0.052	9.2 ± 1.5[c]	135 ± 44	3.1 ± 0.9	-	-	-	-
UTP	0.200 ± 0.004[a]	8.4 ± 0.1	42.5 ± 1.0	2.17 ± 0.18	0.767 ± 0.056[a]	8.1 ± 0.3	10.56 ± 0.86	1.6 ± 0.1
araATP	0.14 ± 0.02[a]	3.1 ±0.5	22.1 ± 4.8	1.2 ± 0.1	0.60 ± 0.19[a]	1.5 ± 0.3	2.49 ± 0.68	1.4 ± 0.3
RBVNTP[d]	2.44 ± 0.92[b]	13.8 ± 2.6[c]	5.6 ± 2.4	-	-	-	-	-
STP	0.20 ± 0.01[a]	1.35 ± 0.03	6.75 ± 0.37	1.09 ± 0.14	-	-	-	-

(a) $[S]_{0.5}$ is the nucleotide concentration that yields half-maximal velocity; (b) K_A value; (c) k_{act} value; (d) [ATP] = [UTP] = 1.0 mM; (e) [ATP] = [STP] =1.0 mM

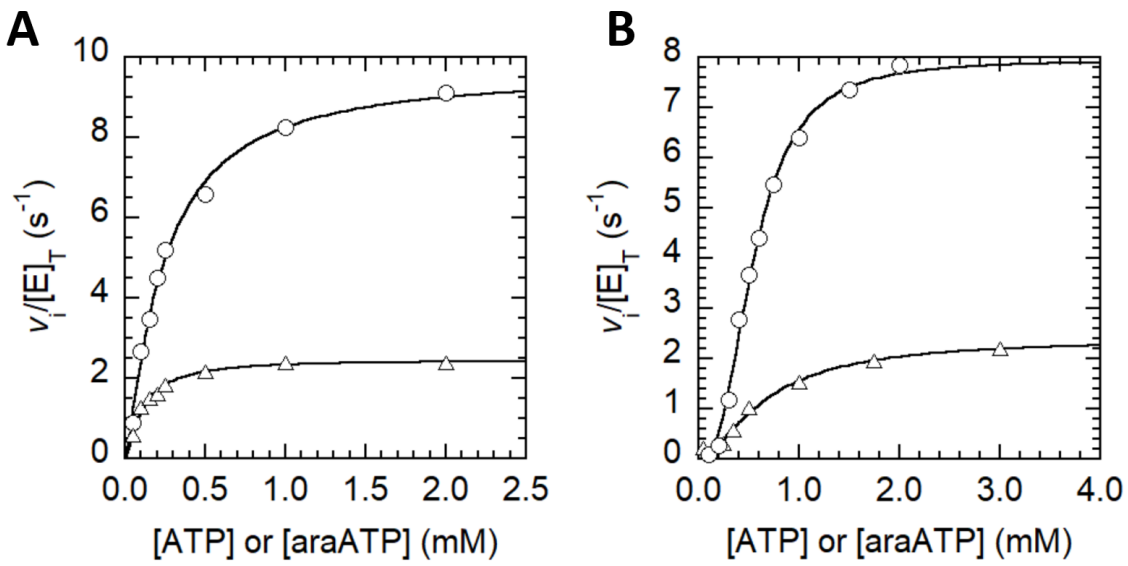

Figure 2.3. Kinetic characterization of ATP and araATP-dependent *ec*CTPS-catalyzed CTP formation. Representative plots of Gln-dependent (**A**) and NH_3-dependent (**B**) *ec*CTPS-catalyzed formation of CTP with various concentration of ATP (○) or araATP (△). All other substrates were maintained at saturating conditions in accord with **Table 5.1**. The concentration of *ec*CTPS were 4.7 µg/mL for araATP-dependent reactions with both Gln and NH_3, 4.7 µg/mL for the ATP-dependent reaction with Gln as the nitrogen source, and 7.6 µg/mL for the ATP-dependent reaction with NH_3 as the nitrogen source. Eqn. 3 was fitted to the initial velocity data. The results are summarized and in **Table 2.1**.

In the synthase domain, the conversion of UTP to CTP proceeds by the ATP-dependent phosphorylation of UTP on the 4-oxygen atom, making the 4-C position electrophilic and susceptible to reaction with ammonia (von der Saal *et al*., 1985). The kinetic data suggest that *ec*CTPS can utilize araATP as an alternative substrate for this phosphorylation. ATP binds in a cleft such that the γ-phosphate is positioned at the exit of the NH_3 tunnel (Endrizzi *et al*., 2004; Lynch *et al*., 2017). Given the activity of *ec*CTPS with araATP, it is likely that the replacement of the D-ribose with D-arabinose in araATP does not completely interrupt binding in this cleft.

Baldwin and colleagues (Endrizzi *et al*., 2005) proposed that recognition of the 2′- and 3′-hydroxyl groups of ATP is not important since they have no direct contacts with the enzyme, although, these groups are proximal to Asp 303 and Lys 306. Furthermore, ATP and dATP were equally effective as substrates with UTP, yielding comparable V_{max}, $[S]_{0.5}$, and Hill coefficient values (Endrizzi *et al*., 2005). However, ddATP was not an efficient substrate (Endrizzi *et al*., 2005), indicating an essential role for the 3′-hydroxyl group in binding and catalysis, or at least one of the 2′- and 3′-hydroxyl groups.

The similarity in binding affinity between ATP and araATP is likely attributed to the analogous nature of the compounds and Baldwin's evidence that recognition of the 2′- and 3′-hydroxyl groups is not required for binding. However, compared with the D-ribose moiety of ATP, the D-arabinose moiety of araATP likely has increased distance between its 2′-hydroxyl group and the conserved Asp 303 residue that prevents the formation of an H-bond. However, this does not seem to affect binding affinity. Given the similarity of kinetic parameters described by Baldwin and colleagues (Endrizzi *et al*., 2005) of dATP to ATP, it could have been predicted that the change in the 2′-hydroxyl would not cause

drastically affect binding affinity, however, the marked reduction in turnover was surprising. It appears that the change in stereochemistry at the 2′-position is disadvantageous to catalysis, likely due to a repositioning of the γ-phosphate so that its transfer is no longer favoured or the loss of the H-bond with Asp 303 results in only a loss of transition state stabilization required for phosphate transfer. Our observation that araATP is a substrate suggests that it is likely that the 3′-hydroxyl group, with the proper stereochemistry of the 3′-C, that is required for activity.

The ability of araATP to replace ATP as a substrate for CTPS had not previously been recognized. Overall, these observations suggest that araATP could assist in maintaining the intracellular CTP pools, though, to a lesser extent than that of ATP, when employed as an antiviral agent. However, the concentration of ATP in mammalian cells is 3.2 ± 1.7 mM (Traut, 1994), and it seems unlikely that araATP would reach such concentrations to serve as a substitute for ATP in CTPS-catalyzed CTP formation.

2.3.2 Effects of Ribavirin-5′-triphosphate (RBVNTP) on *ec*CTPS Activity

The activating effects of GTP have been well studied (Levitzki & Koshland, 1972b; Lunn *et al*., 2008; MacDonnell *et al*., 2004). When Gln is employed as the nitrogen source, GTP is required as a positive allosteric effector to promote catalysis of Gln hydrolysis. Comparison of the initial velocity data obtained for increasing concentrations of GTP or RBVNTP at saturating conditions of ATP, UTP and Gln (in accord with **Table 5.1)** revealed that RBVNTP is an allosteric activator of the Gln-dependent *ec*CTPS-catalyzed formation of CTP (**Figure 2.4**). Eqn. 4 was used to fit the initial velocity data for GTP-dependent activation of Gln-dependent *ec*CTPS-catalyzed formation of CTP.

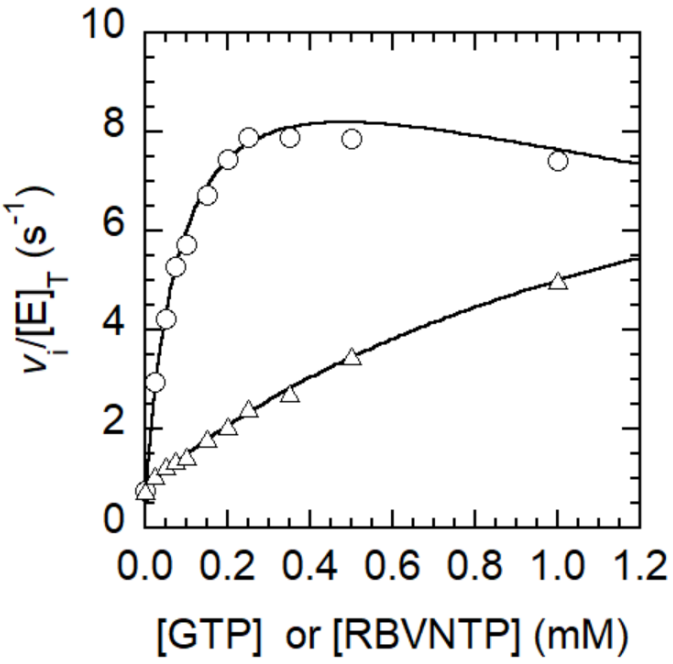

Figure 2.4. Kinetic characterization of GTP- and RBVNTP-dependent activation of Gln-dependent *ec*CTPS activity. Apart from GTP and RBVNTP, all other substrates were at saturating conditions in accord with **Table 5.1**. Eqn. 4 was fitted to the steady-state kinetic data for GTP-dependent activation (○). The k_{act}, K_A, K_{inhib}, and n values for the GTP-dependent activation were 9.2 ± 1.5 s^{-1}, 0.068 ± 0.019 mM, 0.547 ± 0.052 mM, and 3.1 ± 0.9, respectively. Eqn. 5 was fitted to the steady-state kinetic data for RBVNTP-dependent activation (△). The concentration of *ec*CTPS were 4.7 μg/mL for both GTP- and RBVNTP-dependent activation. The k_{act} and K_A values for the RBVNTP-dependent activation were 13.8 ± 2.6 s^{-1} and 2.44 ± 0.92 mM, respectively. The results are summarized in **Table 2.1**.

Unlike GTP, which exhibits inhibition at concentrations above 0.25 mM, RBVNTP did not exhibit inhibition at concentrations up to 1.0 mM, thus, eqn. 5 was fitted to the initial velocity data. A representative comparison of the initial velocities accompanying GTP- and RBVNTP-dependent activation of Gln-dependent CTP formation is presented in **Figure 2.4**.

The kinetic data presented here demonstrate that RBVNTP can behave as an allosteric activator in a similar manner to that of GTP. Although inhibition of *ec*CTPS-catalyzed formation of CTP by RBVNTP was not apparent at concentrations up to 1.0 mM, inhibition by its traditional allosteric activator, GTP, was observed with a K_{inhib} of 0.547 ± 0.052 mM. The k_{act} values for GTP- and RBVNTP-dependent activation were comparable (9.2 ± 1.5 s^{-1} (GTP) and 15.5 ± 4.1 s^{-1} (RBVNTP)); however, there was a ~36-fold increase in the K_A value for RBVNTP relative to GTP (0.068 ± 0.019 mM (GTP) and 2.44 ± 0.92 mM (RBVNTP)), resulting in a 24-fold difference in the catalytic efficiencies for activation (135 ± 44 s^{-1} mM^{-1} (GTP) and 5.6 ± 2.4 s^{-1} mM^{-1} (RBVNTP)). This decrease in the catalytic efficiency of activation for RBVNTP relative to GTP indicates that the enzyme is able to utilize GTP as an allosteric activator much better than RBVNTP, however, it is still important to note that *ec*CTPS can employ RBVNTP as an allosteric inhibitor. Our observation that RBVNTP activates *ec*CTPS-catalyzed Gln-dependent CTP formation is surprising because the structural requirements for activation are quite stringent, with O6 of GTP being absolutely required for activation (Lunn *et al*., 2008). It was previously demonstrated that inosine-5′-triphosphate (ITP) also acts as an allosteric activator, but was bound weakly by the enzyme with a K_A value of 2.9 mM, indicating that the 2-NH_2 group contributes significantly to binding (Lunn *et al*., 2008).

Consequently, the carboxamide group of on the pseudobase of RBVNTP can mimic the O6 interaction with *ec*CTPS to afford activation, but the missing part of the purine structure diminished the binding affinity similar to ITP. Several studies have demonstrated inhibition with GTP (Habrian *et al*., 2016; MacDonnell *et al*., 2004), which appears to arise because saturation of the enzyme with GTP yields a non-productive complex. It is suspected that with increased concentrations of RBVNTP, this complex may form as well; however, it is unlikely that the concentration of RBVNTP would ever reach such a level in cells. Indeed, the concentration of GTP in mammalian cells is 468 ± 224 μM (Traut, 1994). Unfortunately, the total absorbance of the reaction mixture, as well as the high cost of the compound, precluded examination of the effect of RBVNTP at higher (non-physiological) concentrations. Since RBVNTP can replace GTP as an allosteric activator of CTPS, it affords a possible mechanism by which *ec*CTPS can remain active if GTP concentrations are markedly reduced due to the depletion of the GTP pools arising from the inhibition of IMPDH by RBVNMP.

Filament-like structures were discovered in human epithelial type 2 cells, in which further investigations identified hCTPS1 to be one of two key enzymes enriched in such structures (Carcamo *et al*., 2011). DON, acivicin, and ribavirin, exhibited dose-dependent induction of filament-like structures in more than 95% of cells in all cancer cell lines tested as well as mouse primary cells (Carcamo *et al*., 2011). Such findings encouraged us to investigate the effects of RBVNTP on filament assembly by *ec*CTPS. The ability of GTP and RBVNTP to induce formation of *ec*CTPS filaments was evaluated using GTP or RBVNTP as a replacement for CTP and following previously described methods (**Chapter 5.5**). Few filaments of *ec*CTPS are apparent in the absence

of substrates, suggesting a mechanism by which the enzyme polymerizes upon incubation and/or being deposited carbon-coated grids. Neither GTP (**Figure 2.5 panel C**) nor RBVNTP (**Figure 2.5 panel D**) were capable of inducing filament formation by CTPS at concentrations of 1.0 mM. The ability of GTP or RBVNTP to prevent filament formation by *ec*CTPS was evaluated using 1.0 mM of CTP and GTP or RBVNTP. As shown in **Figure 2.5 panels E and F**, neither GTP (1.0 mM) nor RBVNTP (1.0 mM) prevented assembly of CTP-induced *ec*CTPS filaments.

Liu and colleagues (X. Zhou *et al*., 2021) solved the cryo-EM structure of GTP-bound *dm*CTPS, and identified the GTP-interacting residues, which are conserved in *ec*CTPS. In brief, the guanine base of GTP interacts with residues Leu 444, Arg 481, and Phe 373 of the binding monomer and Leu 107 of an adjacent monomer (X. Zhou *et al*., 2021). The ribose ring interacts with Arg 479 and Phe 50, and the triphosphate moiety forms H-bonds with Lys 306, Tyr 307, and Arg 376 (X. Zhou *et al*., 2021). Our observed lack of apparent effects of GTP and RBVNTP on filament assembly by *ec*CTPS is consistent with the observation that the GTP-interacting residues are remote from those residues implicated in *ec*CTPS polymerization (i.e., the linker region α-helix 274–284, α-helix 330–336 of the glutaminase domain (Barry *et al*., 2014), and residues E155 (Barry *et al*., 2014), E149, and F227 (McCluskey & Bearne, 2018a)).

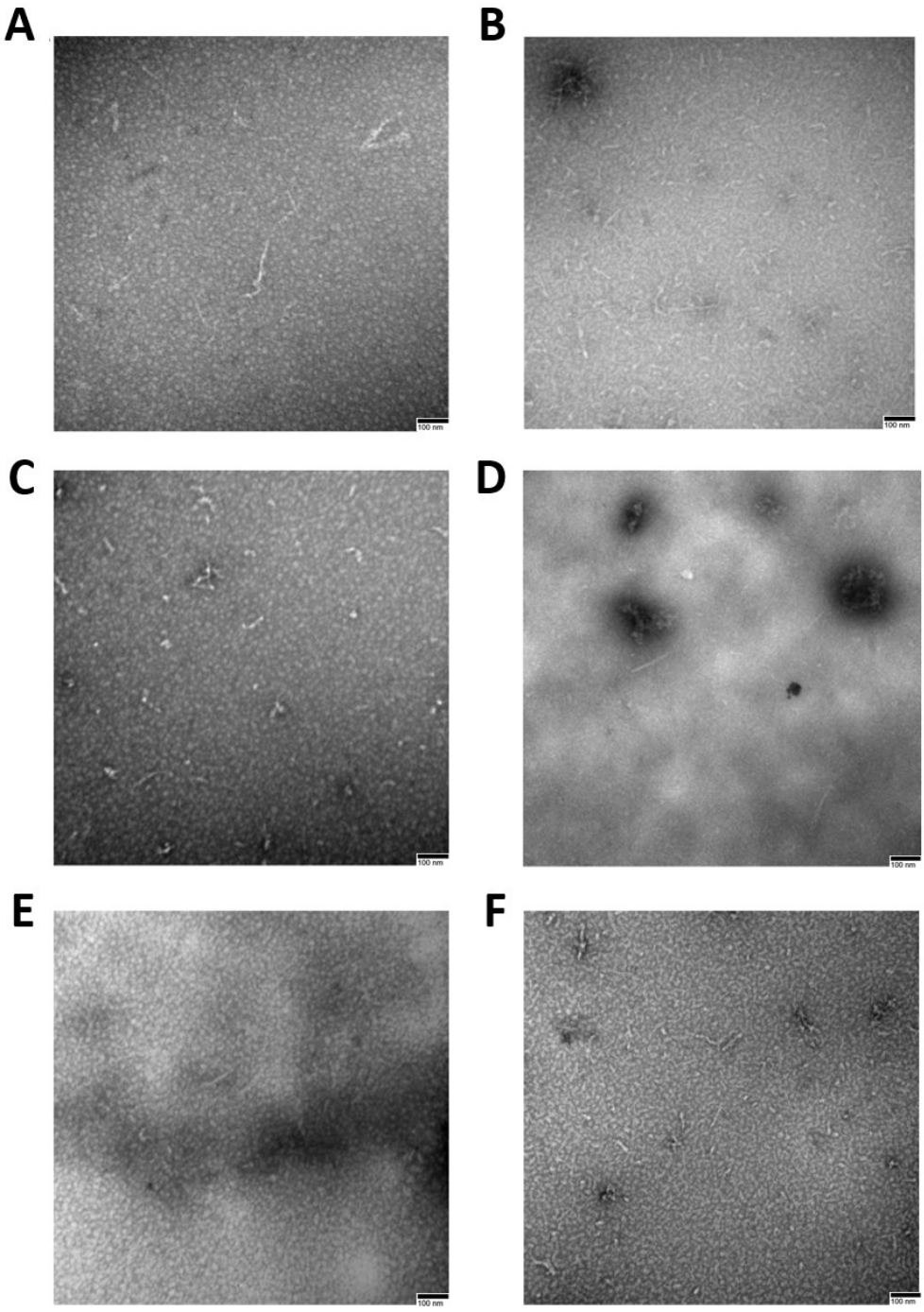

Figure 2.5. Effects of GTP and RBVNTP on filament formation by *ec*CTPS. Few filaments are formed by *ec*CTPS in the absence of nucleotides (**A**). CTP induces polymerization (**B**). GTP (**C**) and RBVNTP (**D**) are not capable of inducing filament formation by *ec*CTPS at concentrations of 1.0 mM. In the presence of CTP (1.0 mM), neither GTP (**E**) nor RBVNTP (**F**), each at 1.0 mM, disrupt CTP-induced filament formation.

2.3.3 Effects of Sofosbuvir-5′-triphosphate on *ec*CTPS Activity

In order to accurately characterize the rates of *ec*CTPS-catalyzed amination of STP, the change in the molar extinction coefficient (ε) accompanying the reaction had to be determined. This was determined by measuring the difference in absorbance at 282 nm for the sofosbuvir nucleoside and its corresponding nucleoside aminated at the 4-position. The extinction coefficient of β-D-2′-deoxy-2′-α-F-2′-β-C-methyluridine (PSI-6206) at 282 nm was estimated at to be 1858 ± 411 M^{-1} cm^{-1} and that of β-D-2′-deoxy-2′-α-F-2′-β-C-methylcytidine (PSI-6130) to be = 5894 ± 275 M^{-1} cm^{-1} at pH 8.0 in assay buffer (**Figure 2.6**). While using ΔA_{291} was suitable to monitor *ec*CTPS activity with the fluorinated analogues, ΔA_{282} presented a greater difference in absorbance between the substrate and the product and was therefore selected as the wavelength at which the *ec*CTPS-catalyzed amination of STP was monitored. Thus, the kinetic parameters for *ec*CTPS-catalyzed turnover of STP were determined using UV spectrophotometry, by following the change in absorbance at 282 nm ($\Delta\varepsilon = 4036 \pm 494$ M^{-1} cm^{-1}).

Because of its current use as an anti-HCV drug (Abraham & Spooner, 2014) and the attention focused on sofosbuvir as an antiviral against SARS-CoV-2 (Jácome *et al*., 2020), we explored the effect of STP on *ec*CTPS activity. While STP did not inhibit CTPS activity, it was a substrate for Gln-dependent *ec*CTPS-catalyzed activity (**Figure 2.7**). The cost of the compound precluded examination of its effect on the less physiologically relevant NH_3-dependent activity.

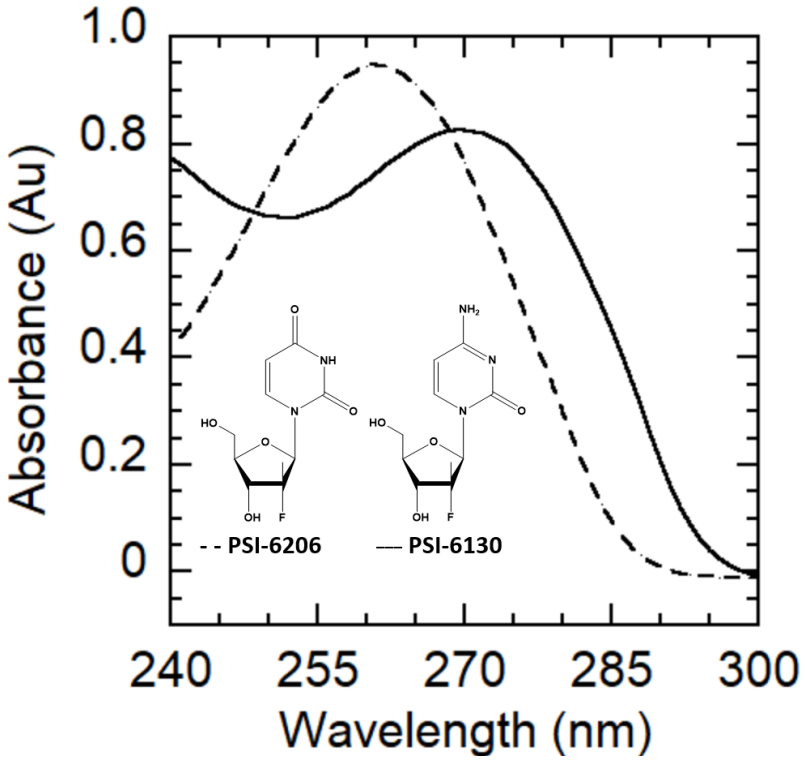

Figure 2.6. Representative UV-absorbance spectra for the determination of Δε. The change in molar extinction coefficient (($\Delta\varepsilon_{282}$ = 4036 M^{-1} cm^{-1}) was estimated using β-D-2′-deoxy-2′-α-F-2′-β-C-methyluridine (dashed line, PSI-6206) (ε =1858 M^{-1} cm^{-1}) and β-D-2′-deoxy-2′-α-F-2′-β-C-methylcytidine (solid line, PSI-6130) (ε =5894 M^{-1} cm^{-1}) at a concentration of 0.1 mM each, in 70 mM HEPES buffer, pH 8.0, containing 0.5 mM EGTA, and 10 mM $MgCl_2$.

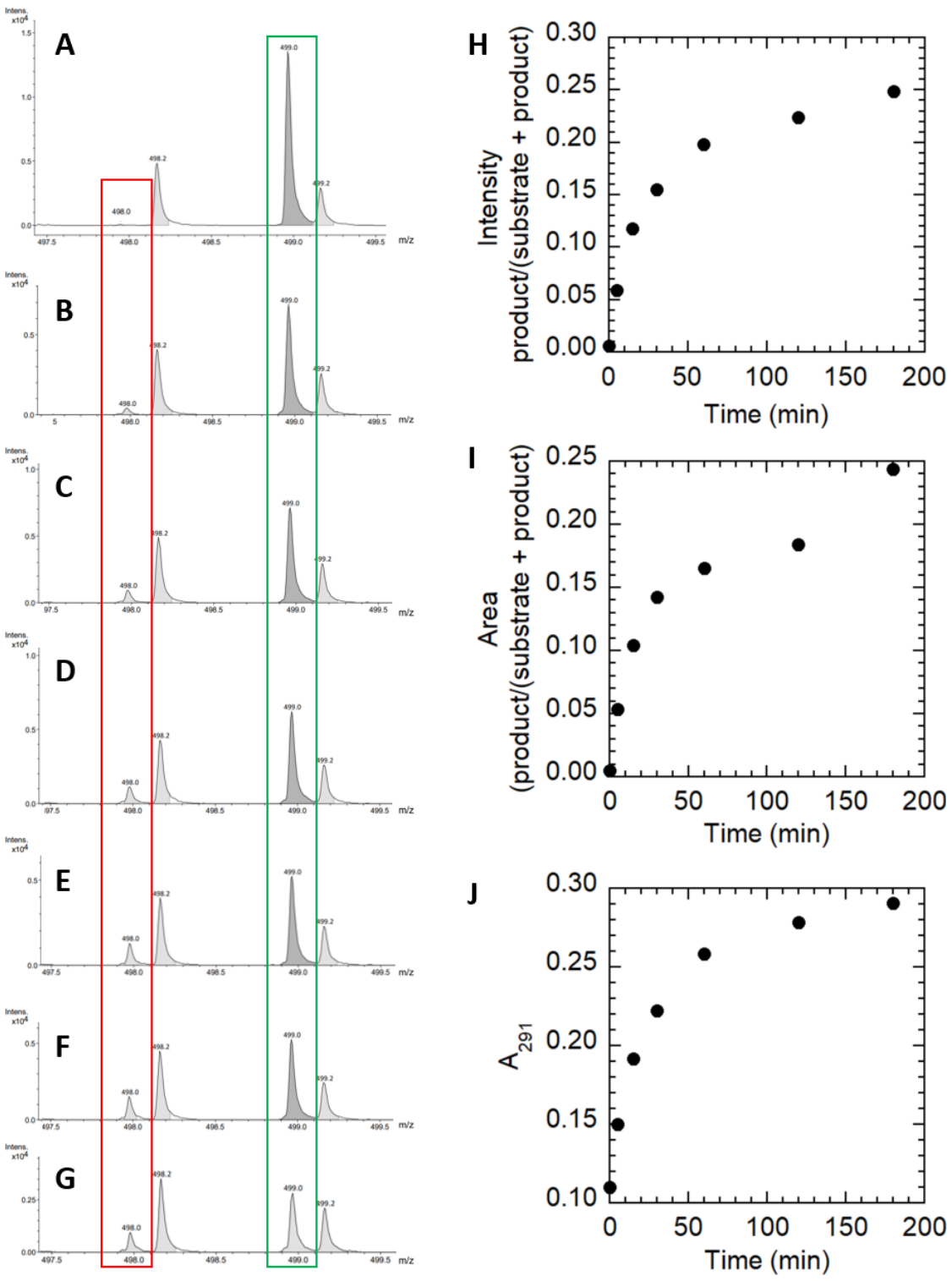

Figure 2.7. ESI-MS analysis demonstrates *ec*CTPS-catalyzed amination of STP. ESI-MS spectra of a sample containing STP (2.0 mM), ATP (1.0 mM), and NH_4Cl (150 mM) in assay buffer, indicating the conversion of substrate (green) to product (red) over time (**A**). Samples of *ec*CTPS (0.5 μM) were incubated with STP (2.0 mM), ATP (1.0 mM),

and NH_4Cl (150 mM) in assay buffer for 5 (**B**), 15 (**C**), 30 (**D**), 60 (**E**), 120 (**F**), and 180 (**G**) min. The peak intensities (**H**) and integrated peak areas (**I**) of the product, divided by the sum of the quantities for the substrate and the product, as well as the A_{291} over the course of the reaction (**J**) are plotted as a function of the incubation time.

We confirmed the formation of aminated STP to yield 4-NH_2-STP using ESI-MS (**Figure 2.7**). The progression of the reaction is demonstrated by peaks corresponding to substrate (m/z = 499.0) and product (m/z = 498.0) (**Figure 2.7.A-G**). In addition, the absorbance at 291 nm was measured at the time points described throughout the reaction. Increasing absorbance at 291 nm (**Figure 2.7.J**) is consistent with increasing peak intensity and area, thus supporting the *ec*CTPS-catalyzed amination of STP. The intensity of peaks corresponding to product were divided by the total intensity (product and substrate) and plotted against the incubation time (**Figure 2.7.H**). Similarly, peaks corresponding to substrate and product were integrated and the area of peaks corresponding to product, divided by the total area of peaks corresponding to substrate and product, were plotted against incubation time (**Figure 2.7.I**). Because of possible differences in sample volumes used in the ESI-MS analyses as well as possible differences in the extent of ionizations, it was necessary to use ratios of the intensities or areas for the product to the total intensities or total integrated peak areas of both the substrate and the product. Upon plotting the increase in intensity and integrated peak areas accompanying product formation over 180 min, it is apparent that the rate of product formation slows considerably by 180 min. The apparent maximal ratio of [product] to total [product + substrate] is ~0.25 by measurement of peak intensity and peak area integration (**Figure 2.7.H-I**). A very small peak at 498.0 was apparent in the

sample without enzyme, indicating the commercial product may contain a small amount of the aminated form of STP.

Given that *ec*CTPS is susceptible to feedback inhibition by CTP, it is possible that the enzymatic reaction was inhibited by the aminated STP formed during the reaction. It would therefore be of interest to test the E149D *ec*CTPS variant, which does not bind CTP (McCluskey *et al*., 2016), for its ability to catalyze the amination of STP. One would expect that there would be more turnover of STP due to the lack of product inhibition. This approach might be useful for industrial bio-production of aminated STP.

STP was able to support Gln-dependent formation of 4-NH_2-STP when the concentration of STP was fixed at 1.0 mM (**Figure 2.7.A**). *ec*CTPS demonstrated similar affinities for Gln with UTP and STP as a substrate (K_m^{UTP} = 0.25 and K_m^{STP} = 0.32 mM). This was not surprising since a 2′-*ribo*-F group does not markedly affect binding of 2′-fluoro-2′-deoxycytidine-5′-triphosphate with *ec*CTPS relative to CTP (McCluskey *et al*., 2016). Interestingly, the Gln-dependent amination of STP was ~8-fold slower than the reaction with UTP (*cf*. k_{cat} values, **Table 2.1**). The increased K_m and decreased k_{cat} of the Gln-dependent amination of STP resulted in a catalytic efficiency that was ~11-fold lower than the Gln-dependent amination of UTP (**Table 2.1**).

When the abilities of STP and UTP to support the Gln-dependent CTP formation were examined by varying their concentrations, *ec*CTPS was found to exhibit the same binding affinities for UTP and STP ($[S]_{0.5} \approx 0.20$ mM) (**Figure 2.8.B**). The Gln-dependent amination of STP is ~6-fold slower than that of Gln-dependent *ec*CTPS-catalyzed conversion of UTP to CTP (*cf*. k_{cat} values, **Table 2.1**). Consequently, the catalytic efficiency of *ec*CTPS-catalyzed amination of STP was also ~6-fold less than

that of the *ec*CTPS-catalyzed conversion of UTP to CTP. ESI-MS demonstrated that up to 3 h, *ec*CTPS aminates ~25% of available substrate, likely because product inhibition of *ec*CTPS then slows the reaction rate.

Few UTP analogues have been found to serve as substrates for *ec*CTPS. The ability of STP to replace UTP as a substrate for *ec*CTPS has not previously been recognized. Overall, these observations suggest that STP could be aminated *in vivo*, leading to formation of another antiviral agent (i.e., see references ((Stuyver *et al*., 2006)) and (Clark *et al*., 2005)).

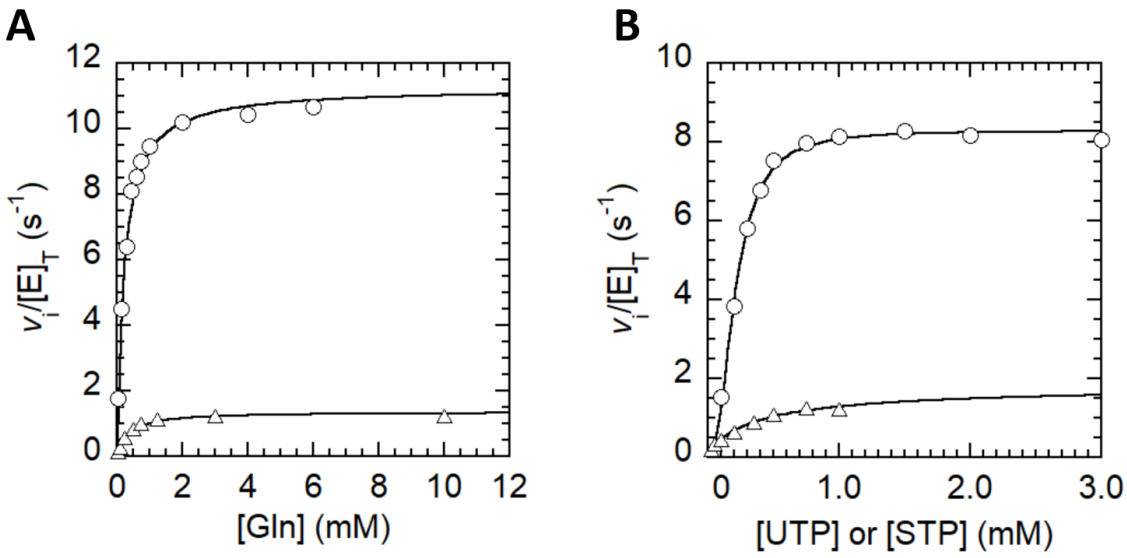

Figure 2.8. Kinetic characterization of STP as a substrate of *ec*CTPS. Representative plots of the initial velocities of Gln-dependent *ec*CTPS-catalyzed CTP formation at a fixed concentration of UTP (○) or STP (△) (1.0 mM each) and varying the concentrations of Gln (0.05 – 10.00 mM) (**A**) and at a fixed concentration of Gln (6.0 mM) and varying concentrations of UTP (○) or STP (△) (0.1 – 3.0 mM and 0.025 – 1.000 mM, respectively) (**B**). All other substrates were at saturating conditions in accord with **Table 5.1**. The concentrations of *ec*CTPS in the Gln-dependent activity were 6.3 µg/mL when UTP was at saturating conditions and 3.8 µg/mL when STP was at saturating conditions (**A**). The concentrations of *ec*CTPS in the Gln-dependent activity were 3.8 µg/mL when STP was the variable substrate (**B**), and 7.6 µg/mL when UTP was the variable substrate (**B**). The curves shown are fits of eqns. 1 (**A**) and 2 (**B**) to the steady-state kinetic data. The corresponding kinetic parameters are summarized in **Table 2.1.**

In the absence of NTPs, *ec*CTPS does not polymerize into filaments (**Figure 2.9. panel A**); however, the presence of CTP at a concentration of 1.0 mM is sufficient to induce polymerization (**Figure 2.9.B**). Because of the similar binding affinity of UTP and STP, one could expect disassembly of *ec*CTPS filaments by STP at concentrations similar to those at which UTP induces disassembly of filaments (i.e., 1.0 mM (McCluskey & Bearne, 2018a)). However, this was not the case, since an abundance of filaments were observed in samples containing 1.0 mM CTP and 1.0 mM STP (**Figure 2.9.C**). Upon increasing the concentration of STP to 5.0 mM, filaments became less abundant (**Figure 2.9.D**). This observation, along with the utilization of STP as a substrate, is consistent with STP binding at the overlapping UTP- and CTP-binding sites (Endrizzi *et al*., 2005) and displacing CTP. Thus, STP can replace UTP both as a substrate for *ec*CTPS, albeit less efficient, and prevent filament assembly. The effects of STP on filament formation by *ec*CTPS indicates that upon employing sofosbuvir as an antiviral drug, it may affect the regulation of CTPS, and thus, pyrimidine metabolism.

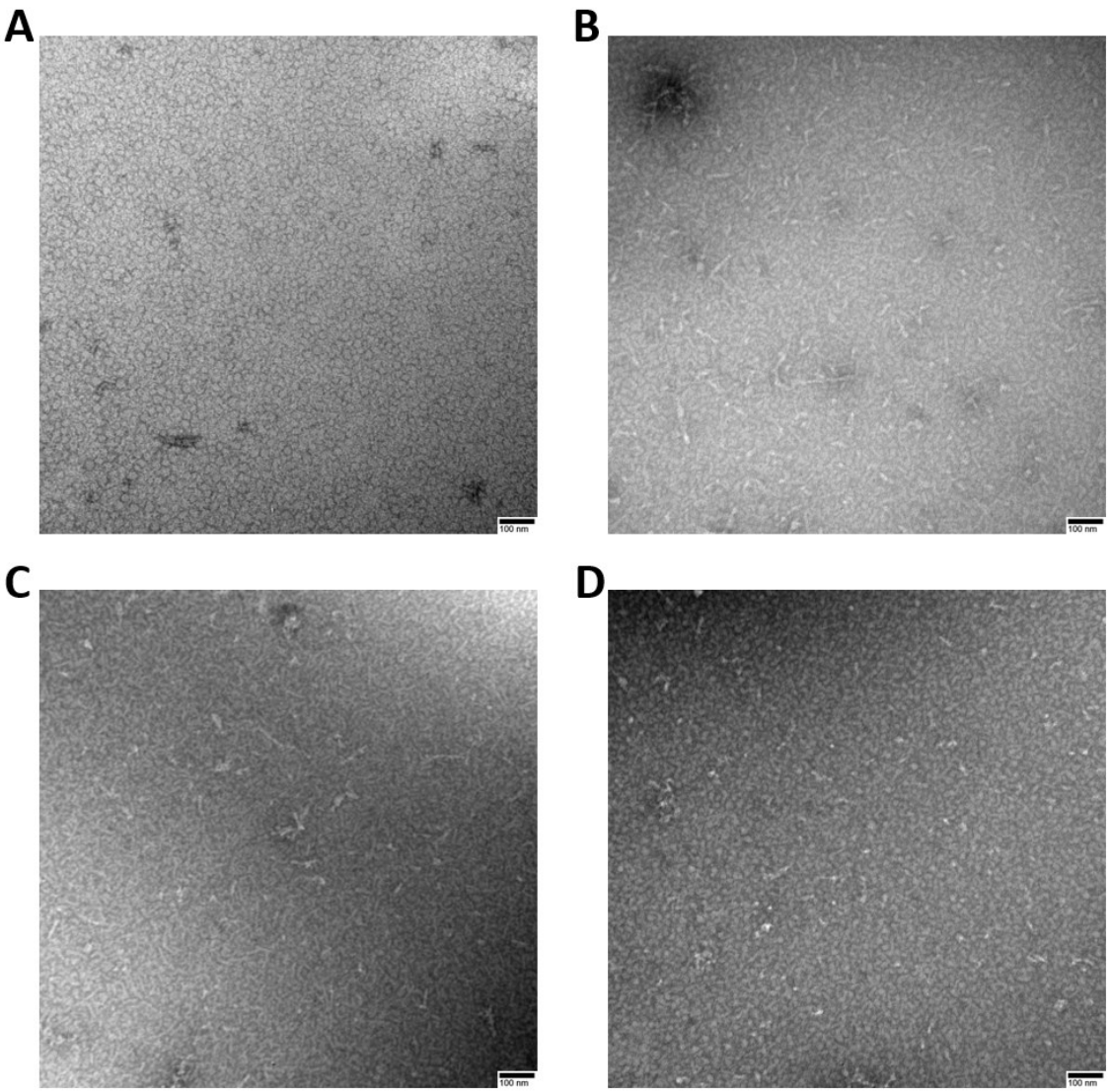

Figure 2.9. Effect of STP on filament formation by *ec*CTPS. Representative electron micrographs of *ec*CTPS in the absence of nucleotides **(A)** and in the presence of CTP (1.0 mM) with either 0 **(B)**, 1.0 mM **(C)**, or 5.0 mM **(D)** STP present. Increasing the concentration of STP caused a marked reduction in the presence of CTP-induced *ec*CTPS filaments.

2.3.4 Effects of N^4-OH-CTP on *ec*CTPS Activity

Anion-exchange chromatography of the mixture resulting from the reaction of hydroxylamine with CTP on a DEAE-Sephadex A-25 column with elution by a TEAB (0.1-1.0 M) stepwise gradient yielded three distinct products as judged from observed the absorbance trace at 260 nm (**Figure 2.10**). Fractions corresponding to the three distinct peaks (A, B and C) in **Figure 2.10** were pooled, lyophilized several times, and submitted for ESI-MS analysis (**Figure 2.11**). The apparent concentrations of TEAB at which the nucleotides corresponding to peaks A, B and C were eluted were 0.4 mM, 0.8 mM, and 1.0 mM respectively. Mass spectrometry revealed that N^4-OH-CMP was the predominant species present in pooled fractions corresponding to peak A (**Figure 2.11.A**). N^4-OH-CDP was the predominant species present in pooled fractions corresponding to peak B (**Figure 2.11.B**). Additionally, N^4-OH-CMP appeared to be present in the sample – likely due to the fragmentation of a phosphate group from N^4-OH-CDP during ESI-MS analysis. Fractions corresponding to peak C contained N^4-OH-CTP, as shown in the low-resolution (**Figure 2.11.C**) and high-resolution (**Figure 2.11.D**) mass spectra. A significant peak was apparent at the exact mass corresponding to N^4-OH-CDP. Again, this is likely due to the fragmentation of a phosphate group from N^4-OH-CTP, which is consistent with the literature (Strzelecka *et al*., 2017)

Samples corresponding to the isolated N^4-OH-CMP, N^4-OH-CDP, and N^4-OH-CTP were subjected to analysis by ion-pairing reversed-phase HPLC to determine their purity. Distinct, single peaks were apparent in all samples (**Figure 2.12**). The increase in retention time between the monophosphate (A), diphosphate (B) and triphosphate (C) is

consistent with increasing retention times of UMP, UDP, and UTP (**Figure 2.13**), as well as published literature (Contreras-Sanz *et al*., 2012; Shi *et al*., 2008).

The concentration of N^4-OH-CTP was determined using ^{1}H NMR spectroscopy with integration of the H6-proton (**Figure 2.14**). Peaks were assigned based on the chemical shift assignments for CTP (Wishart *et al*., 2009). Additionally, the presence of the triphosphate moiety was confirmed using ^{31}P NMR spectroscopy: signals (202 MHz, D_2O) δ -10.10 (d, J = 19.4 Hz), - 11.44 (d, J = 20.2 Hz), -23.13 (t, J = 19.8 Hz). The assignment was based on the published chemical shift assignments for N^4-OH-CTP (EIDD-2061) (Painter *et al*., 2016).

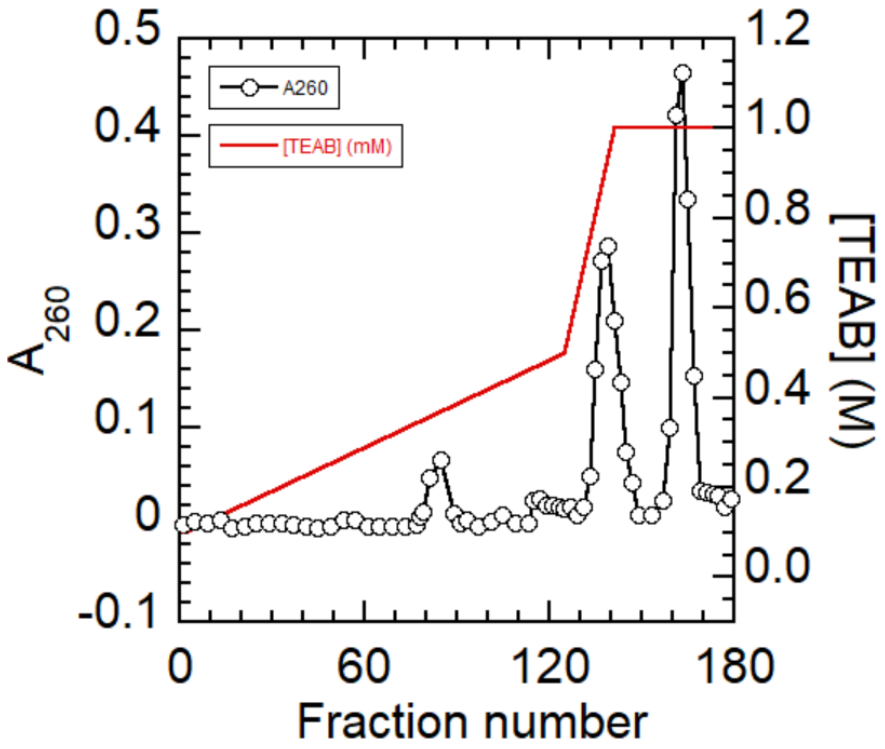

Figure 2.10. Purification of N^4-OH-CTP using anion-exchange chromatography. Representative plot displaying absorbance (260 nm) of fractions collected from the elution of the reaction mixture for the preparation of N^4-OH-CTP using a DEAE-Sephadex A-25 column and a stepwise TEAB (0.1-1.0 M) gradient. Fractions corresponding to the peaks designated A, B, and C were collected individually and analyzed using ESI-MS (**Figure 2.11**).

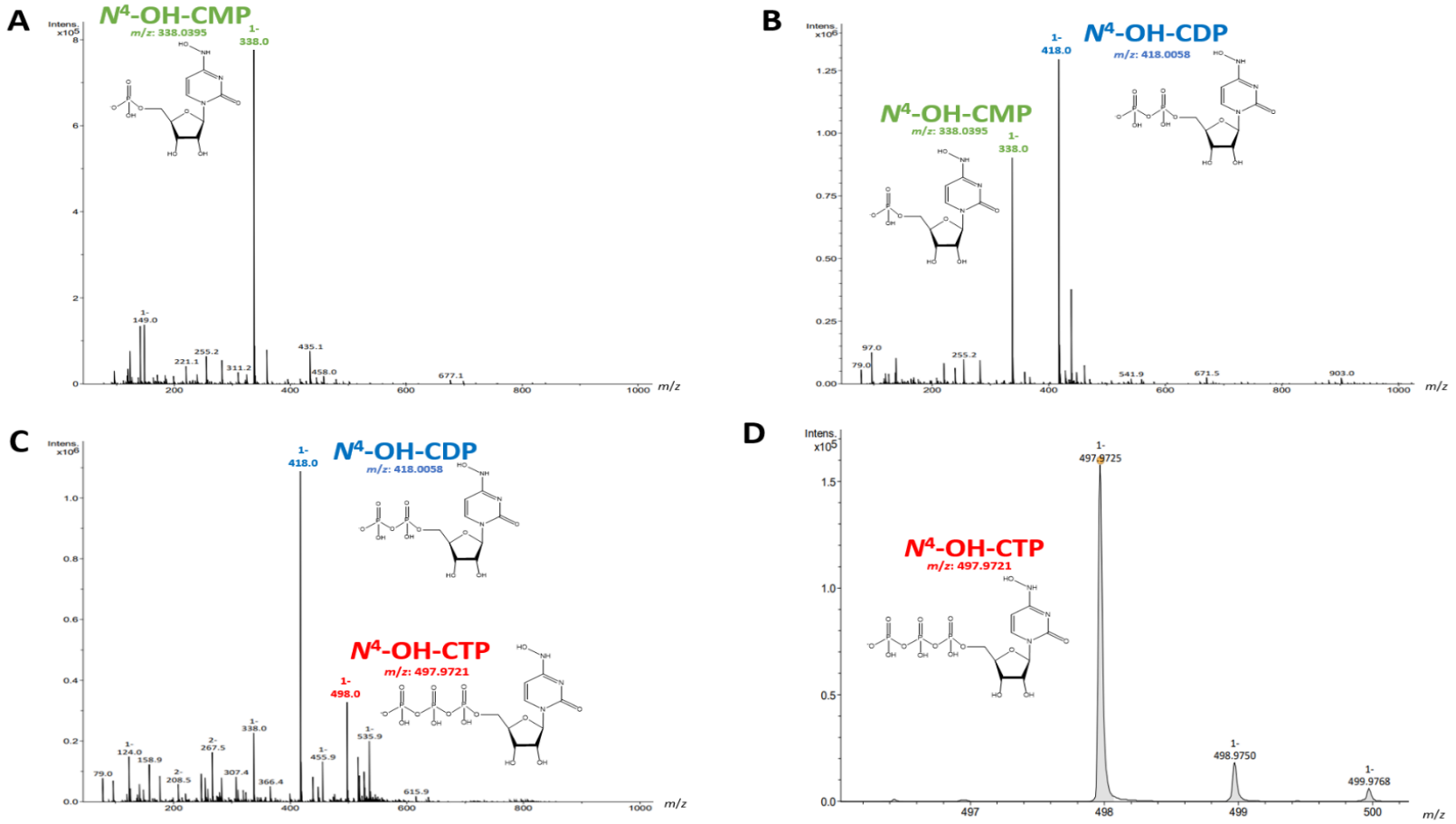

Figure 2.11. Identification of N^4-OH-CTP by ESI-MS in negative ion mode. Representative low-resolution spectra of product from pooled fractions corresponding to peak A, B, and C (**Figure 2.10**). N^4-OH-CMP (green) was identified in sample A (**A**). N^4-OH-CDP (blue) and N^4-OH-CMP were identified in sample B (**B**). N^4-OH-CTP (red) and N^4-OH-CDP (blue) were identified in sample C (**C**). High resolution spectrum of the peak at *m/z* 498.0 corresponding to N^4-OH-CTP (**D**). Expected mass $[M - H^+]^-$ = 497.9721, found 497.9725.

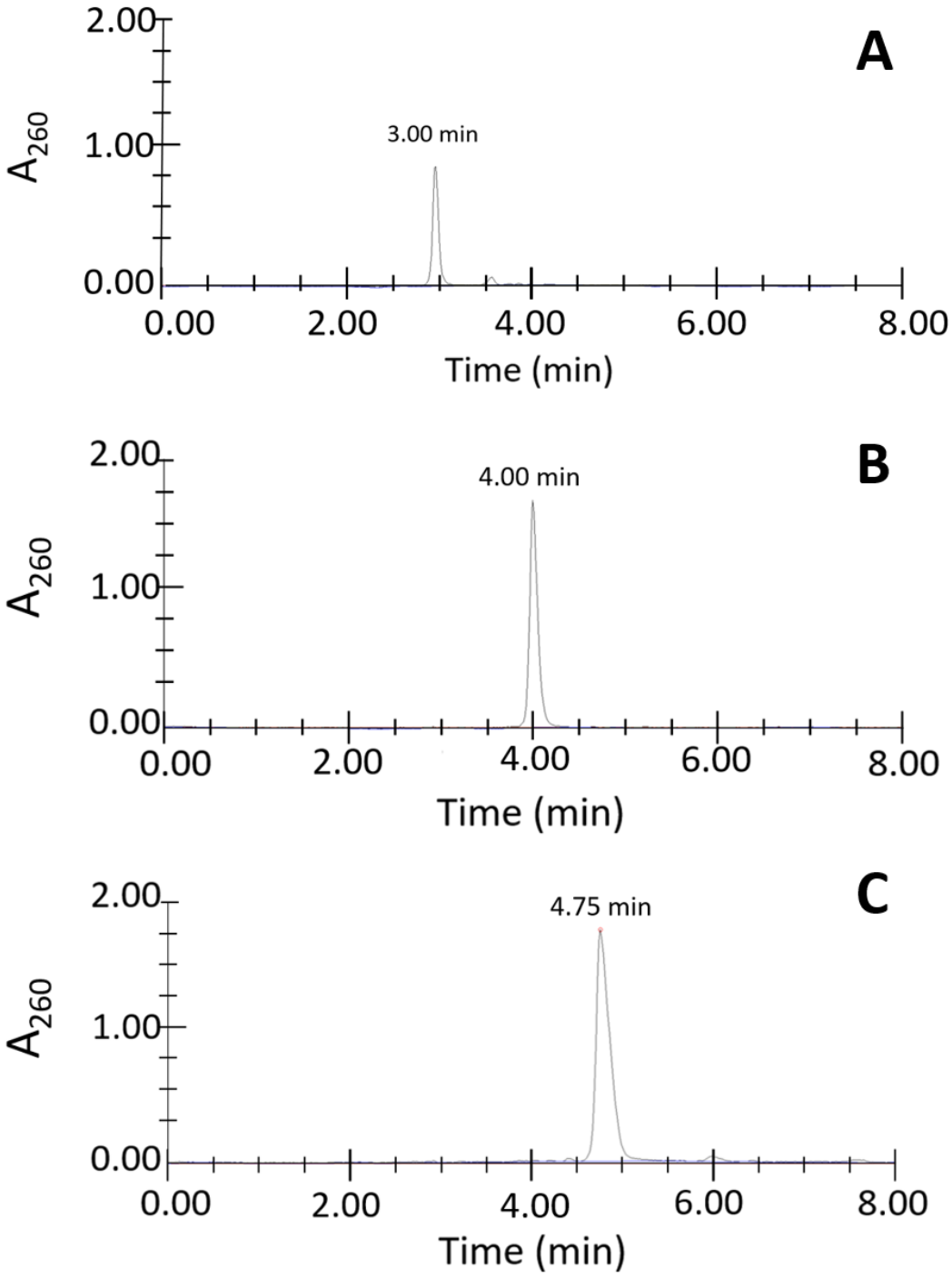

Figure 2.12. Ion-pairing reversed-phase HPLC of fractions from sample A, B, and C for the preparation of N^4-OH-CTP. Absorbance at 260 nm of 20-µL samples from peak A (N^4-OH-CMP), (**A**) peak B (N^4-OH-CDP), (**B**) and peak C (N^4-OH-CTP) (**Figure 2.10**). An increased retention time is observed from the monophosphate to diphosphate and triphosphate species in accord with **Figure 2.13**.

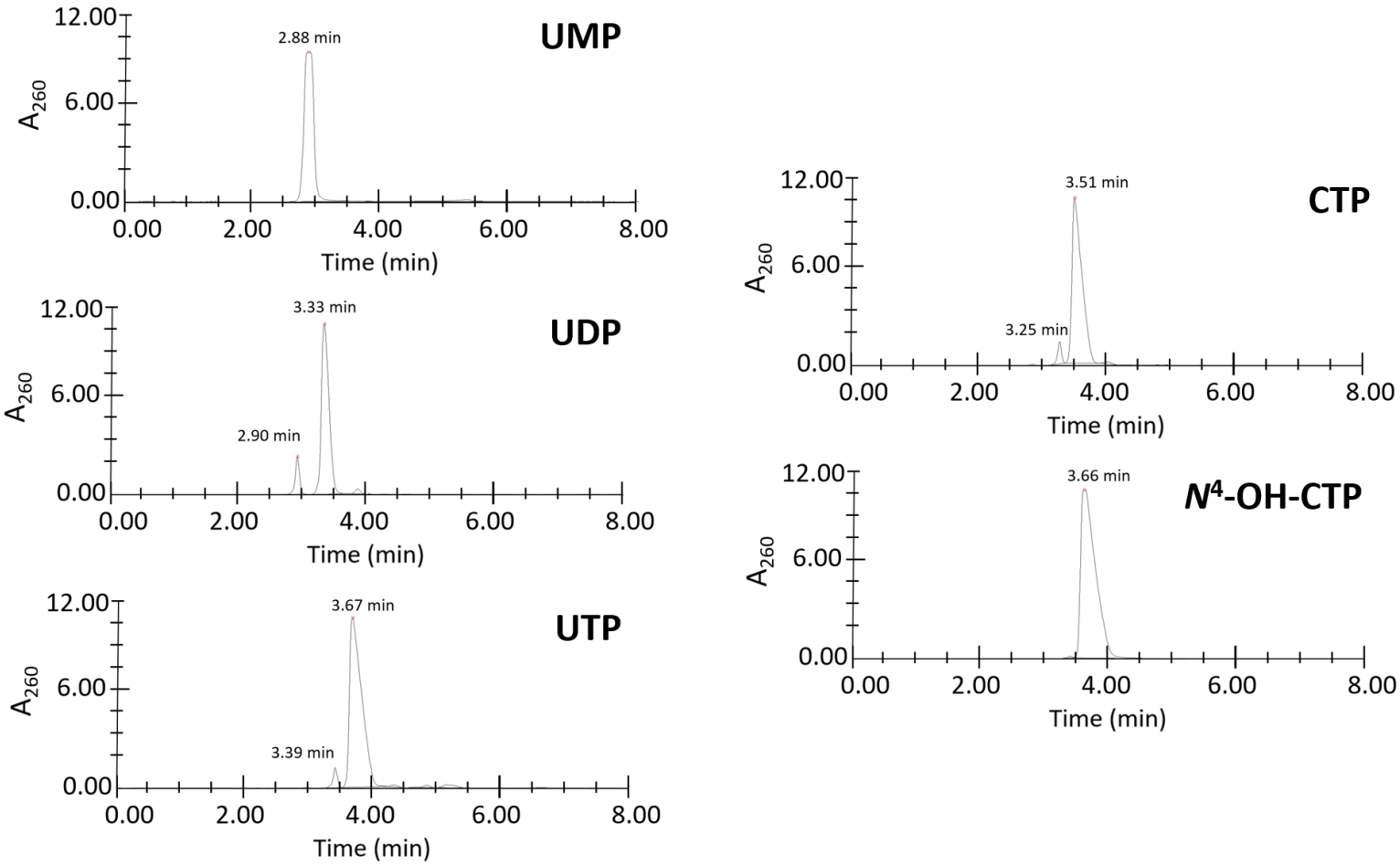

Figure 2.13. Ion-pairing reversed-phase HPLC indicating increasing retention times of nucleotide mono-, di-, and triphosphates. Absorbance at 260 nm of 20-µL samples of UMP, UDP, UTP, CTP and N^4-OH-CTP. An increased retention time is observed from the monophosphate to diphosphate and triphosphate species. CTP and N^4-OH-CTP elute at a similar retention time to UTP.

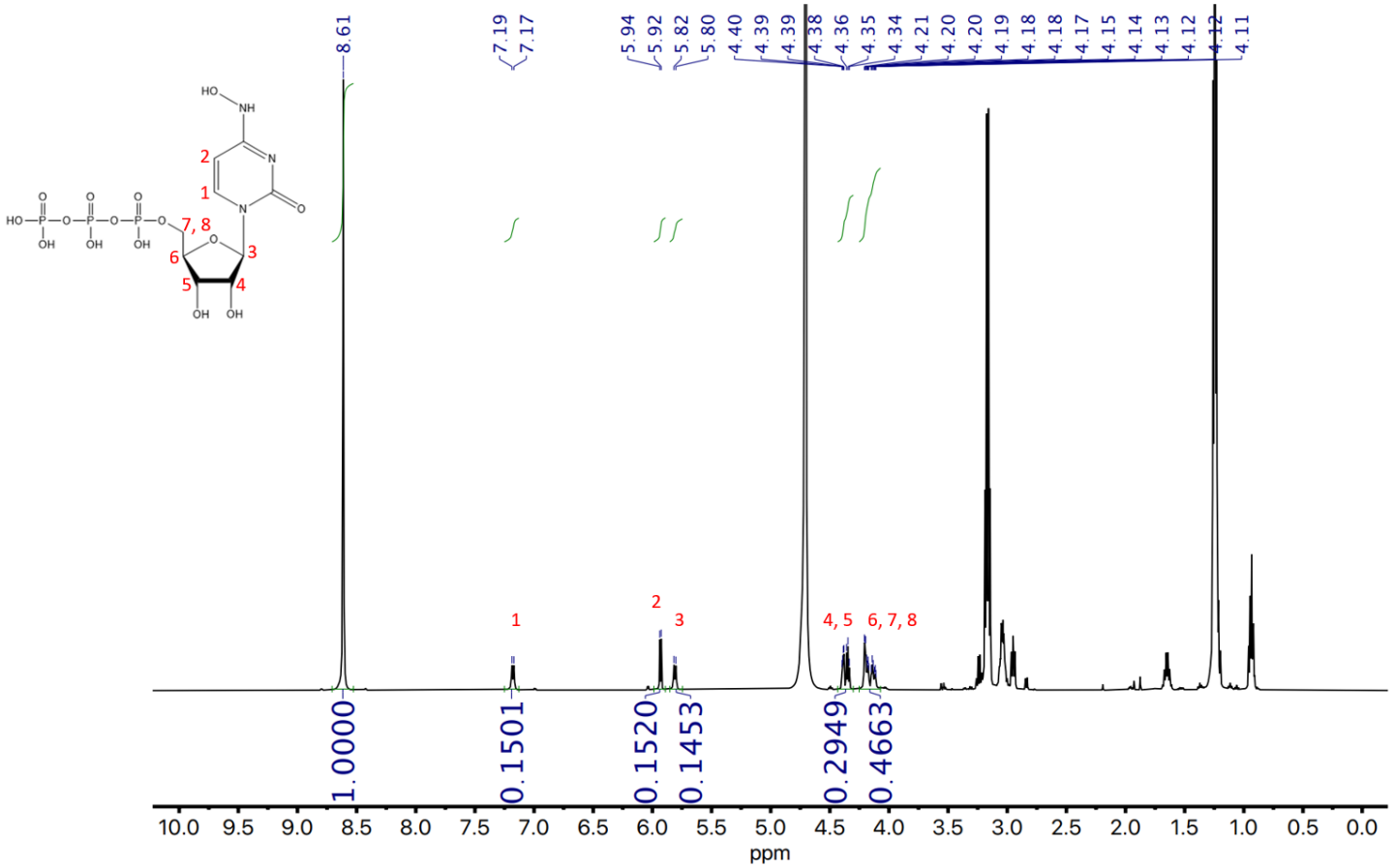

Figure 2.14. Representative ^{1}H NMR spectrum for quantification of N^4-OH-CTP. The concentration of N^4-OH-CTP was determined using ^{1}H NMR with integration of the doublet H6-proton (δ 7.18 ppm) compared to the integral for an internal pyrazine standard at (5 mM, δ 8.61 ppm).

Preliminary modeling studies using the published structure of CTPS with bound CTP (Endrizzi *et al*., 2004) suggested that an enhanced interaction might arise from H-bonding between the N^4-hydroxyl group and Lys 196 (**Figure 2.2**) (Bearne, S.L., personal communication). To investigate this, we measured the inhibition of *ec*CTPS by CTP and N^4-OH-CTP at two fixed concentrations of UTP (0.05 and 0.20 mM) with Gln as the nitrogen source. The concentration of ATP, GTP, and Gln were fixed at saturating conditions as given in **Table 5.1**. The relative initial velocities (v_i/v_o) were plotted against the concentration of inhibitor and eqn. 6 was fitted to the data. IC_{50} values for the inhibition of *ec*CTPS by CTP were $IC_{50}^{[UTP]=0.05\ mM} = 107 \pm 4$ μM and $IC_{50}^{[UTP]=0.20\ mM}$ 234 ± 21 μM (**Figure 2.16, Table 2.2**), which are comparable to previously published data (McCluskey *et al*., 2016). Interestingly, IC_{50} values for the inhibition of *ec*CTPS by N^4-OH-CTP were ~9-fold higher, $IC_{50}^{[UTP]=0.05\ mM}$ 986 ± 50 μM and $IC_{50}^{[UTP]=0.20\ mM}$ 1730 ± 251 μM (**Figure 2.17, Table 2.2**), indicating that this CTP analogue was not bound by *ec*CTPS with greater affinity than CTP.

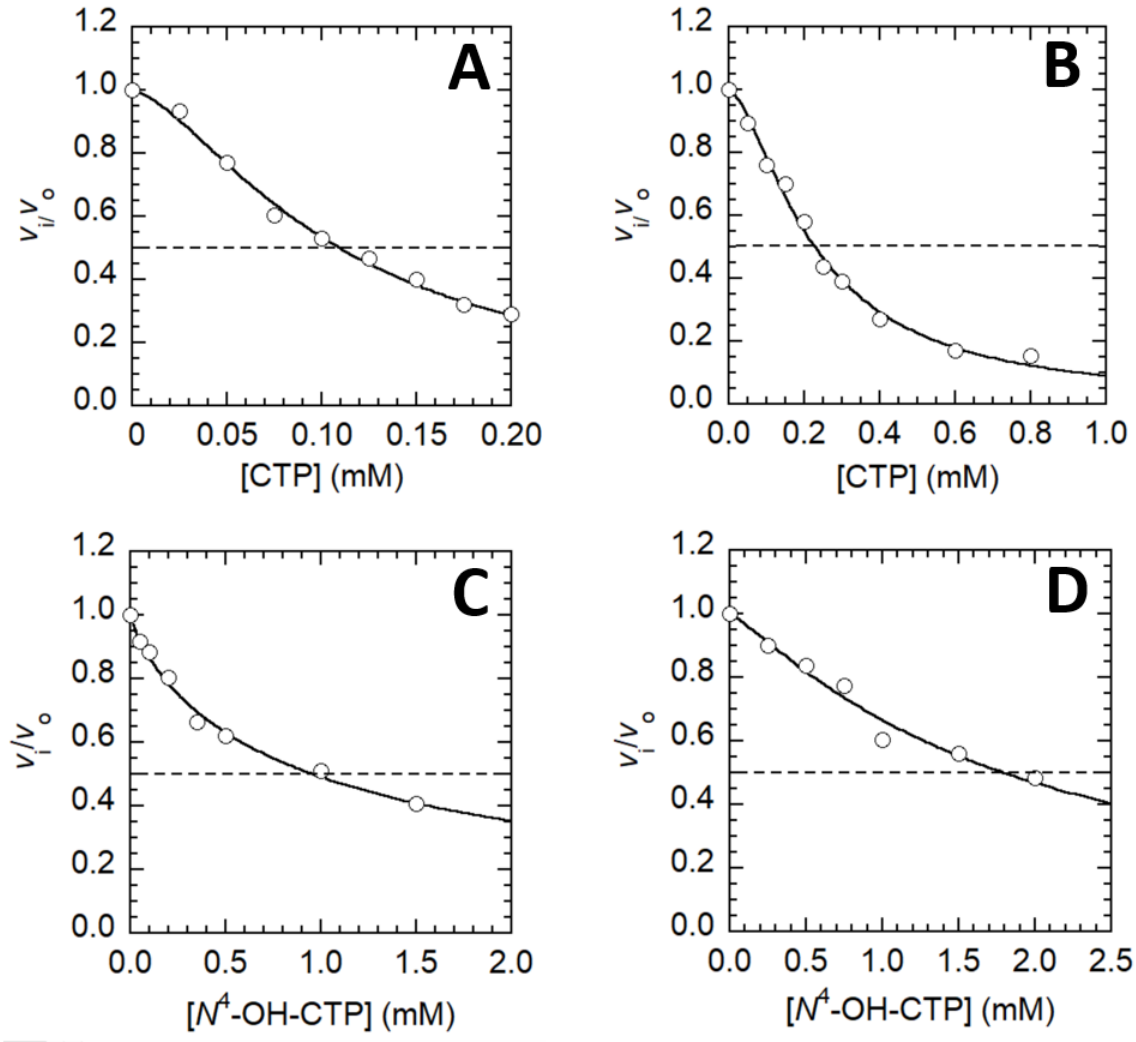

Figure 2.15. Representative plots for the determination of the IC_{50} values for the inhibition of the Gln-dependent CTP formation by CTP and N^4-OH-CTP. Inhibition by CTP (A, B) and N^4-OH-CTP (C, D) was measured at [UTP] = 0.05 mM (A, C) and [UTP] = 0.20 mM (B, D). The concentration of ATP, GTP, and Gln were fixed at 1.0 mM, 0.25 mM, and 6.0 mM, respectively. The concentrations of *ec*CTPS were 19.0 (**A**), 7.5 (**B**), and 3.2 (**C, D**) µg/mL. The curve is a non-linear regression fit of eqn. 6 to the relative velocities (v_i/v_o). The IC_{50} and n values were determined in triplicate and are given in **Table 2.2**.

Table 2.2. Inhibition of Gln-dependent *ec*CTPS-catalyzed production of CTP by CTP and N^4-OH-CTP

Inhibitor	[UTP] = 0.05 mM		[UTP] = 0.20 mM		K_i (μM)
	IC_{50} (μM)	*n*	IC_{50} (μM)	*n*	
CTP	107 ± 4	1.6 ± 0.1	234 ± 21	1.6 ± 0.1	108 ± 29
N^4-OH-CTP	986 ± 50	0.8 ± 0.1	1730 ± 251	1.3 ± 0.2	383 ± 76

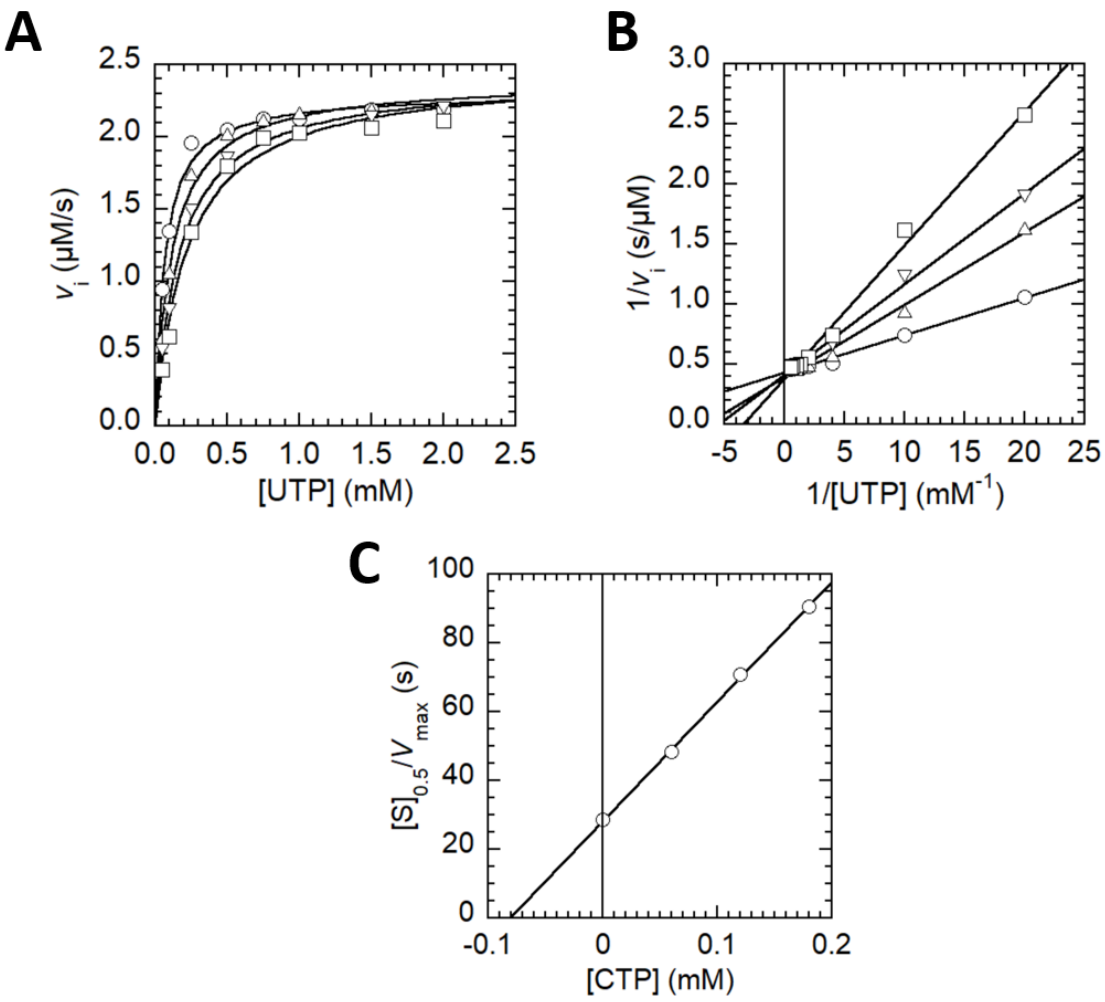

Figure 2.16. Representative plots showing competitive inhibition of Gln-dependent CTP formation by CTP. *ec*CTPS activity was assayed with UTP as the variable substrate and various fixed concentrations of CTP (0 (○), 0.06 (△), 0.12, (▽) and 0.18 (□) mM). The initial velocity data were plotted as a Michaelis-Menten plot (**A**), to which eqn. 2 was fitted. The initial velocity data were re-plotted as a double reciprocal plot to which eqn. 7 was fitted (**B**). Apparent $\frac{[S]_{0.5}}{V_{max}}$ values were replotted against the concentration of CTP (**C**) and the K_i value was determined to be 108 ± 29 μM. The concentration of *ec*CTPS was 5.0 μg/mL. The results are summarized in **Table 2.2**.

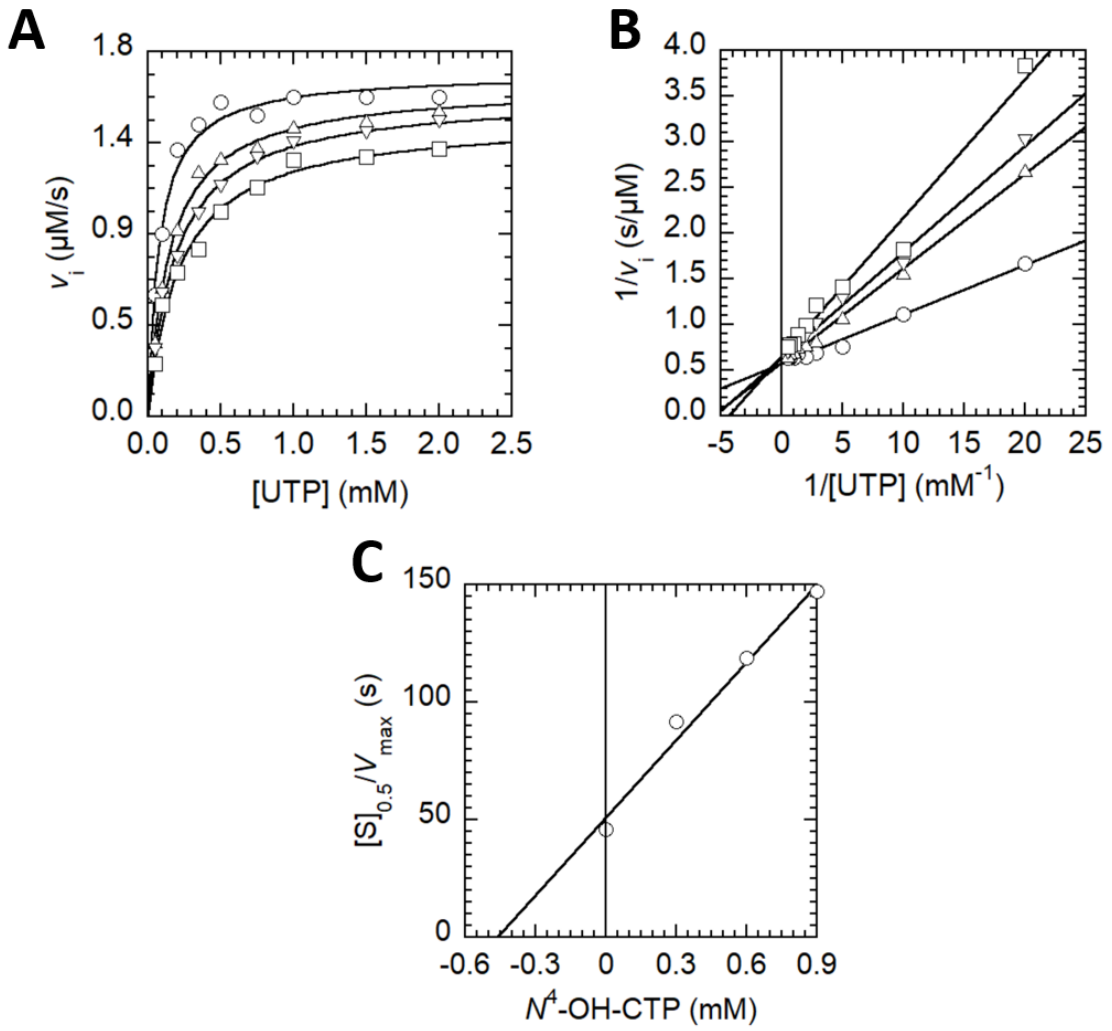

Figure 2.17. Representative plots showing competitive inhibition of Gln-dependent CTP formation by N^4-OH-CTP. *ec*CTPS activity was assayed with UTP as the variable substrate and various fixed concentrations of CTP (0 (○), 0.3 (△), 0.6 (▽), and 0.9 mM(□)). The initial velocity data were plotted as a Michaelis-Menten plot (**A**), to which eqn. 2 was fitted. The initial velocity data were re-plotted as a double reciprocal plot to which eqn. 7 was fitted (**B**). Apparent $\frac{[S]_{0.5}}{V_{max}}$ values were replotted against the concentration of N^4-OH-CTP (**C**) and the K_i value was determined to be 383 ± 76 μM. The concentration of *ec*CTPS was 3.9 μg/mL. The results are summarized in **Table 2.2**.

The N^4 exocyclic atom of CTP is not directly contacted by *ec*CTPS, however, a water-mediated hydrogen bond to the Gly 146 backbone carbonyl oxygen provides potential recognition of amino group at the 4-position of CTP (Endrizzi *et al*., 2005). Given the analogous structure of N^4-OH-CTP to CTP, other residues essential in the recognition of CTP (or a CTP analogue) are not expected to be impacted by the substitution at N^4. The increased IC_{50} value of N^4-OH-CTP, relative to CTP suggests that the proposed enhanced interaction with Lys 196 may not occur and an altered interaction with Gly 146 may diminish the recognition of N^4-OH-CTP by *ec*CTPS. The $IC_{50}^{[UTP]=0.05\ mM}$ values were significantly lower than $IC_{50}^{[UTP]=0.20\ mM}$ values, consistent with other CTP-analogues that act as a competitive inhibitor with respect to UTP (McCluskey *et al*., 2016). To verify that N^4-OH-CTP acts as competitive inhibitors, we performed kinetic studies to investigate the mode of inhibition and the value of the inhibition constant (K_i) of both CTP and N^4-OH-CTP.

The steady-state initial velocity data did not demonstrate significant cooperativity to justify using the Michaelis-Menten equation modified by a Hill number (eqn. 3), thus, eqn. 2 was fitted to the data (**Figure 2.17.A**). In accord with previously published data (McCluskey *et al*., 2016), a competitive inhibition pattern by CTP was observed with respect to UTP upon replotting the initial velocity data in a double reciprocal plot, wherein the lines of best fit intersected on the $1/v_i$ axis (**Figure 2.17.B**). The apparent $\frac{[S]_{0.5}}{V_{max}}$ values, corresponding to the slopes of these lines in the double-reciprocal plot (but derived from non-linear regression analysis of the Michaelis-Menten plot in **Figure 2.17.A**) were replotted against the concentration of CTP to estimate the K_i value (**Figure 2.17.C**). Similarly, N^4-OH-CTP demonstrated competitive inhibition with respect to UTP

(**Figure 2.17.B**). The K_i values presented in **Table 2.2** indicate that the binding affinity of N^4-OH-CTP is decreased ~3.5-fold relative to that of CTP, which agrees with the higher IC_{50} values exhibited for inhibition by N^4-OH-CTP relative to CTP.

The mechanism by which NHC induces cell death is well understood. In brief, NHC is phosphorylated to its active 5′-triphosphate form, which is incorporated into the genome of new virions, resulting in the accumulation of inactivating mutations (Painter *et al*., 2019; Urakova *et al*., 2018). Furthermore, NHC exhibits antiviral activity against multiple coronaviruses, including SARS-CoV-2 (Sheahan *et al*., 2020; Zandi *et al*., 2020), and displays synergistic activity with other antiretroviral protease inhibitors against SARS-CoV-2 (Ianevski *et al*., 2020). The present work demonstrates that the active metabolite of NHC can weakly inhibit *ec*CTPS activity. The ability of N^4-OH-CTP to inhibit *ec*CTPS has not previously been recognized. Overall, these observations suggest that N^4-OH-CTP, in addition to causing mutation in the viral genome, could also reduce the intracellular CTP pools when employed as an antiviral agent, thereby possibly potentiating the antiviral effect of NHC.

Given the ability of CTP to induce *ec*CTPS polymerization, exploring the effects of N^4-OH-CTP on filament formation was of interest. Since the 4-amino group is not directly contacted by *ec*CTPS (Endrizzi *et al*., 2005), it seems likely that the binding of N^4-OH-CTP should mimic CTP and induce polymerization of *ec*CTPS. Indeed, N^4-OH-CTP (1.0 mM) was sufficient to induce filament assembly by *ec*CTPS (**Figure 2.18 panel B**). Despite a decrease in binding affinity by N^4-OH-CTP (**Table 2.2**), the *ec*CTPS filaments induced by N^4-OH-CTP displayed no distinct differences from those induced by CTP with regards to size or abundance (**Figure 2.18 panel A**). Thus, it is apparent that

N^4-OH-CTP can behave as a product-analogue inhibitor and as a ligand to induce a filamentous form of *ec*CTPS. Such findings should be considered when investigating the effects of NHC as an antiviral drug.

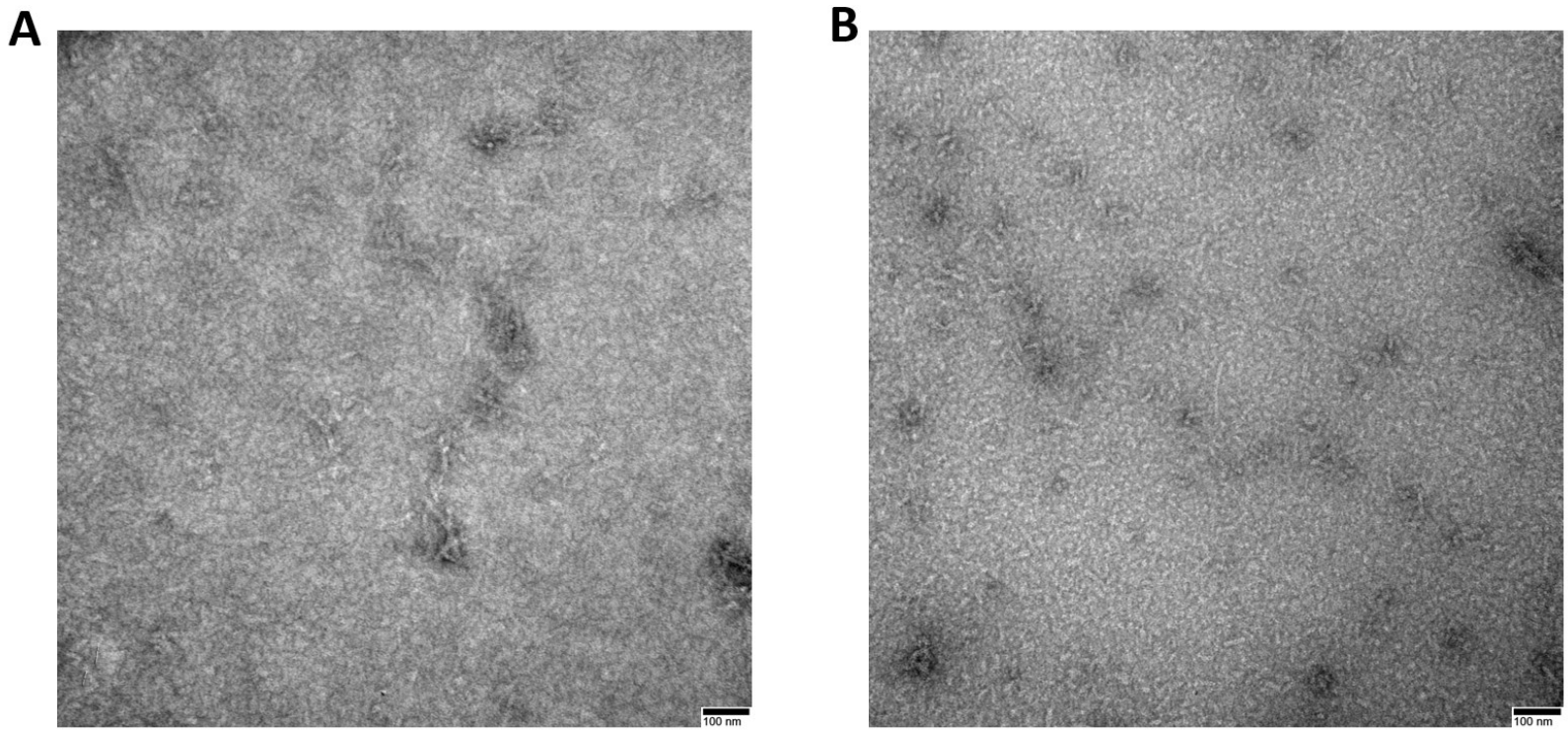

Figure 2.18. N^4-OH-CTP can induce *ec*CTPS polymerization. Representative electron micrograph of *ec*CTPS in the presence of CTP (1.0 mM) (**A**) and N^4-OH-CTP (1.0 mM) (**B**).

2.4 CONCLUSIONS AND FUTURE DIRECTION

In this chapter, we explored the effects of specific antiviral nucleotide analogues on the activity of *ec*CTPS, as well as their effects on filament formation by *ec*CTPS. AraATP was recognized as a substrate, although it had catalytic efficiency values ~2.5 - 5-fold lower relative to activity with ATP as a substrate (**Table 2.1**). RBVNTP was an allosteric activator of *ec*CTPS; however, it exhibited a ~24-fold decrease in catalytic efficiency relative to GTP (**Table 2.1**). Neither GTP nor RBVNTP had an apparent effect on filament assembly, or the prevention of filament assembly by CTP as assessed using TEM (**Figure 2.5**). Upon administration as antiviral prodrugs, the corresponding metabolites araATP and RBVNTP afford possible mechanisms by which CTPS can remain active when intracellular pools of substrates are diminished as well as assist in maintaining intracellular pools of CTP.

*ec*CTPS recognized STP as a substrate for amination (**Figure 2.7**), forming an alternative antiviral metabolite (4-NH_2-STP). The catalytic efficiency for STP as a substrate was reduced ~6-fold relative to that observed for UTP (**Table 2.1**). Similar to UTP, STP was able to disrupt filament formation (**Figure 2.9**), likely due to the binding at the overlapping UTP/CTP-binding site. The 4-NH_2-STP formed via *ec*CTPS-catalyzed amination of STP may be incorporated into the viral RNA and lead to chain termination, thereby, providing an additional mechanism by which sofosbuvir demonstrates antiviral activity. STP may also afford a mechanism by which CTPS remains active when the concentration of UTP is low since it also regulates polymerization of the enzyme.

N^4-OH-CTP was synthesized, purified, and assessed as an inhibitor of *ec*CTPS. Similar to feedback inhibition by the product CTP, N^4-OH-CTP acts as a competitive

inhibitor (**Figure 2.17**). Despite a proposed enhanced interaction of N^4-OH-CTP with *ec*CTPS due to the lack of contacts between the N^4 exocyclic atom and the enzyme, N^4-OH-CTP demonstrated a ~3.5-fold decrease in binding affinity relative to CTP (*cf.* K_i values, **Table 2.2**). Furthermore, N^4-OH-CTP was able to induce filament formation by *ec*CTPS. In addition to causing mutations in the viral genome, N^4-OH-CTP could reduce the intracellular CTP pools by inhibition of CTPS and the promotion of enzyme polymerization into inactive filaments, thereby potentiating the antiviral effects of NHC.

The effects that these 5′-triphosphates of specific antiviral agents have on *ec*CTPS should be considered when assessing the antiviral prodrugs for the treatment of SARS-CoV-2. Since CTPS structure and function is conserved amongst various organisms, using *ec*CTPS as a model system provides a framework for the effects of the 5′-triphosphates of antiviral agents on humans upon administration for the infections of COVID-19. Future investigations should focus on the effects of araATP, RBVNTP, STP, and N^4-OH-CTP on hCTPS1 and hCTPS2 activity and its ability to form filaments. In addition, the effects of other 5′-triphosphates of antiviral agents on *ec*CTPS activity and filament formation should be examined to provide a better understanding of possible effects of repurposing known antiviral drugs for the treatment of COVID-19.

CHAPTER 3: ADENOSINE-5′-(3-THIO)-TRIPHOSPHATE (ATPγS) AS A LIGAND FOR *ec*CTPS

3.1 INTRODUCTION

ATP is found in every living organism and plays a central role in many metabolic pathways and the regulation of enzyme activity. Numerous ATP analogues have been synthesized to probe the role of ATP in biological systems (Yount, 1975). A variety of derivatives of ATP exist, which have modifications of the adenine base, the ribose moiety, or the 5′-triphosphate chain. ATP-utilizing systems vary enormously in their specificity; an analogue that provides insight in one biochemical system may be futile in another. In general, there are two main types of investigations for which ATP analogues are particularly useful. First, fluorescent, spectroscopic probes, are often used to report on the action of ATP in nucleotide-interacting systems while having minimal effects on the molecule's properties (Hiratsuka, 2003). 2′,3′-O-Trinitrophenyl-adenosine-5′-monophosphate (TNP-AMP), was the first fluorescent analogue used as a substrate for G-proteins and ATP-binding proteins (Tao & Lamkin, 1981). Another example of a fluorescent ATP analogue is the fluorophore-conjugated ATP analogue *N*-methyl-anthraniloyl-ATP (mantATP). It has been used for example, to study the kinetics of human kinesin Eg5 motors using the change of fluorescence intensity as a readout (Cochran *et al*., 2004).

Second, non-hydrolysable analogues such as adenosine 5′-[β,γ-imido]triphosphate (ADPNP), Adenosine-5′-[(β,γ)-methyleno]triphosphate (AMPPCP), and ATPγS (**Table 3.1**) are often employed to study the mechanism of enzymes that utilize ATP as a substrate (Bagshaw, 2001). In particular, ATPγS is a substrate and inhibitor of ATP-

dependent enzyme systems and is hydrolyzed very slowly by phosphatases and most ATPases (Peck & Herschlag, 2003). For example, adenosine triphosphatase exhibits a 9-fold reduction in k_{cat} for Mg- ATPγS relative to MgATP (Yates & Duance, 1976). In the *ec*CTPS-catalyzed production of CTP from UTP, ATP is hydrolyzed at the β-γ linkage to yield ADP. CTP synthesis requires the presence of both the nucleotide substrates ATP and UTP, and in their absence, only Gln hydrolysis takes place. Levitzki and Koshland (Levitzki & Koshland, 1972b) utilized ADPNP as a non-hydrolysable analogue to uncouple the production of CTP from Gln hydrolysis. They measured the glutaminase activity of the dimer in the absence of ATP and UTP and compared it to the glutaminase activity of the tetramer in the presence of ADPNP and UTP and found that the k_{cat} value for Gln hydrolysis increased nearly 6-fold in the presence of ADPNP and UTP.

Willemoës and Sigurskjold (Willemoës & Sigurskjold, 2002) investigated the steady state kinetics of *Lactococcus lactis* CTPS-catalyzed Gln hydrolysis uncoupled from CTP formation using ADPNP and ATPγS. ATPγS was a more potent inhibitor of CTPS activity than ADPNP (IC_{50} ~1 mM for ATPγS versus ~8 mM for ADPNP) and thus, was selected ATPγS as an appropriate analogue of ATP to use in studies designed to investigate the glutaminase half reaction and its response to the allosteric activation by GTP in the presence of (unreactive) ATPγS and UTP (Willemoës & Sigurskjold, 2002) Use of ATPγS and UTP ensured that the enzyme was in its tetrameric form but could not form CTP. Interestingly, they observed that GTP-dependent activation of the uncoupled glutaminase reaction never obtained the same rate as GTP-activated CTP synthesis when the active site was saturated with UTP and ATPγS. Theses authors concluded that the additional activation arose from the formation of the phosphorylated UTP intermediate,

which could not form in the presence of ATPγS (Willemoës & Sigurskjold, 2002). Levitzki and Koshland initially proposed a mechanism shown in scheme 1A in which the nascent ammonia attacks the UTP molecule prior to activation by ATP (Levitzki & Koshland, 1971), however, based on positional isotope exchange experiments (Lewis & Villafranca, 1989), suggested that the ATP molecule activates the UTP molecule first, followed by attack from nascent ammonia as indicated in Scheme 1B. It is this activated form of UTP that Willemoës and Sigurskjold (Willemoës & Sigurskjold, 2002) proposed as a co-activator of the *L. lactis* enzyme-catalyzed hydrolysis of Gln, along with GTP.

Scheme 3.1. Proposed mechanisms of CTP synthesis at the synthase domain

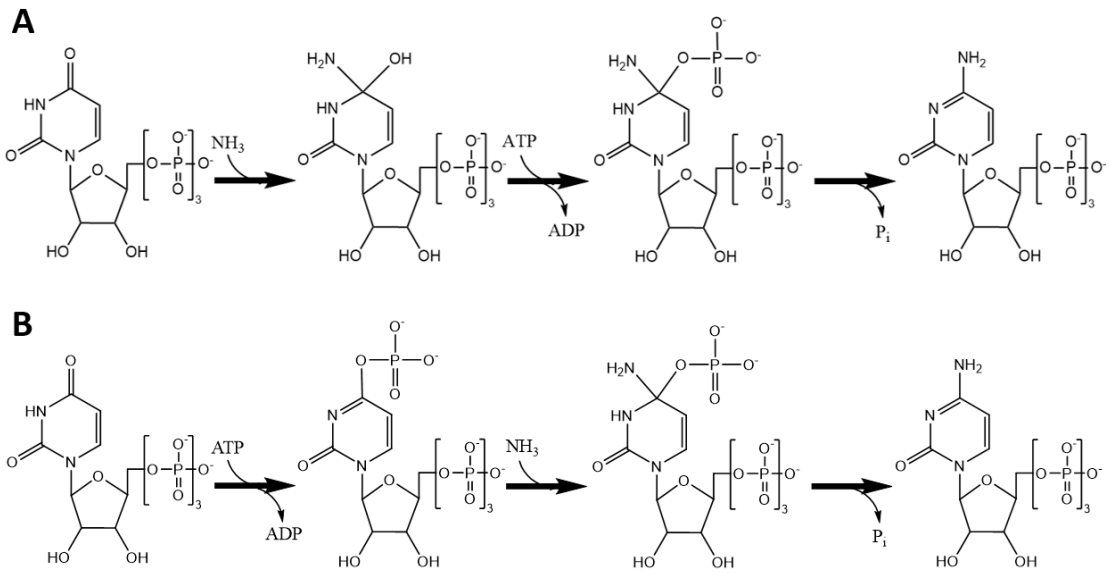

There are currently no structures of *ec*CTPS with ATP bound; however, Baldwin and colleagues (Endrizzi *et al*., 2005) solved the structure of ADP-bound *ec*CTPS (PDB: 2AD5). Kollman and colleagues (Lynch *et al*., 2017) solved structures of filamentous *ec*CTPS bound to ADP (PDBs: 5U6R, 5U3C). Kollman and colleagues also solved the

structure of ATP-bound hCTPS1 (PDB: 5U03), ADPNP-bound hCTPS1 (PDB: 7MGZ), ADP-bound hCTPS2 (PDB: 6PK7) (Lynch *et al*., 2021), and ATP-bound hCTPS2 (PDB: 6PK4) (Lynch & Kollman, 2020). Furthermore, the structure of *Mycobacterium tuberculosis* CTPS with the non-hydrolyzable ATP analogue AMPPCP (PDB: 4ZDK) has been solved (Mori *et al*., 2015).

Table 3.1. Structures of common nonhydrolyzable ATP analogues and fluorescent derivatives

General purpose	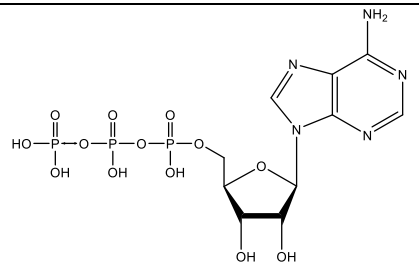 ATP		
Fluorescent derivatives	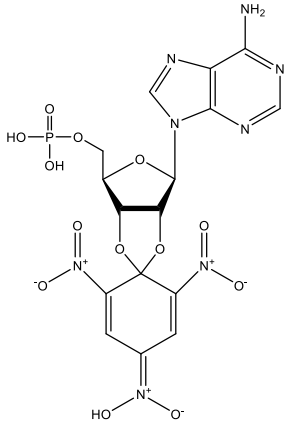 TNP-AMP	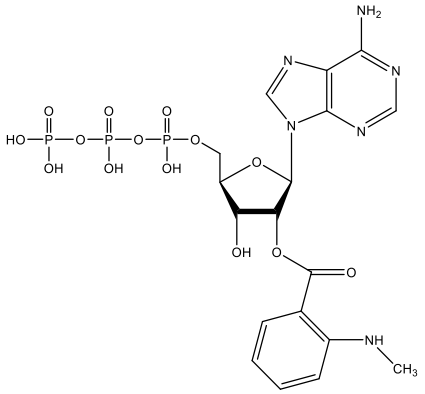 mantATP	
Nonhydrolyzable analogues	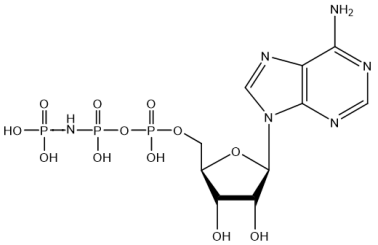 ADPNP	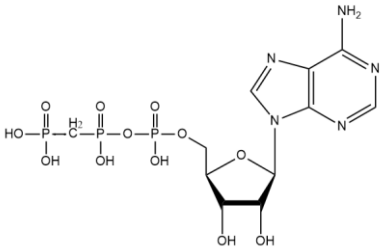 AMPPCP	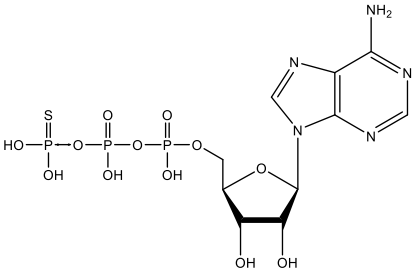 ATPγS

The inhibition of *ec*CTPS has been investigated primarily with use of CTP, GTP, and Gln analogues, as well as nicotinamides (Bearne *et al*., 2001; Habrian *et al*., 2016; MacDonnell *et al*., 2004; McCluskey *et al*., 2016). There have been fewer investigations of inhibition of *ec*CTPS by ATP analogues. In this chapter, we explore the kinetic properties of ATPγS as a ligand for *ec*CTPS. ATPγS proved to be a relatively potent inhibitor of *ec*CTPS activity in the presence of GTP and with Gln as the nitrogen source (**Table 3.2**). In addition, the effects of ATPγS on filament formation by *ec*CTPS were investigated using transmission electron microscopy.

3.2 MATERIALS AND METHODS

All materials are described in **Chapter 5.1**. Kinetic investigations and the effects of NTPs on filament formation by *ec*CTPS were completed as described in **Chapter 5** except for an increased concentration of NTPs (2.0 mM) in filament studies.

3.3 RESULTS AND DISCUSSION

3.3.1 ATP-dependent *ec*CTPS Activity

The k_{cat} and $[S]_{0.5}$ values for the ATP-dependent activity of *ec*CTPS were determined using Gln and NH_3 as the nitrogen sources (**Figure 3.1**). *ec*CTPS activity was assayed with fixed saturating concentrations of UTP (1 mM), NH_4Cl (150 mM) or Gln (6 mM), and various concentrations of ATP (0.05 – 2.0 mM). When Gln was used as the nitrogen source, the concentration of GTP was maintained at saturating conditions (0.25 mM). The kinetic parameters are given in **Table 3.2**.

Upon comparison of the ATP-dependent activity between the reactions utilizing either Gln or NH_3, as the two nitrogen sources, the $[S]_{0.5}$ when Gln is the nitrogen source is less than half that observed when NH_3 is the nitrogen source. The k_{cat} values are comparable, though the catalytic efficiency of the Gln-dependent activity is nearly 4 times that of the NH_3-dependent activity. Possibly, the difference between the $[S]_{0.5}$ values may arise from the enzyme undergoing conformational changes upon interactions with GTP, that also affect ATP-binding affinity. GTP has demonstrated an inhibitory effect in the NH_3-dependent activity, though it acts as an allosteric activator when Gln is used as the nitrogen source (MacDonnell *et al*., 2004). *ec*CTPS demonstrates cooperativity upon binding both ATP and UTP (Long & Pardee, 1967). This is supported by the cooperativity indicated by the Hill number of $n = 3.0 \pm 0.5$ for the formation of CTP with NH_3 as the nitrogen source. The formation of CTP, however, does not appear to show cooperativity with a Hill coefficient of $n = 1.18 \pm 0.01$.

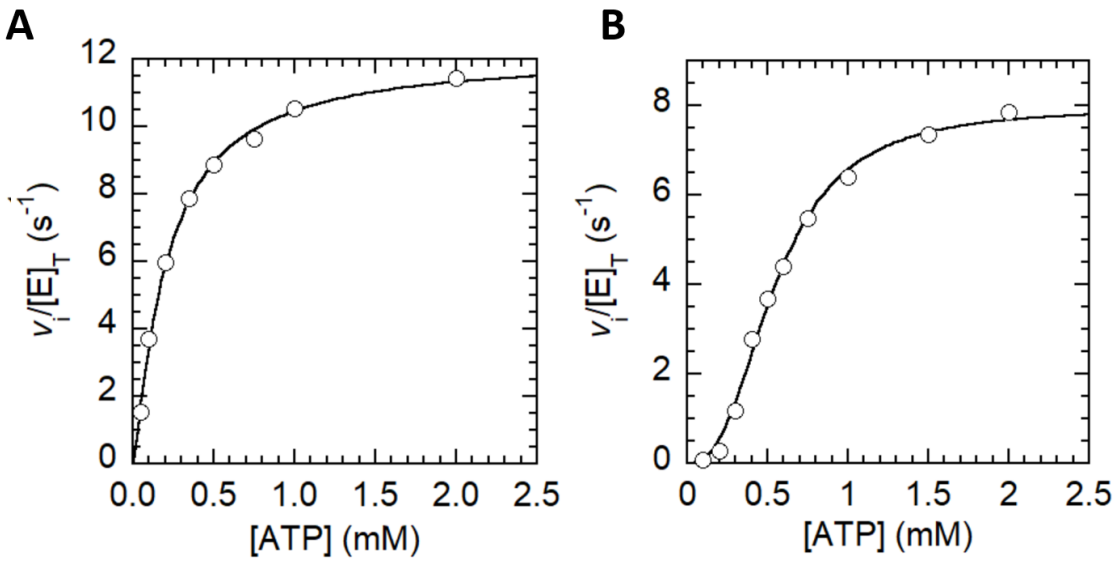

Figure 3.1. Representative plots for the kinetic characterization of ATP-dependent *ec*CTPS activity. Dependence of the Gln-dependent (**A**) and NH_3-dependent (**B**) formation of CTP on the concentration of ATP. All other substrates were at saturating concentrations. Eqn. 3 was fitted to the steady-state kinetic data. The k_{cat}, $[S]_{0.5}$, and n values for the Gln-dependent assay were 11.6 ± 0.6 s^{-1} and 0.21 ± 0.02 mM, and 1.18 ± 0.01 respectively. The k_{cat}, $[S]_{0.5}$, and n values for the NH_3-dependent assay were 8.0 ± 0.1 s^{-1} and 0.57 ± 0.03 mM, and 3.0 ± 0.5, respectively. The results are summarized in **Table 3.2**.

3.3.2 Inhibition of *ec*CTPS by ATPγS

IC_{50} values were determined by monitoring the rate of Gln- or exogenous NH_3-dependent CTP production in the presence of increasing amounts of ATPγS (**Figure 3.2**). The concentration of ATP was held roughly equal to the $[S]_{0.5}$ value for both Gln- or exogenous NH_3-dependent CTP production as determined previously (0.2 and 0.55 mM, respectively) (**Figure 3.2**). Eqn. 6 was fitted to the kinetic (v_i/v_o) data. All other substrates were held at saturating concentrations in accord with **Table 5.1**. For reactions using Gln as a substrate, GTP was present at 0.25 mM. The IC_{50} values were 83 μM and 671 μM for the *ec*CTPS-catalyzed Gln-dependent and NH_3-dependent reactions, respectively. Interestingly, it appears that the affinity for ATPγS is enhanced in the presence of Gln and GTP. This finding is qualitatively in agreement with the observation that the $[S]_{0.5}$ value for ATP is also lower for the Gln-dependent CTP formation relative to the $[S]_{0.5}$ value observed for the NH_3-dependent CTP formation (**Figure 3.2**).

To explore the inhibition in more detail, a full kinetic study was conducted to determine the mode of inhibition and the value of the inhibitor constant (K_i). A competitive inhibition pattern was observed with respect to ATP upon replotting the initial velocity data in a double reciprocal plot, wherein the lines of best fit intersected on the $1/v_i$ axis (**Figure 3.3**). The apparent $\frac{[S]_{0.5}}{V_{max}}$ values, corresponding to the slopes of these lines (but derived from non-linear regression analysis of the Michaelis-Menten plot in **Figure 3.3A**) were replotted against concentration of ATPγS to determine the K_i value. Interestingly, the NH_3-dependent CTP production demonstrated cooperativity and eqn. 3 was fitted to the initial velocity data. Again, a competitive inhibition pattern was observed with respect to ATP upon replotting the initial velocity data in a double

reciprocal plot. The apparent $\frac{[S]_{0.5}{}^{n}}{V_{max}}$ values, (but derived from non-linear regression analysis of the Michaelis-Menten plot in **Figure 3.4A**) were replotted against the concentration of ATPγS to determine the K_i value.

The K_i values reveal that the binding affinity of ATPγS is enhanced nearly 5-fold when Gln is the nitrogen source as opposed to NH_3, which is again in agreement with the increased affinity exhibited for ATP in the presence of GTP and Gln as the nitrogen source (**Figure 3.1**). This behaviour supports the notion that ATPγS is bound by *ec*CTPS in a similar manner to ATP.

Since the ATP-, UTP-, and CTP-binding sites are all located in the synthase domain, it could be expected that the binding of ATPγS would have little effect on the rate of Gln hydrolysis, which occurs at the glutaminase domain. However, as mentioned in the **Chapter 3.1**, when *ec*CTPS is incubated in the presence of GTP, UTP and ADPNP there is an increase in glutaminase activity rates arising from the presence of the nucleotides (Levitzki & Koshland, 1972b). In contrast, in *L. lactis* CTPS, k_{cat} values for the uncoupled glutaminase activity in the presence of ATPγS do not reach the same level as Gln hydrolysis coupled to CTP synthesis (Willemoës & Sigurskjold, 2002). Had studies been conducted to determine the inhibitory effects of ATPγS on only the glutaminase activity of *ec*CTPS in absence of UTP, it is possible that there would be minimal difference between uncoupled glutaminase activity and CTP production in the presence of UTP and ATP, similar to what was observed by Levitzki and Koshland (Levitzki & Koshland, 1972b).

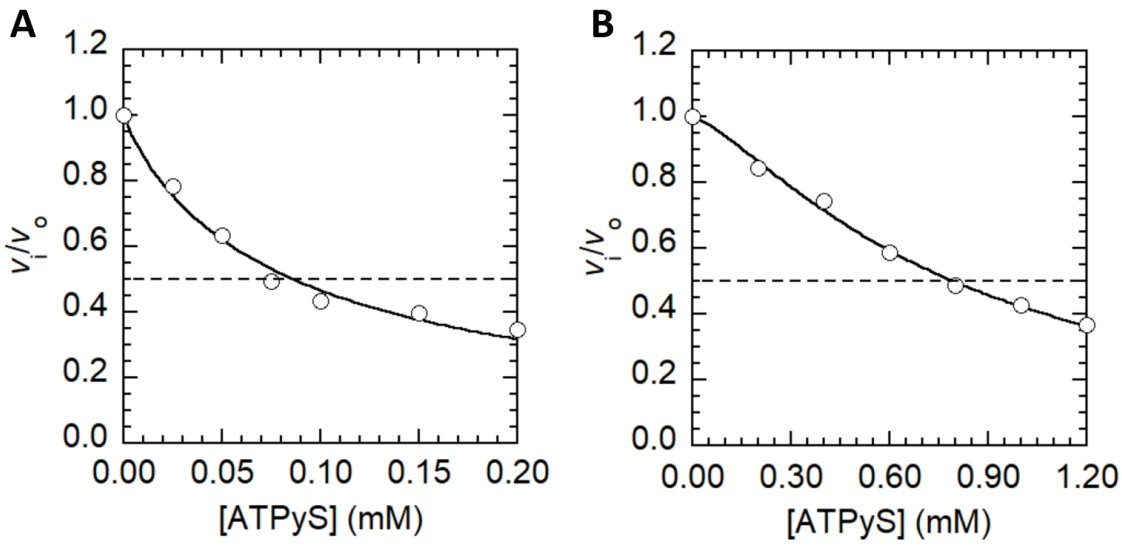

Figure 3.2. Representative plots of the ATPγS-dependent inhibition of *ec*CTPS activity. ATPγS-dependent inhibition of *ec*CTPS-catalyzed formation of CTP with Gln (**A**) or NH_3 (**B**) as the nitrogen source. The concentration of ATP was maintained at a constant concentration of 0.2 mM and 0.55 mM for the Gln and NH_3 reactions respectively. All other substrates were at saturating conditions in accordance with **Table 5.1**. Eqn. 6 was fitted to the steady-state kinetic data. The IC_{50}^{Gln} and *n* values were 83 ± 16 μM and 0.9 ± 0.1 respectively. The IC_{50}^{NH3} and *n* values were 671 ± 99 μM and 1.3 ± 0.2 respectively. The results are summarized in **Table 3.2**.

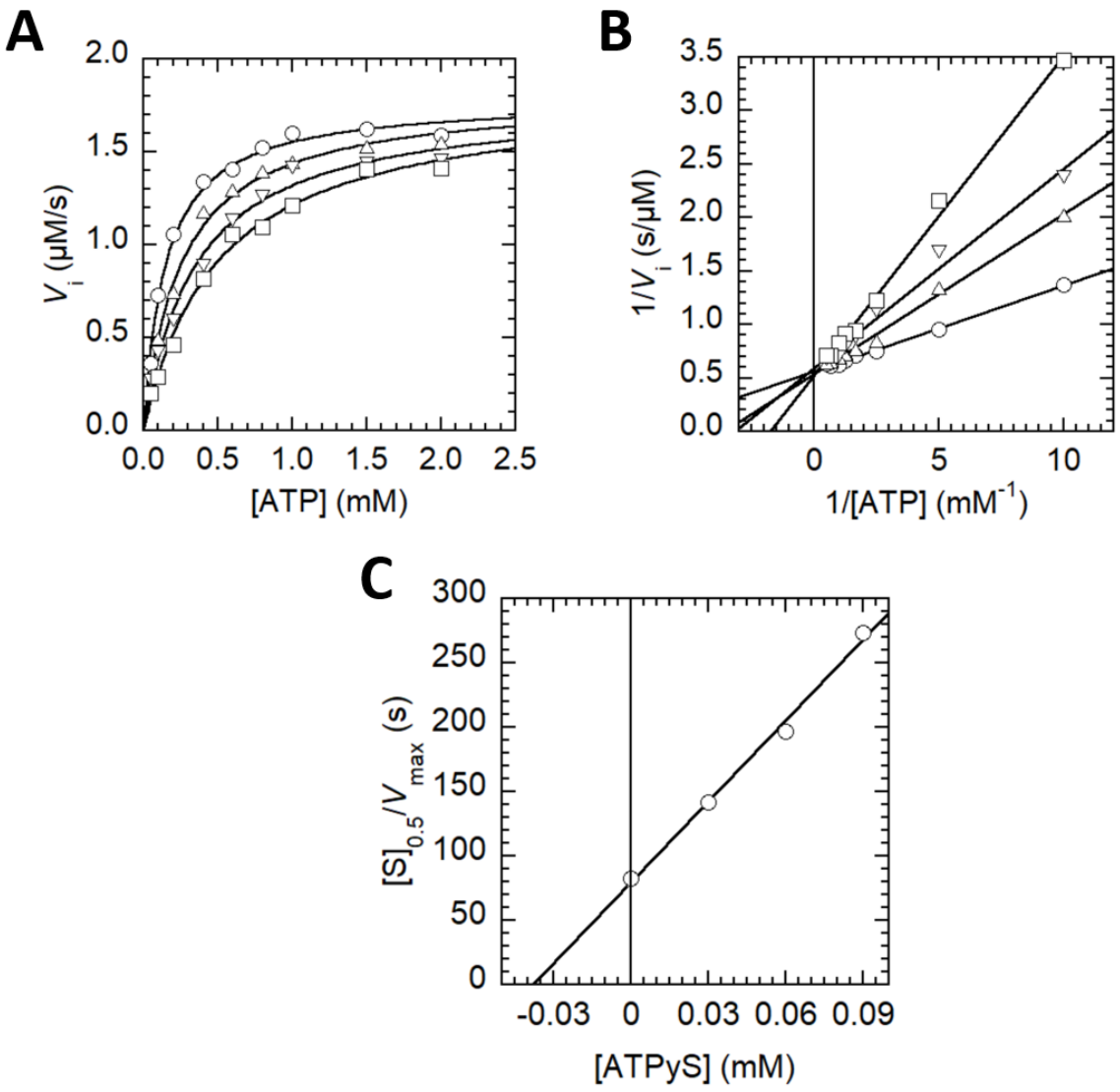

Figure 3.3. Representative plots of the competitive inhibition of Gln-dependent CTP formation by ATPγS. ATP-dependent CTPS activity was assayed with various concentrations of ATPγS (0 (○), 0.03 (△), 0.06 (▽), and 0.09 (□) mM). The data were plotted as a Michaelis-Menten plot (**A**), to which eqn. 2 was fitted. Data were plotted as a double reciprocal plot to which eqn. 7 was fitted (**B**). Apparent $\frac{[S]_{0.5}}{V_{max}}$ values replotted against the concentration of ATPγS (**C**). The K_i value was determined to be 36.1 ± 1.7 μM. The results are summarized in **Table 3.2**.

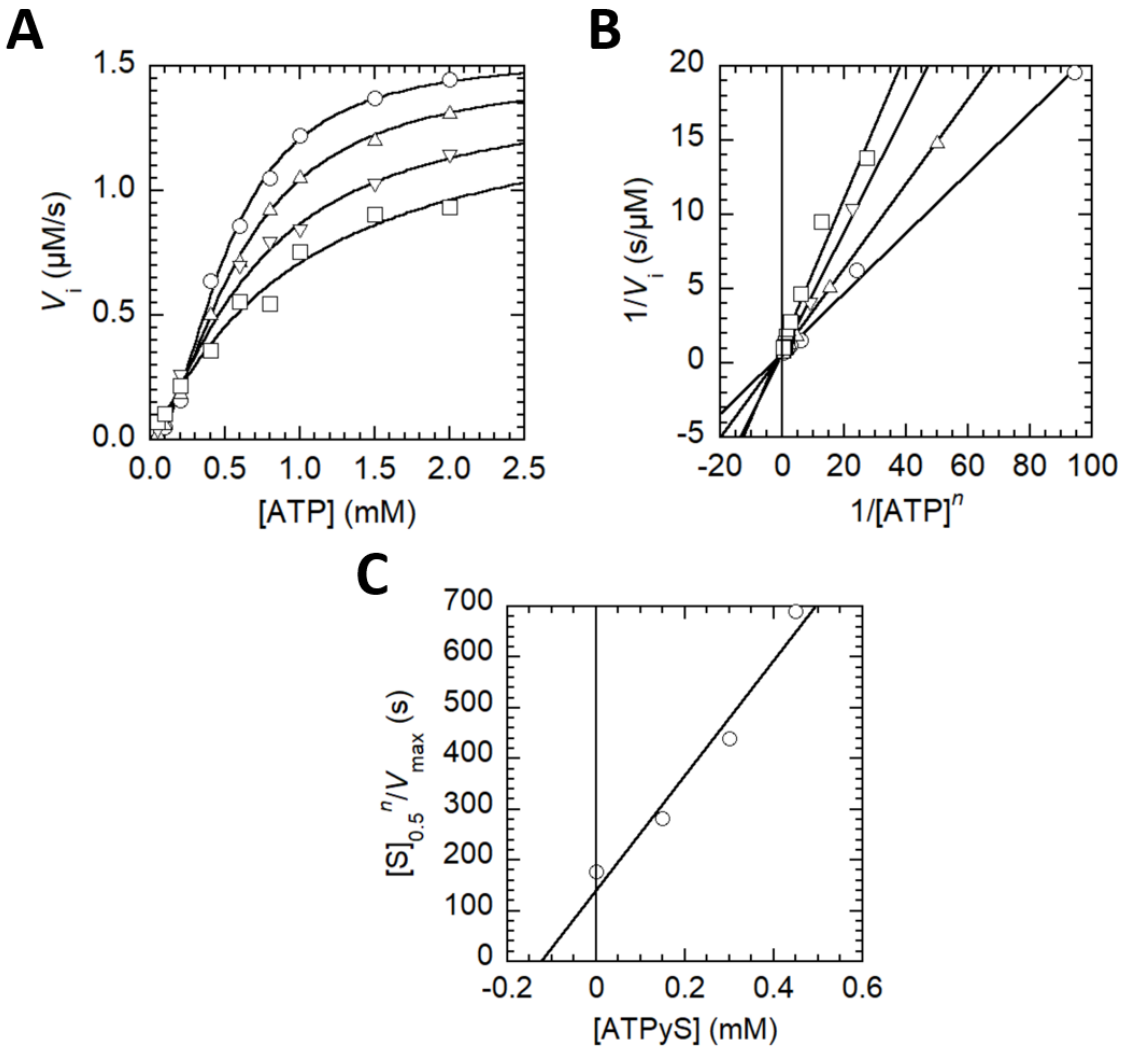

Figure 3.4. Representative plots of the competitive inhibition of NH_3-dependent CTP formation by ATPγS. ATP-dependent CTPS activity was assayed with various concentrations of ATPγS (0 (○), 0.15 (△), 0.3 (▽), and 0.45 (□) mM). The data were plotted as a Michaelis-Menten plot (**A**), to which eqn. 3 was fitted. Data were plotted as a double reciprocal plot, to which eqn. 8 was fitted (**B**). Apparent $\frac{[S]_{0.5}{}^n}{V_{max}}$ values replotted against the concentration of ATPγS (**C**). The K_i value was determined to be 170 ± 39 μM. The results are summarized in **Table 3.2**.

Table 3.2. Kinetic parameters for ATP-dependent activity and the inhibition of *ec*CTPS by ATPγS

Nitrogen source	Kinetic Parameters						
	ATP-dependent activity				Inhibition by ATPγS		
	k_{cat} (s^{-1})	$[S]_{0.5}$ (mM)	$k_{cat}/[S]_{0.5}$ (s^{-1} mM^{-1})	*n*	IC_{50} (μM)	*n*	K_i (μM)
Gln	11.6 ± 0.6[a]	0.21 ± 0.02[a]	55.2 ± 6.0	1.18 ± 0.01[a]	83 ± 16[b]	0.9 ± 0.1[b]	36.1 ± 1.7
NH_3	8.0 ± 0.1[a]	0.57 ± 0.03[a]	14.13 ± 0.75	3.0 ± 0.5[a]	671 ± 99[b]	1.3 ± 0.2[b]	170 ± 39

[a] Values from **Table 2.2**

[b] The concentration of ATP was held roughly equal to $[S]_{0.5}$ (i.e., 0.20 mM (Gln) and 0.55 mM (NH_3)).

3.3.3 Effects of ATPγS on Filament Formation by *ec*CTPS

CTP induces filament formation in *ec*CTPS as illustrated in **Figure 3.5 panel A**. Despite the inhibition of *ec*CTPS activity by ATPγS, it alone cannot induce filament formation. Indeed, the majority of structures observed by transmission electron microscopy were small and round shaped, possibly indicating the presence of tetramers (**Figure 3.5, Panel B**). Previous studies have revealed that CTP-dependent filament formation is hindered by the addition of substrate UTP (McCluskey & Bearne, 2018a). However, neither ATP nor ATPγS disrupted CTP-dependent filament formation at concentrations of 2.0 mM as illustrated in **Figure 3.5**, **panels C and D,** respectively. No apparent changes in size or abundance of the filaments were observed for the *ec*CTPS sample treated with CTP alone (**Figure 3.5**, **Panel A**), relative to the samples treated with CTP and ATP or CTP and ATPγS (**Figure 3.5**, **panels C and D,** respectively).

CTP and UTP share an overlapping binding site for their 5′-triphosphate moieties in the synthase domain of *ec*CTPS (Endrizzi *et al*., 2004). Levitzki and Koshland initially proposed that UTP or ATP must be present for the transition of the enzyme from a dimer to a tetramer (Levitzki & Koshland, 1972a), however, others found that CTP alone can induce formation of tetramers (Han *et al*., 2005). Gitai and colleagues (Ingerson-Mahar *et al*., 2010) discovered filamentous CTPS in *Caulobacter crescentus* in the presence of ATP, UTP, GTP and Gln. This was later attributed to the production of CTP during the incubation period (Barry *et al*., 2014). Gitai and colleagues (Barry *et al*., 2014) suggested that polymerized enzyme is disrupted by binding its substrates ATP and UTP; however, McCluskey and Bearne (McCluskey & Bearne, 2018a) found that UTP alone was sufficient to disassemble filaments. Despite the ATP-binding site also being located at the

synthase domain, the binding of ATP or ATPγS does not impede filament formation. ATPγS inhibits the enzyme, rendering it incapable of catalyzing the conversion of UTP to CTP, however, all active sites are solvent accessible (Barry *et al*., 2014), indicating that ATPγS and CTP are not mutually exclusive binders of *ec*CTPS. This is reflected in **Figure 3.5, panel D**, in which ATPγS did not disrupt filament size or abundance.

As discussed in more detail in **Chapters 1.6** and **4**, there are two discrete segments that constitute the filament assembly contacts: the linker region α-helix 274–284, and the short α-helix 330–336 of the glutaminase domain (Barry *et al*., 2014). None of these residues are in direct contact with bound ADP in the *ec*CTPS crystal structures, consistent with the observation that ATP and ATPγS have no apparent effect on polymerization. Analysis of an *ec*CTPS•ATPγS complex may offer new information on the action of ATP-mediated activation of the UTP molecule in the synthase domain.

Recently, researchers have discovered a second CTP-binding site that overlaps the ATP-binding site in hCTPS1, hCTPS2, and *dm*CTPS (Lynch *et al.*, 2021; X. Zhou *et al*., 2021). Kollman and colleagues (Lynch *et al*., 2021) were able to selectively target hCTPS1 and hCTPS2 using a family of small molecule inhibitors targeting the second CTP-binding site. Despite *ec*CTPS sharing 40% amino acid sequence identify and 60% similarity, to hCTPS1 (Endrizzi *et al*., 2004), CTP has not been observed in this second site in existing crystal structures of CTP-bound *ec*CTPS (Endrizzi *et al*., 2005; Lynch *et al*., 2017). The apparent absence of a secondary CTP-binding site is likely due to various amino acid substitutions in the *E. coli* enzyme, including K306, which is proposed to clash with CTP (Lynch *et al*., 2021).

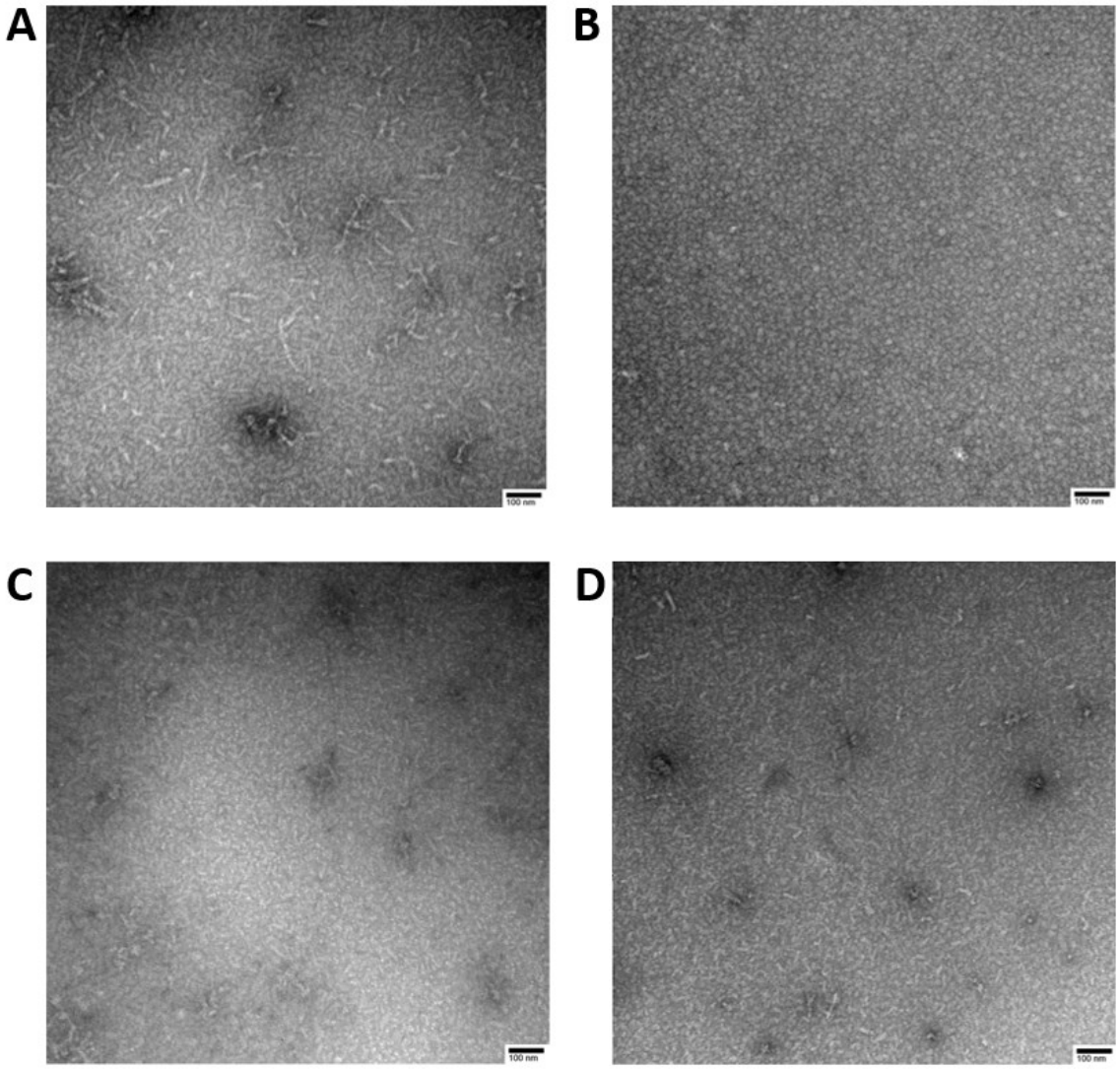

Figure 3.5. Effects of CTP, ATP, and ATPγS on filament formation by *ec*CTPS. (**A**) CTP induces filament formation by *ec*CTPS. (**B**) ATPγS is unable to induce filament formation alone. Addition of ATP (**C**) or ATPγS (**D**) to CTP has no apparent effect on CTP-dependent filament abundance or size. Concentrations of CTP, ATP, and ATPγS are all 2.0 mM.

3.4 CONCLUSIONS AND FUTURE DIRECTION

ATPγS was assessed as a ligand of *ec*CTPS and found to be a competitive inhibitor with respect to ATP. IC_{50} values were determined by monitoring the rate of Gln- or exogenous NH_3-dependent CTP production in the presence of increasing amounts of ATPγS. The binding affinity of *ec*CTPS to ATPγS was enhanced in the presence of Gln and GTP (**Figure 3.2**), in agreement with the observation that the $[S]_{0.5}$ value for ATP was also lower with Gln-dependent CTP formation relative to the $[S]_{0.5}$ value observed with NH_3-dependent CTP formation (**Table 3.2**). Further inhibition studies revealed that ATPγS was a competitive inhibitor of *ec*CTPS with respect to ATP, supporting the notion that ATPγS is bound by *ec*CTPS in a similar manner to ATP. The K_i value with respect to ATP when Gln was utilized as the nitrogen source was estimated to be 36.1 ± 1.7 μM (**Figure 3.3**), ~12-fold less than the most potent *ec*CTPS inhibitor to date (dF-dCTP), which has a K_i value of 3.0 ± 0.1 μM with respect to UTP. Despite the inhibition of *ec*CTPS activity by ATPγS, it alone cannot induce filament formation (**Figure 3.5**). An analysis of ATPγS-bound *ec*CTPS crystal structures is of interest, as it could reveal considerable information on the basis by which ATPγS inhibits *ec*CTPS with such potency and the positioning of the γ-phosphate transfer to active the bound UTP molecule.

CHAPTER 4: KINETIC CHARACTERIZATION AND INHIBITION OF C268A *ec*CTPS VARIANT BY CTP AND dF-dCTP

4.1 INTRODUCTION

As discussed in **Chapter 1.6**, one of the ways that CTPS responds to cellular metabolic demands for CTP is by forming filamentous structures composed of tetramers. *ec*CTPS, the two isoforms of human CTPS (hCTPS1 and hCTPS2), and *dm*CTPS undergo global conformational changes upon transitioning from tetrameric to filamentous states (Lynch *et al.*, 2017; Lynch & Kollman, 2020; X. Zhou *et al*., 2021; Zhou *et al*., 2019). The interdomain linker (residues 267-286) was recently proposed to play a role in facilitating the stacking of the tetramers into the filamentous state (Lynch *et al*., 2017). This stacking of the tetramers is facilitated by interaction of α-helical secondary structure elements, specifically α-helix 274-284 of the linker segment and α-helix 330-336 of the glutaminase domain (**Figure 4.1**). (Endrizzi *et al*., 2005; Lynch *et al*., 2017). Although there have been several investigations of the effect of amino acid substitutions in the glutaminase domain (Willemoës *et al*., 2005), the synthase domain (McCluskey & Bearne, 2018a), and the ammonia tunnel (Lunn & Bearne, 2004; McCluskey & Bearne, 2018a, 2018b), few investigations have been conducted in the interdomain linker.

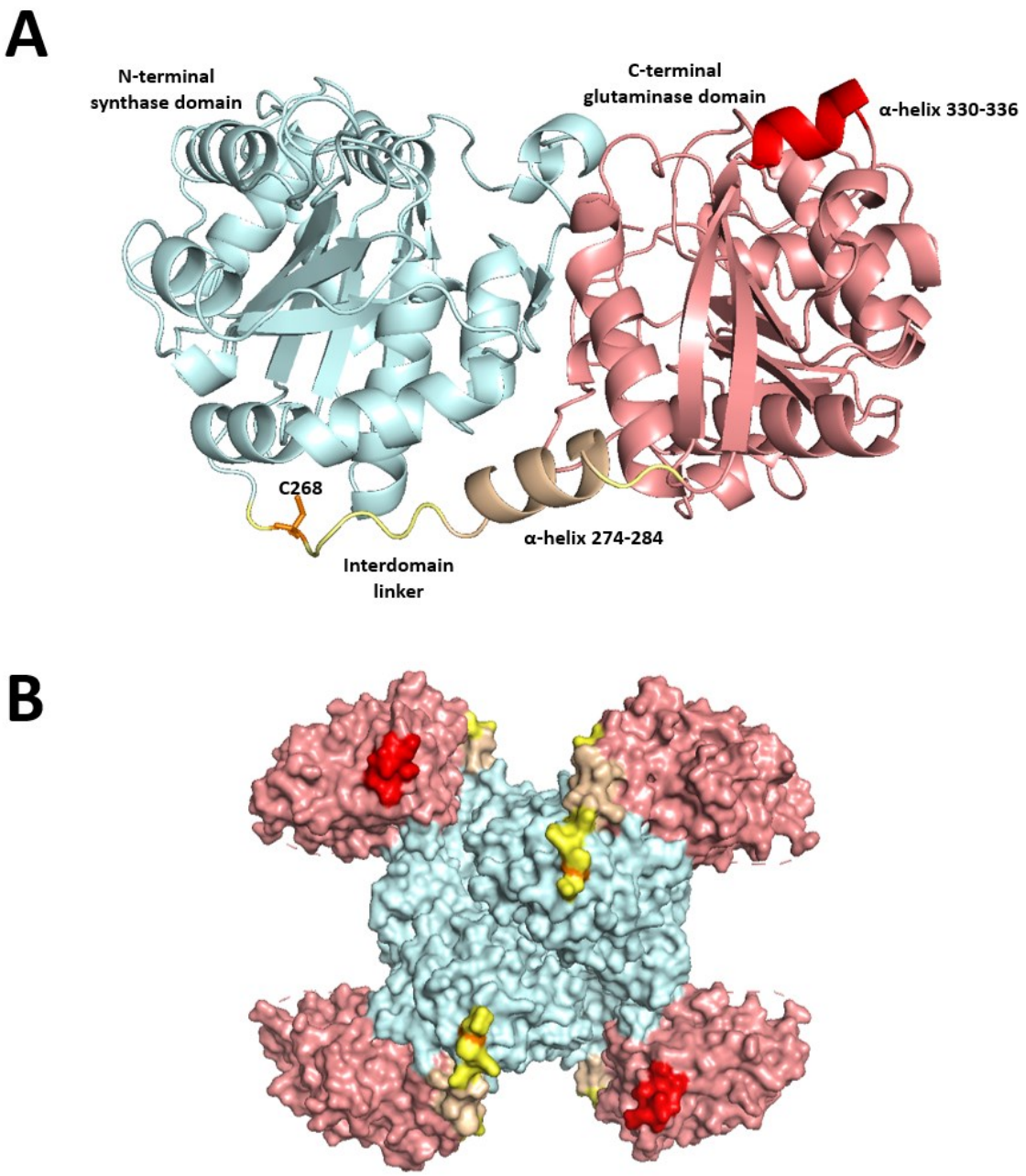

Figure 4.1. Structure of CTP-bound *ec*CTPS highlighting the linker region. The X-ray crystal structure of monomeric (**A**) and tetrameric (surface representation) (**B**) wild-type *ec*CTPS highlighting the N-terminal synthase domain (residues 1-266, light cyan), the C-terminal glutaminase domain (residues 287-544, salmon), the interdomain linker (residues 267-286, yellow), residue C268 (orange), α-helix 274-284 of the interdomain linker (wheat), and α-helix 330-336 of the glutaminase domain (red). (PDB: 7R64, unpublished). Images were rendered using PyMOL v. 2.3.2.

In the CTP-bound tetramer, the subunit interface is altered relative to the apoenzyme tetramer structures, compacting the CTPS subunits more tightly around the bound CTP (Endrizzi *et al*., 2004, 2005). The compaction of subunits was even more pronounced in the tetramers comprising CTPS filaments (Lynch *et al*., 2017). It was previously unknown whether this alteration of the tetramer interface was initiating polymerization or resulting from filament assembly. Kollman and colleagues (Lynch *et al*., 2017) solved the X-ray crystal structure of the complex of the C268A *ec*CTPS variant with bound CTP (PDB: 5TKV) and this structure revealed a tetramer with a state of compaction nearly identical to that observed for the tetramers comprising the filament of *ec*CTPS with bound CTP (PDB: 7R64, unpublished). The conformational changes between the CTP-bound C268A *ec*CTPS structure and wild-type apo state are largely rigid body motions, wherein the subunits in each state were structurally very similar (Lynch *et al*., 2017). The primary exception was a 3.6-Å shift of helix 218-228 closer to the bound CTP on an adjacent monomer, such that Phe 227 packs against the pyrimidine moiety of CTP (Lynch *et al*., 2017). This shift in the position of the helix stabilizes the filament conformation by repositioning Asn 229 at the base of helix 218-228, thus, creating a new hydrogen bond network with Arg 158 and Glu 155 forming a salt bridge across the tetramer interface (Lynch *et al*., 2017). These changes alter the relative orientations of the polymerization interfaces and positions them to allow assembly only in the CTP-bound state, consequently, supporting the notion that CTP binding allosterically controls *ec*CTPS filament assembly by directly inducing a filament-competent conformation of *ec*CTPS (Lynch *et al*., 2017). Despite differences in the

conformational changes aforementioned, Kollman reported identical k_{cat} and CTP inhibition effects for both the C268A and wild-type *ec*CTPS variants.

Due to its critical role in nucleotide metabolism, CTPS has been recognized as a therapeutic target for the development of antiviral (De Clercq, 1993; Kang *et al*., 1989), anticancer (Endrizzi *et al*., 2004; Kizaki *et al*., 1985; Kizaki *et al*., 1980; Williams *et al*., 1978), and immunosuppressive agents (Lynch *et al*., 2021; Martin *et al*., 2014). CTPS exhibits feedback inhibition by the product. Indeed, CTP inhibits *ec*CTPS with an IC_{50} of 107 ± 4 μM (**Table 2.2**). Pyrimidine analogues such as CPEC-5′-triphosphate (IC_{50} ~6 μM) (Kang *et al*., 1989) inhibit CTPS and are particularly effective at inhibiting CTPS when used in combination with other cytidine analogues (Bierau *et al*., 2003; Verschuur *et al*., 2004). As discussed in **Chapter 2.**1, by inhibiting CTPS activity, CPEC-5′-triphosphate reduces CTP pools, thereby promoting the incorporation of cytidine analogues into DNA and inhibiting DNA synthesis (Verschuur *et al*., 2002). However, resistance to CPEC has been observed in cancer cells with adaptations that reduce the feedback inhibition by CTP and other analogues (Blaney *et al*., 1993; Zhang *et al*., 1993) Furthermore, cardiotoxic effects have been observed in clinical trials (Schimmel *et al*., 2007). Other CTP analogues have also been explored as CTPS inhibitors with the most potent, to date, being dF-dCTP (IC_{50} ~1.2 μM (McCluskey *et al*., 2016)). Unlike CPEC, gemcitabine is commonly used for the treatment of solid tumours and tends to be well tolerated (Heinemann *et al*., 1995; Toschi *et al*., 2005).

McCluskey and Bearne (McCluskey & Bearne, 2018a) proposed that the potent inhibition of *ec*CTPS by dF-dCTP was likely due to interactions between the 2′-*arabino* fluorine group and a hydrophobic pocket formed by residues Q114, V115, and I116 on an

interdigitating loop from an adjacent subunit that forms part of the CTP-binding site. Additionally, dF-dCTP induces inhibitory filament formation at a lower concentration than CTP (McCluskey & Bearne, 2018a). McCluskey and Bearne (McCluskey & Bearne, 2018a) also found that substitutions of Phe 227 (F227A and F227L) obviated the ability of resulting variants to undergo large scale filament assembly, supporting the role of Phe 227 as a 'sensor' of CTP that promotes filament assembly. Further investigations on the origins of the potent inhibition of dF-dCTP by *ec*CTPS included solving the tetrameric structures of *ec*CTPS in complex with CTP (2.0 Å), 2′-*ribo*-F-dCTP (2.0 Å), 2′-*arabino*-F-CTP (2.3-Å), dF-dCTP (2.2 Å), dF-dCTP and ADP (2.1 Å), and dF-dCTP and ATP (2.6 Å) at the indicated resolutions (McLeod *et al*., unpublished).

In this chapter, we characterize the C268A *ec*CTPS variant with respect to its kinetic parameters (k_{cat}, K_m) and inhibition by CTP and dF-dCTP. This information, along with the structural information, provides insights into the structural basis by which dF-dCTP inhibits *ec*CTPS with such potency and induces formation of a filament-competent conformation.

Table 4.1. Structures of CTP and fluorinated analogues

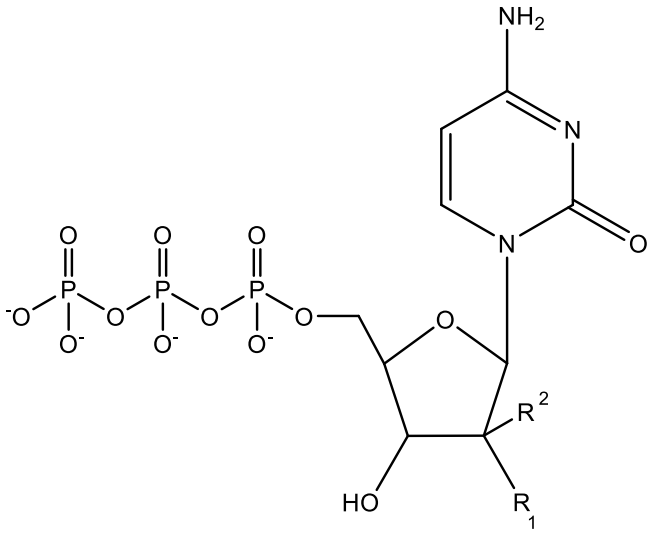	**R_1**	**R_2**
CTP	OH	H
arabinocytidine-5′-triphosphate (araCTP)	H	OH
2′-fluoro-2′-deoxycytidine-5′-triphosphate (F-dCTP)	F	H
2′-fluoro-2′- deoxyarabinocytidine-5′-triphosphate (F-araCTP)	H	F
gemcitabine-5′-triphosphate (dF-dCTP)	F	F

4.2 MATERIALS AND METHODS

All materials are described in **Chapter 5.1**. All methods follow those described in **Chapter 5** unless otherwise stated.

4.2.1 Site-directed Mutagenesis

The pET-15b-CTPS1 plasmid (Bearne *et al*., 2001) containing the open reading frame encoding *ec*CTPS was used as the template for site-directed mutagenesis, following a protocol similar to that described for the Q5 mutagenesis kit (New England BioLabs) following the inverse PCR-based method (Dominy & Andrews, 2003). Reactions were conducted using Phusion High-Fidelity DNA Polymerase (New England Biolabs). The forward (F) and reverse (R) synthetic deoxyoligonucleotide primers used to incorporate the mutation into the open reading frame were 5′-CTTAAACGC**A**CCGGAAGCGAATCTG-3′ (F) and 5′-CTGAATCGTTTACAAATATAATCGTC-3′ (R), where the codon encoding residue 268 is underlined and the altered base is shown in boldface. Mutant plasmids were used to transform *E. coli* DH5α cells using heat shock (Greene & Sambrook, 2012), which were used for plasmid maintenance. The entire plasmid open reading frame was commercially sequenced (Robarts Research Institute, London ON) to verify that no other mutations in the nucleotide sequence were introduced.

4.2.2 Expression and Purification of Recombinant C268A *ec*CTPS

E. coli BL21(DE3) cells transformed with the pET-15b-CTPSC268A plasmid were used to produce recombinant enzyme as described in **Chapter 5.2**. The enzyme was

purified as described for wild-type *ec*CTPS, except that the Ni^{2+}-NTA column was washed stepwise with wash buffer containing 5-60 mM imidazole, then bound enzyme was eluted with buffer containing 250 mM imidazole. Protein concentrations were estimated using the Bio-Rad protein assay (Bio-Rad Laboratories, Mississauga, ON, Canada) with BSA standards.

4.2.3 Enzyme Assays

The rates of *ec*CTPS-catalyzed conversion of UTP into CTP and the associated kinetic parameters were determined as described in **Chapter 5.3**. Values of k_{cat} were calculated using the molecular weights for the His_6-tagged, recombinant enzyme monomers of 62,911 Da (wild-type) and 62,878 Da (C268A) calculated from the primary sequence using the ExPASy ProtParam program (Gasteiger *et al*., 2003). IC_{50} values for the inhibition of the wild-type and C268A *ec*CTPS variants by CTP or dF-dCTP were determined by monitoring the initial rates for the conversion of UTP to CTP with Gln (6.0 mM) as the nitrogen source, together with fixed concentrations of UTP (0.05 mM or 0.20 mM) and varying concentrations of CTP (0 – 1000 μM) or dF-dCTP (0 – 20 μM). The IC_{50} and n values were determined by fitting eqn. 6 to the relative initial velocities (v_i/v_o) obtained at the indicated concentrations using nonlinear regression analysis and the program KaleidaGraph v. 4.02 from Synergy Software. All kinetic parameters were determined in triplicate and average values are reported. The reported errors are the standard deviations.

4.3 RESULTS & DISCUSSION

4.3.1 Generation of C268A *ec*CTPS Variant

The C268A *ec*CTPS variant was purified using metal ion affinity chromatography and pure protein was obtained as indicated on the SDS-PAGE gel (**Figure 4.2**). Interestingly, the affinity of the C268A variant for the Ni^{2+}-NTA matrix was not as high as the wild-type enzyme. The C268A variant was eluted partially by the wash buffer containing 60 mM imidazole and completely by the 250 mM imidazole-containing buffer. On the other hand, more stringent conditions were required for the elution of the wild-type enzyme (i.e., typically using EDTA-containing strip buffer after the column was washed with the wash buffer containing 250 mM imidazole). This observation suggests that the C268A and wild-type *ec*CTPS variants may have different conformations that affect the exposure of the His_6-tag on these proteins.

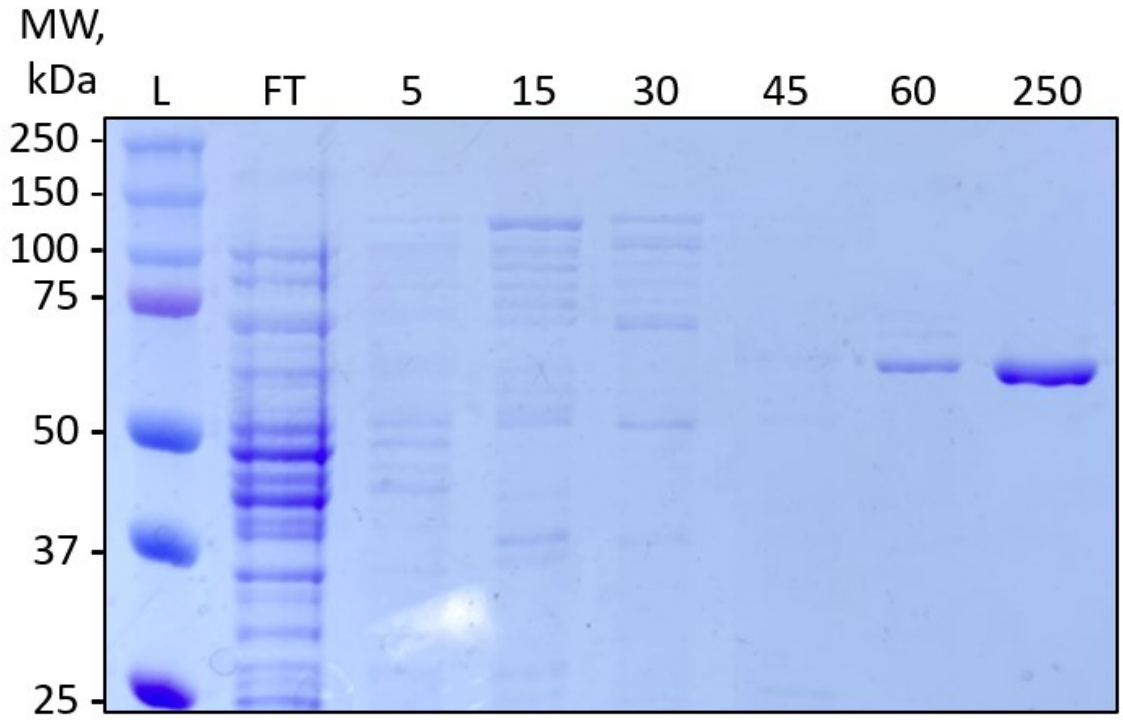

Figure 4.2. Representative 10% SDS-PAGE electrophoretogram for the purification of the *ec*CTPS C268A variant. Lane "L" corresponds to the molecular weight ladder. Lane "FT" corresponds to the flow-through of the clarified lysate. Lanes designated 5, 15, 30, 45, 60, and 250 correspond the concentration of imidazole (mM) in the wash buffer.

4.3.2 Kinetic Characterization of C268A *ec*CTPS Variant

To fully characterize the kinetic properties of the C268A *ec*CTPS variant, we assessed its turnover numbers and catalytic efficiency (k_{cat}/K_m) with Gln and NH_3 as the nitrogen sources. The k_{cat}, K_m, and catalytic efficiency values were nearly identical between the wild-type and the C268A variants (**Table 4.2, Figure 4.3**). The K_m^{Gln} is significantly lower than $K_m{}^{NH3}$ indicating the enzymes' greater binding affinity for its natural substrate and in the presence of GTP. Values of k_{cat} are comparable between Gln- and NH_3- dependent reactions for both *ec*CTPS variants. Thus, the comparison of kinetic parameters between wild-type and variant *ec*CTPS indicate that the C268A mutation has no obvious effect on catalytic activity.

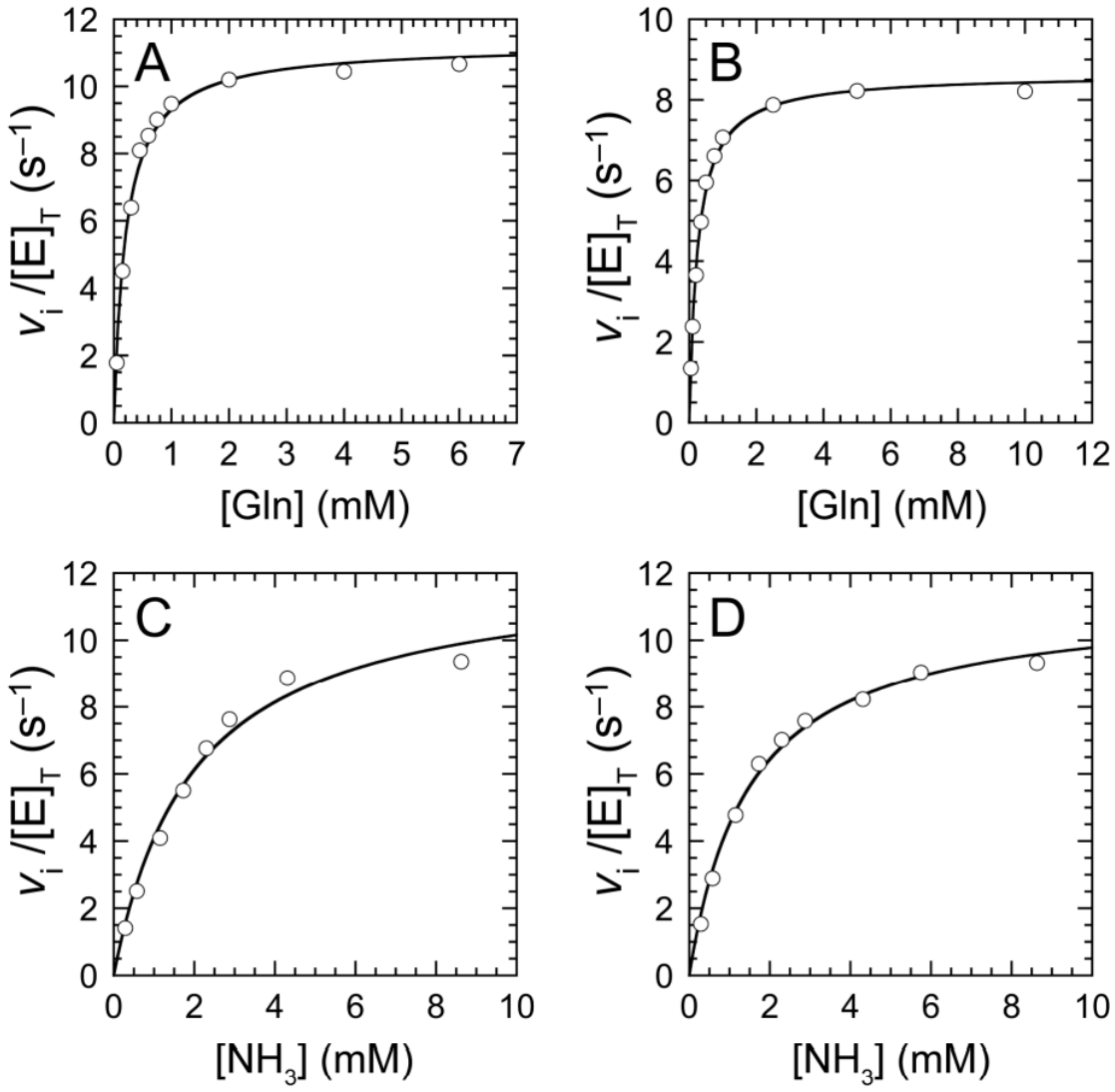

Figure 4.3. Representative Michaelis-Menten plots for the determination of the kinetic parameters for Gln- (A, B) and NH_3-dependent (C, D) CTP formation catalyzed by the wild-type (A, C) and C268A *ec*CTPS (B, D) variants. The concentrations of ATP and UTP were both fixed at 1.0 mM. The concentrations of the wild-type and C268A *ec*CTPS variants were typically 5.1– 20 μg/mL and 4.2 μg/mL, respectively. Eqn. 2 was fitted to the initial velocity data. The kinetic parameters were determined in triplicate and are given in **Table 4.2**.

Table 4.2. Kinetic parameters for Gln- and NH_3-dependent CTP formation catalyzed by wild-type and C268A *ec*CTPS variants

CTPS variant	kinetic parameters					
	Gln-dependent CTP formation			NH_3-dependent CTP formation		
	K_m (mM)	k_{cat} (s^{-1})	k_{cat}/K_m ($mM^{-1}\ s^{-1}$)	K_m (mM)	k_{cat} (s^{-1})	k_{cat}/K_m ($mM^{-1}\ s^{-1}$)
wild-type[a]	0.25 ± 0.04	11 ± 1	44 ± 12	1.7 ± 0.2	11 ± 2	6 ± 1
C268A	0.27 ± 0.02	8.8 ± 0.2	33 ± 2	1.5 ± 0.3	11.3 ± 0.4	8 ± 1

[a] Values for wild-type *ec*CTPS are in excellent agreement with those published previously (Bearne *et al*., 2001; McCluskey *et al*., 2016).

4.3.3 Inhibition of C268A *ec*CTPS Variant by CTP and dF-dCTP

The IC_{50} values and representative plots for the inhibition of wild-type *ec*CTPS and C268A *ec*CTPS variant by product CTP and dF-dCTP are presented (**Table 4.3, Figs. 4.4 and 4.5**). Since the C268A variant with bound CTP has a global conformation similar to that of the filament-like, 'closed' conformation of dF-dCTP-bound wild-type *ec*CTPS (McLeod *et al*., unpublished), one could anticipate that the C268A variant will bind dF-dCTP with increased potency relative to wild-type enzyme. However, both the wild-type and C268A *ec*CTPS variants exhibit nearly identical IC_{50} values for inhibition by CTP (**Table 4.3**), which agrees with observations made by Kollman and co-workers (Lynch *et al*., 2017). The IC_{50} values for the inhibition of wild-type *ec*CTPS by dF-dCTP (**Table 4.3**) were similar to those previously published (McCluskey *et al*., 2016) ($IC_{50}^{[UTP]\,=\,0.05\ mM}$ = 1.2 μM, $IC_{50}^{[UTP]\,=\,0.20\ mM}$ = 3.9 μM). Interestingly, dF-dCTP also inhibited both the wild-type and C268A variants to the same degree (**Table 4.3**). In addition, both CTP and dF-dCTP exhibited more potent inhibition when the concentration of UTP was held at 0.05 mM (**Figure 4.5**) rather than 0.20 mM (**Figure 4.4**), providing further evidence for the overlapping nature of the UTP- and CTP-binding sites (Endrizzi *et al*., 2005).

Holyoak and colleagues (McLeod *et al.*, unpublished) discovered structural similarities upon comparison of the filamentous wild-type *ec*CTPS-CTP co-crystal, the tetrameric C268A *ec*CTPS-CTP co-crystal, and the tetrameric wild-type *ec*CTPS-dF-dCTP co-crystal. More specifically, there were no significant differences in the binding modes of dF-dCTP to wild-type *ec*CTPS and CTP binding to C268A *ec*CTPS variant (McLeod *et al.*, unpublished). In both cases, the nucleotide was bound as the metal-

nucleotide complex, suggesting that the filament-forming competent state also allows for the preferential binding of the metal-nucleotide complex (McLeod *et al.*, unpublished). The metal-nucleotide complex slightly rearranges the CTP-binding site, which may be a reasonable explanation for the potent inhibition of *ec*CTPS by dF-dCTP. Additionally, upon comparison of structures mentioned above, Holyoak and colleagues (McLeod *et al.*, unpublished) found that there was slight movement in the position of the bound nucleotides, and an alteration of the conformation of the peptide bond for S14 such that the α-phosphate oxygens of both dF-dCTP bound to wild-type *ec*CTPS and CTP bound to C268A *ec*CTPS variant were positioned closer to S14. These observations, again, revealed similar behaviour between the C268A-CTP and wild-type-dF-dCTP complexes.

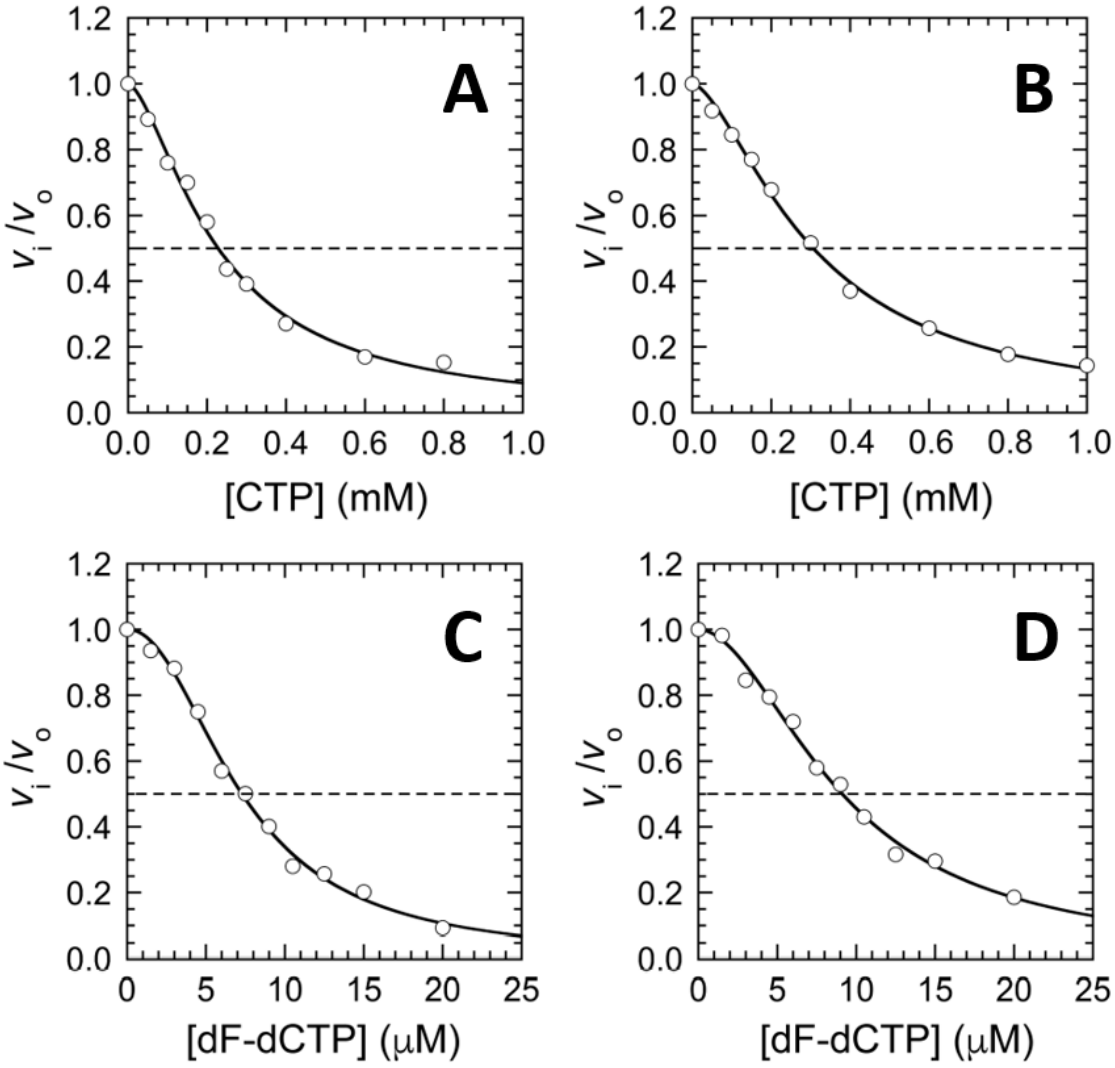

Figure 4.4. Representative plots for the determination of IC_{50} values for the inhibition of the Gln-dependent CTP formation by the wild-type (A, C) and C268A *ec*CTPS (B, D) variants by CTP (A, B) and dF-dCTP (C, D) with [UTP] = 0.20 mM. The concentration of ATP and Gln were fixed at 1.0 mM and 6.0 mM, respectively. The concentrations of the wild-type and C268A *ec*CTPS variants were 5.1– 20 and 4.2 μg/mL, respectively. The curve is a non-linear regression fit of the data to eqn. 6. The IC_{50} and *n* values were determined in triplicate and are given in **Table 4.3**.

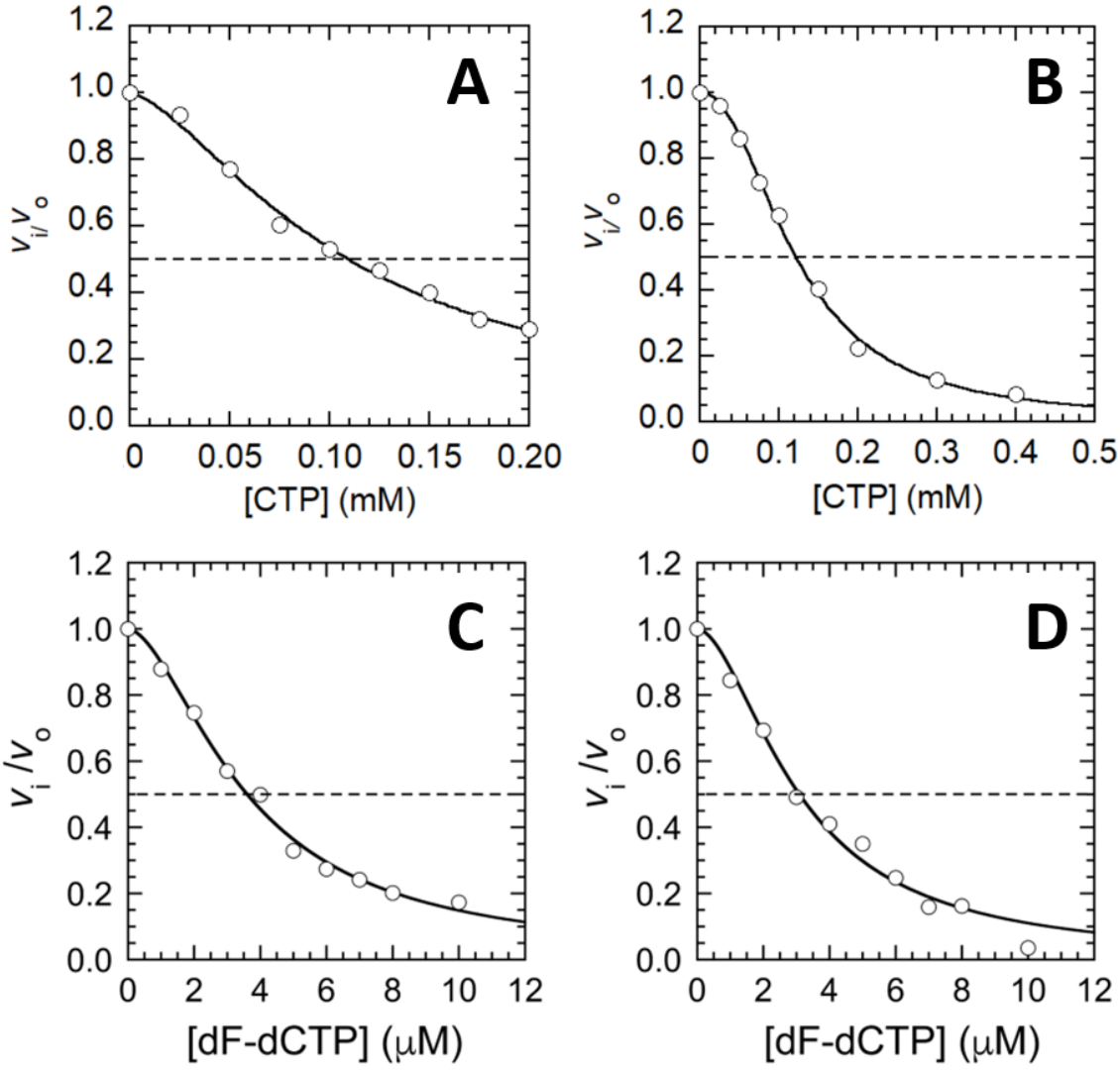

Figure 4.5. Representative plots for the determination of IC_{50} values for the inhibition of the Gln-dependent CTP formation by the wild-type (A, C) and C268A *ec*CTPS (B, D) variants by CTP (A, B) and dF-dCTP (C, D) with [UTP] = 0.05 mM. The concentration of ATP and Gln were fixed at 1.0 mM and 6.0 mM, respectively. The concentrations of the wild-type and C268A *ec*CTPS variants were 5.1 and 4.2 μg/mL, respectively. The curve is a non-linear regression fit of the data to eqn. 6. The IC_{50} and *n* values were determined in triplicate and are given in **Table 4.3**.

.

Table 4.3. IC_{50} values for the inhibition of the wild-type and C268A *ec*CTPS variants by CTP and dF-dCTP

CTPS variant	kinetic parameters							
	inhibition by CTP				inhibition by dF-dCTP			
	[UTP] = 0.05 mM		[UTP] = 0.20 mM		[UTP] = 0.05 mM		[UTP] = 0.20 mM	
	IC_{50} (µM)	*n*	IC_{50} (µM)	*n*	IC_{50} (µM)	*n*	IC_{50} (µM)	*n*
wild-type	107 ± 4	1.6 ± 0.1	234 ± 21	1.6 ± 0.1	3.8 ± 0.2	1.8 ± 0.2	7.3 ± 0.3	2.0 ± 0.1
C268A	131 ± 20	1.8 ± 0.5	259 ± 42	1.5 ± 0.1	3.2 ± 0.1	1.7 ± 0.1	9.6 ± 0.8	1.9 ± 0.2

In the C268A *ec*CTPS•CTP complex, Holyoak and colleagues (McLeod *et al.*, unpublished) noted that F227 underwent a transition from a disordered to ordered state, thereby forming a π-stacking interaction with the cytosine moiety of CTP. They observed the same F227 conformation in the *ec*CTPS•F-araCTP and *ec*CTPS•dF-CTP structures, indicating its role in the enhanced interaction of 2′-F-*arabino*-containing CTP derivatives. Holyoak *et al.* (McLeod *et al.*, unpublished) confirmed the proposal by McCluskey *et al.* (McCluskey *et al*., 2016) that this residue plays a role in mediating an enhanced binding interaction with the 2′-F-*arabino* group, specifically, through a hydrophobic pocket arising from F227 and residues on the interdigitating loop from an adjacent subunit (**Figure 4.6**) McLeod *et al.*, unpublished). Additionally, F227 has been implicated in filament formation because of a change in location concomitant with a shift of the 218-228 helix, thereby rearranging the CTP-binding pocket and subsequently promoting polymerization (Endrizzi *et al*., 2004, 2005; Lynch *et al*., 2017). Holyoak and colleagues (McLeod *et al.*, unpublished) found that the mobility of F227 in the *ec*CTPS•CTP and *ec*CTPS•F-dCTP complexes (i.e., based on diffuse electron density) is markedly reduced when a CTP analogue bearing the 2′-F-*arabino* group is present (i.e., F-ara-CTP and dF-dCTP). By stabilizing the conformation of F227 and the 218-228 helix in the filament competent state, dF-dCTP can promote filament formation more effectively than CTP. As observed in polymerization studies by McCluskey and Bearne, (McCluskey & Bearne, 2018a) dF-dCTP induced polymerization at lower concentrations than CTP and F227 variants were unable to undergo large-scale filament formation. F227 acts as a polymerization 'switch' but does not contribute to binding of CTP analogues that lack a 2′-F-*arabino* group (McCluskey & Bearne, 2018a), McLeod *et al.*,

unpublished). The C268A *ec*CTPS variant for which the tetramers preferentially assume a 'filament-like' conformation *in crystallo* (PDB: 5TKV) has the F227 side chain in the same stabilized conformation as observed for the *ec*CTPS•F-araCTP and *ec*CTPS•dF-dCTP complexes (McLeod *et al.*, unpublished). Although one might anticipate that this rearrangement of the CTP-binding site with the formation of the metal-nucleotide complex, the concomitant changes in the S14-ligand interaction distances, and the reduction of mobility of F227 in the C268A variant would play a role in the strong binding of dF-dCTP, the lack of change in the potency of inhibition of the C268A variant by both CTP and dF-dCTP relative to wild-type (**Table 4.3, Figs. 4.4, 4.5**), suggests that this is not the case.

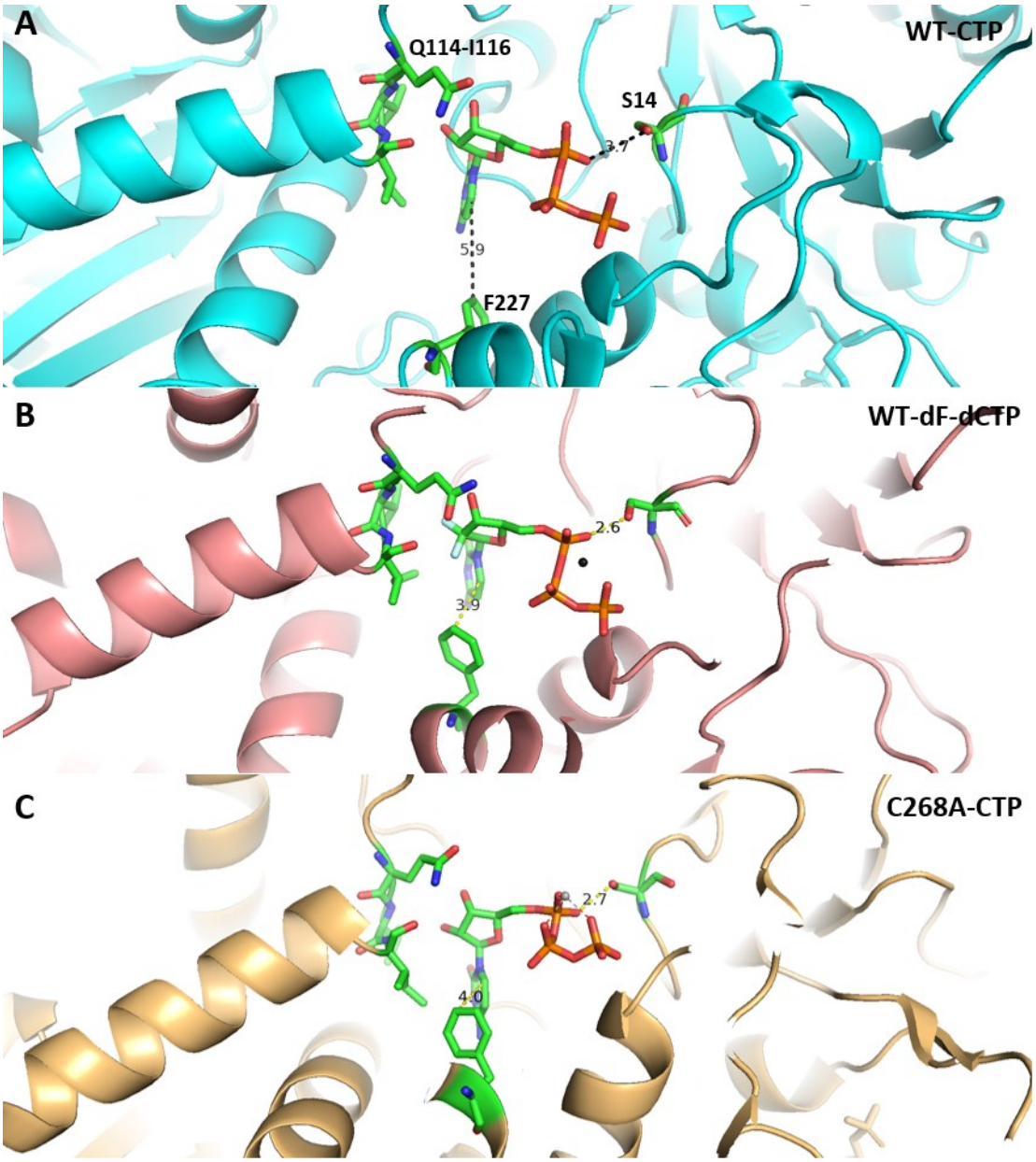

Figure 4.6. Interactions of S14, F227, and the interdigitating loop bearing Q114, V115, and I116 of wild-type *ec*CTPS with CTP (A), dF-dCTP (B), and C268A *ec*CTPS with CTP (C). Changing binding interactions observed in the CTP (**A**, cyan, PDB: 7R6E), dF-dCTP (**B**, salmon, PDB: 7R64), and C268A-CTP (**C**, bright orange, PDB: 5TKV) complexes are highlighted as yellow dashed lines. Atoms are colored as green (carbons), red (oxygen), blue (nitrogen), orange (phosphorous), light blue (fluorine), light grey (magnesium), and dark grey (sodium). The hydrophobic pocket (Q114-I116) contributing to the binding of the fluorine groups, the side chain of F227 interacting with the cytosine ring, and the side chain of S14 interacting with the α-phosphate oxygens of CTP and dF-dCTP are shown coloured by element. Interaction distances are in Å. Images were rendered using PyMOL v. 2.3.2.

4.4 CONCLUSIONS AND FUTURE DIRECTION

The open reading frame encoding the C268A *ec*CTPS variant was created using site-directed mutagenesis and overexpressed. Comparison of the kinetic parameters of the purified C268A variant with those of wild-type *ec*CTPS revealed no differences arising as a result of the amino acid substitution. Conformational changes between CTP-bound wild-type enzyme, dF-dCTP-bound wild-type enzyme and the CTP-bound C268A enzyme, namely rearrangement of CTP-binding site, changes in the S14-ligand interaction distances, and stabilization of F227, revealed striking similarities in the latter two cases. The nearly identical k_{cat}, K_m, and IC_{50} values for inhibition of wild-type and C268A variants by CTP and dF-dCTP indicate that conformational changes alone do not account for the tight-binding exhibited by dF-dCTP.

While binding of dF-dCTP to wild-type *ec*CTPS positions the S14 roughly ~1.1 Å closer to the α-phosphate oxygens of bound dF-dCTP, as it does in the structure of the C268A *ec*CTPS-CTP variant co-crystal (**Figure 4.6**), a tighter association with CTP or dF-dCTP was not observed, suggesting that this interaction does not dramatically impact binding affinity. It would be interesting to explore substitutions of this residue to further probe its role in the conformational changes accompanying binding of dF-dCTP. For example, substitution of Ser 14 by another polar uncharged amino acid with a longer side chain (e.g., S14N and S14Q) might prevent the movement of S14 such that the filament-like conformation cannot be obtained. It would be necessary, however, to also determine if failure to observe filament formation arose from inability of CTP or dF-dCTP to induce the appropriate conformational change or if the substitution simply weakened the binding affinity of CTP and dF-dCTP.

The structural basis for the inhibition of *ec*CTPS by dF-dCTP serves as framework for further inhibitor design. The 2′-*arabino* fluorine group should be exploited in the future design of small molecule inhibitors for *ec*CTPS. It would also be of interest to investigate the inhibition of the two human isoforms of CTPS by dF-dCTP and other fluorinated CTP analogues such as sofosbuvir-5′-triphosphate. The *ec*CTPS amino acid sequence shares 40% identity with human hCTPS1 and X-ray crystal structures show conservation of structurally and functionally important residues (Endrizzi *et al*., 2004; Kursula *et al*., 2006; Yamauchi *et al*., 1990). The two human isoforms share 75% sequence identity but have distinct physiological roles. hCTPS1 filaments assemble in an 'active', substrate-bound conformation (Lynch *et al*., 2017) whereas hCTPS2 filaments dynamically switch between substrate- and product-bound conformations to produce highly cooperative regulation (Lynch & Kollman, 2020). It is unknown whether dF-dCTP is capable of inducing conformational changes in hCTPS1 & 2 that promote filament formation or disassembly. Understanding the structural consequences of dF-dCTP binding to hCTPS in general may be necessary for the further development of anticancer drugs based on CTP or dF-dCTP analogues (Lynch *et al*., 2021).

CHAPTER 5: GENERAL METHODS

5.1 MATERIALS

All chemicals, unless stated otherwise, were from Sigma-Aldrich Canada Ltd. (Oakville, ON, Canada). GTP, araATP, and ribavirin-5′-triphosphate were purchased from Jena Bioscience (Jena, Germany). NaCl, Tris base, bis acrylamide, sodium bicarbonate, hydroxylamine hydrochloride, acetonitrile, and dialysis tubing were purchased from Fisher Scientific (Ottawa, ON, Canada). Tryptone, yeast extract, ampicillin, IPTG, imidazole, SDS, TEMED, and EGTA were purchased from Bishop (Burlington, ON, Canada). Sofosbuvir-5′-triphosphate (STP) was purchased from Toronto Research Chemicals (Toronto, ON, Canada) and Sierra Bioresearch (Tucson, AZ, USA). β-D-2′-deoxy-2′-α-F-2′-β-C-methyluridine was obtained from SynInnova (Edmonton, AB, Canada) and β-D-2′-deoxy-2′-α-F-2′-β-C-methylcytidine was obtained from BLDpharm (Cincinnati, OH). His·Bind resin (Novagen) was purchased from EMD Millipore (San Diego, CA, USA). Protein purification columns and APS were purchased from Bio-Rad (Mississauga, ON, Canada). For HPLC experiments, a Waters 510 pump and a controller were used for solvent delivery. Injections were made using a Rheodyne 7725i sample injector fitted with a 20-µL injection loop, and a Waters 486 absorbance detector was used to detect nucleotides. Kinetic studies were conducted using an HP 8453 UV-vis diode array spectrophotometer. Quartz cuvettes were purchased from Hellma analytics (Müllheim, Germany). High resolution (HR) electrospray ionization (ESI) mass spectra (MS) were collected using a Bruker microTOF Focus orthogonal ESI-TOF mass spectrometer instrument operating in negative mode.

^{1}H NMR spectra were obtained using a Bruker AV 500 MHz spectrometer at the Dalhousie University Nuclear Magnetic Resonance Research Resource Centre (NMR-3). Transmission electron microscopy was conducted at the Faculty of Medicine EM Core Facility at Dalhousie University. Copper 200 mesh grids (Edge Scientific, ON, Canada) were formvar and carbon-coated by Mary Ann Trevors.

5.2 EXPRESSION AND PURIFICATION OF RECOMBINANT *ec*CTPS

Wild-type *ec*CTPS was purified from *E. coli* BL21(DE3) cells transformed with the pET-15b-CTPS1 plasmid as described previously (Bearne *et al*., 2001). Inoculums were prepared by culturing *E. coli*, transformed with pET-15b-CTPS, overnight at 37 ℃ in Luria-Bertani medium (LB: 1% w/v NaCl, 1% w/v tryptone, 0.5% w/v yeast extract, pH 7.5) containing 0.1 mg/mL ampicillin. This inoculum (10 mL) was added to LB medium (1 L), and cultures were grown with shaking at 37 ℃. When the cultures obtained an OD_{600} of 0.5-0.6, gene expression was induced by the addition IPTG to a final concentration of 1.0 mM. The cultures were grown for an additional 7-8 h at 37 ℃. The cells were harvested by centrifugation (3795 × *g*) for 10 min at 4 ℃. The supernatant was discarded, and the pellet resuspended in Binding Buffer (5 mM imidazole, 0.5 M NaCl, 20 mM Tris-HCl, pH 7.9). The cells were lysed by sonication (5 × 30 s with 30 s intervals on ice) with a Branson Sonifier 250 (power setting 5). The crude lysate was clarified by centrifugation at 146550 × *g*, for 35 min, at 4 ℃.

Soluble *ec*CTPS bearing an N-terminal His_6-tag was purified by metal ion affinity chromatography using established protocols (Novagen, 1997). Fractions were collected after washing the column with 25 mL of Binding Buffer and 15 mL of Wash Buffer (60

mM imidazole, 0.5 M NaCl, 20 mM Tris-HCl pH 7.9). Elution of the desired protein was achieved with 6 mL of Strip Buffer (100 mM EDTA, 0.5 M NaCl, 20 mM Tris-HCl pH 7.9). The fraction containing CTPS was dialyzed (MWCO of 12 000 - 14 000 Da) against assay buffer (70 mM HEPES buffer, pH 8.0, containing 0.5 mM EGTA, and 10 mM $MgCl_2$), for 24 h at 4 °C. Purity of recombinant enzyme preparations were assessed using SDS-PAGE (10%) analysis, and the enzyme concentration was determined using Bradford assays conducted according to the manufacturer's directions (Bio-Rad Laboratories, Missisauga, ON) with bovine serum albumin standards. The N-terminal His_6-tag was not removed from the protein.

5.3 ENZYME ASSAYS

CTPS activity was determined at 37 °C using a continuous spectrophotometric assay as previously described (Bearne *et al*., 2001). In brief, the rate of *ec*CTPS-catalyzed conversion of UTP to CTP was measured by following the change in absorbance at 291 nm ($\Delta\varepsilon = 1331\ M^{-1}cm^{-1}$) for 60 s. Saturating conditions of substrates are summarized in **Table 5.1**. Reactions were conducted in assay buffer and typically contained *ec*CTPS (20 μg/mL) and nucleotides UTP and ATP at saturating conditions in a total volume of 0.3 mL in a 0.2-cm quartz cuvette. Enzyme and nucleotides were pre-incubated at 37 °C for 2 min followed by the addition of the ammonia source (Gln or NH_4Cl) to initiate the reaction. For reactions using NH_4Cl as the substrate (5.0-150 mM), KCl was used to maintain ionic strength at 0.25 M. The $[NH_3]$ present at pH 8.0 was calculated using a p*K*a (NH_4^+) of 9.24 (i.e., $[NH_3] = 0.0575 \cdot [NH_4Cl]_{total}$) (Iyengar & Bearne, 2003). For reactions using Gln as the substrate (0.05-6.00 mM), the concentration of GTP was

maintained at a saturating concentration. GTP-dependent activation assays were conducted using Gln (6.0 mM) as the substrate and varying the concentration of GTP (0.25-0.80 mM) with the concentrations of UTP and ATP saturating and CTPS concentrations of 14-70 μg/mL. The kinetic parameters for UTP (0 – 3.0 mM) were obtained by following Gln-dependent CTP formation with saturating concentrations of GTP and ATP, and concentrations of CTPS 60-80 μg/mL. The kinetic parameters for ATP (0 – 2.0 mM) were obtained by following Gln-dependent CTP formation with saturating concentrations of GTP and UTP, and concentrations of CTPS 60-80 μg/mL. The values of k_{cat} and K_m were determined by fitting eqn. 2 to initial velocity data using non-linear regression analysis and the program KaleidaGraph v. 4.02 from Synergy Software (Segel, 1975). Similarly, k_{cat}, $[S]_{0.5}$, and n (Hill coefficient) values for ATP, UTP, and STP as substrates were determined by fitting eqn. 3 to the corresponding initial velocity data (Koshland & Levitzki, 1974). For the activation and inhibition of CTPS by GTP, the values of K_A, k_{act}, and K_{inhib} were obtained by fitting eqn. 4 to the initial velocity data as described previously (Lunn *et al*., 2008). For the activation of CTPS by RBVNTP, the values of K_A and k_{act} were obtained by fitting eqn. 5 to the initial velocity data. Turnover numbers (k_{cat}) were calculated using the molecular weight for the His_6-tagged, recombinant enzyme monomer of 62,911 Da calculated from the primary sequence using the ExPASy ProtParam program (Gasteiger *et al*., 2003). When substrates other than Gln or NH_3 were varied, K_m was replaced with $[S]_{0.5}$. All kinetic parameters were determined in triplicate and average values are reported. The reported errors are the standard deviations.

$$v_{\mathrm{i}} = \frac{k_{\mathrm{cat}}[\mathrm{E}]_{\mathrm{T}}[\mathrm{S}]}{(K_{\mathrm{m}} + [\mathrm{S}])} \tag{2}$$

$$v_{\mathrm{i}} = \frac{k_{\mathrm{cat}}[\mathrm{E}]_{\mathrm{T}}[\mathrm{S}]^{n}}{({K_{\mathrm{m}}}^{n} + [\mathrm{S}]^{n})} \tag{3}$$

$$\frac{v_{\mathrm{i}}}{[\mathrm{E}]_{\mathrm{T}}} = \frac{k_{\mathrm{o}} + \left(\frac{k_{\mathrm{act}}[\mathrm{A}]}{K_{\mathrm{A}}}\right)}{1 + \frac{[\mathrm{A}]}{K_{\mathrm{A}}} + \left(\frac{[\mathrm{A}]}{k_{\mathrm{inhib}}}\right)^{n}} \tag{4}$$

$$\frac{v_{\mathrm{i}}}{[\mathrm{E}]_{\mathrm{T}}} = \frac{k_{\mathrm{o}} + \frac{k_{\mathrm{act}}[\mathrm{A}]}{K_{A}}}{1 + \frac{[\mathrm{A}]}{K_{\mathrm{A}}}} \tag{5}$$

Table 5.1. Saturating concentrations of *ec*CTPS substrates

Nitrogen source	substrate				
	ATP	**UTP**	**GTP**	**Gln**	**NH_4Cl**
Gln	1.0 mM	1.0 mM	0.25 mM	6.0 mM	-
NH_3	1.0 mM	1.0 mM	-	-	150 mM

5.4 INHIBITION ASSAYS

IC_{50} values were determined by monitoring the rate of Gln- or exogenous NH_3-dependent CTP production in the presence of increasing amounts of inhibitor. Typically, all ligands were maintained at saturating concentrations in accord with **Table 5.1** unless otherwise stated. Relative velocities (v_i/v_o) were fitted with curves in accord with eqn. 6 to obtain values for IC_{50} and n.

The inhibition of *ec*CTPS by various inhibitors (CTP, **Chapter 2 & 4**, N^4-OH-CTP, **Chapter 2**, ATPγS, **Chapter 3**, and dF-dCTP, **Chapter 4**) was studied. Competitive inhibition constants (K_i) were determined by following both the NH_3- and Gln-dependent formation of CTP from UTP using either Gln (6.0 mM) or NH_4Cl (150 mM) as the nitrogen source in the presence of fixed concentrations of inhibitor. Michaelis-Menten plots were constructed for each concentration of inhibitor and eqn. 2 was fitted to the Gln-dependent initial velocity data using non-linear regression analysis. Eqn. 3 was fitted to the NH_3-dependent initial velocity data using non-linear regression analysis. Lineweaver Burk (double reciprocal) plots of Gln-dependent reactions were constructed by plotting the values of $\frac{1}{v_i}$ against $\frac{1}{[S]}$ in accord with eqn. 7. The apparent $\frac{[S]_{0.5}}{V_{max}}$ values, corresponding to the slopes of these lines (but derived from non-linear regression analysis of the Michaelis-Menten plots) were replotted against concentration of inhibitor to estimate the K_i. Alternatively, for NH_3-dependent reactions, values of $\frac{1}{v_i}$ were plotted against $\frac{1}{[S]^n}$ in accord with eqn. 8. The apparent $\frac{[S]_{0.5}{}^n}{V_{max}}$ values derived from non-linear regression analysis of the Michaelis-Menten plots were replotted against the concentration of the inhibitor to estimate the K_i value.

$$\frac{v_{\mathrm{i}}}{v_{\mathrm{o}}} = \frac{{\mathrm{IC}_{50}}^{n}}{{\mathrm{IC}_{50}}^{n} + [\mathrm{I}]^{n}} \tag{6}$$

$$\frac{1}{v_i} = \frac{K_{\mathrm{m}}}{V_{\mathrm{max}}[\mathrm{S}]} + \frac{1}{V_{\mathrm{max}}} \tag{7}$$

$$\frac{1}{v_{\mathrm{i}}} = \frac{{K_{\mathrm{m}}}^{n}}{V_{\mathrm{max}}[\mathrm{S}]_{0.5}^{n}} + \frac{1}{V_{\mathrm{max}}} \tag{8}$$

5.5 ELECTRON MICROSCOPY

The ability of nucleotide analogues to induce or disrupt filament formation by *ec*CTPS was assessed by TEM using a protocol similar to those described previously (Barry *et al*., 2014; McCluskey & Bearne, 2018a). *ec*CTPS (15 μM) was incubated in assay buffer and various nucleotide-5′-triphosphates for 30 min at 37 °C. Samples were diluted 10-fold using assay buffer containing 50% glycerol before being deposited on Formvar-coated carbon grids (TAAB Laboratories, Berkshire, UK) for uranyl acetate (0.7%) staining. Negative stain transmission electron micrographs were obtained using a JEOL 1230 transmission electron microscope.

CHAPTER 6: CONCLUSIONS

In this thesis, we (i) explored the effects of specific antiviral nucleotide analogues on the activity of *ec*CTPS, as well as their effects on filament formation by *ec*CTPS, (ii) the role of ATPγS as a ligand, and (iii) the inhibition of the C268A variant of *ec*CTPS by dF-dCTP to further our understanding of how dF-dCTP inhibits *ec*CTPS activity.

The antiviral metabolites araATP and RBVNTP were recognized as a substrate and allosteric activator, respectively, although they demonstrated decreased catalytic effects relative to ATP and GTP. AraATP and RBVNTP afford possible mechanisms by which CTPS can remain active when intracellular pools of substrates are diminished and could assist in maintaining intracellular pools of CTP. STP was recognized as a substrate for amination, forming an alternative antiviral metabolite (4-NH_2-STP), which may be incorporated into the viral RNA and lead to chain termination, thereby, providing an additional explanation for the antiviral activity of sofosbuvir. Similar to UTP, STP was able to disrupt filament formation. N^4-OH-CTP was synthesized, purified, and shown to be an inhibitor of *ec*CTPS, although with decreased binding affinity relative to CTP. Similar to CTP, N^4-OH-CTP was able to induce filament formation by *ec*CTPS, suggesting that when administered as an antiviral, in addition to causing mutations in the viral genome, N^4-OH-CTP could reduce the intracellular CTP pools by inhibition of CTPS, thereby potentiating the antiviral effects of NHC. The effects that these 5′-triphosphates of specific antiviral agents have on *ec*CTPS should be considered when assessing the antiviral prodrugs for the treatment of SARS-CoV-2.

ATPγS was found to be a competitive inhibitor of *ec*CTPS. The K_i value when Gln was utilized as the nitrogen source was estimated to be 36.1 ± 1.7 μM with respect to

ATP, ~12-fold less than the most potent *ec*CTPS inhibitor to date (dF-dCTP). Despite the inhibition of *ec*CTPS activity by ATPγS, it alone cannot induce filament formation. Future investigations with ATPγS should include an analysis of the ATPγS-bound *ec*CTPS crystal structure, since it could reveal considerable information on the basis by which ATPγS inhibits *ec*CTPS.

The C268A *ec*CTPS variant was created using site-directed mutagenesis and overexpressed. Comparison of the kinetic parameters (k_{cat}, K_m, and IC_{50} values for inhibition by CTP and dF-dCTP) of the purified C268A variant with those of wild-type *ec*CTPS revealed no differences arising as a result of the amino acid substitution. This indicated that conformational changes alone do not account for the tight-binding exhibited by dF-dCTP. The structural basis for the inhibition of *ec*CTPS by dF-dCTP serves as framework for further inhibitor design.

REFERENCES

Abeles, R. H., & Beck, W. S. (1967). The mechanism of action of cobamide coenzyme in the ribonucleotide reductase reaction. *J Biol Chem*, *242*(16), 3589-3593.

Abraham, G. M., & Spooner, L. M. (2014). Sofosbuvir in the treatment of chronic hepatitis C: new dog, new tricks. *Clin Infect Dis*, *59*(3), 411-415. https://doi.org/10.1093/cid/ciu265

Agostini, M. L., Pruijssers, A. J., Chappell, J. D., Gribble, J., Lu, X., Andres, E. L., . . . Denison, M. R. (2019). Small-Molecule Antiviral β-d-N 4-Hydroxycytidine Inhibits a Proofreading-Intact Coronavirus with a High Genetic Barrier to Resistance. *J Virol*, *93*(24). https://doi.org/10.1128/JVI.01348-19

Alothaid, H., Aldughaim, M. S. K., El Bakkouri, K., AlMashhadi, S., & Al-Qahtani, A. A. (2020). Similarities between the effect of SARS-CoV-2 and HCV on the cellular level, and the possible role of ion channels in COVID19 progression: a review of potential targets for diagnosis and treatment. *Channels (Austin)*, *14*(1), 403-412. https://doi.org/10.1080/19336950.2020.1837439

Bagshaw, C. (2001). ATP analogues at a glance. *J Cell Sci*, *114*(Pt 3), 459-460.

Bakovic, M., Fullerton, M. D., & Michel, V. (2007). Metabolic and molecular aspects of ethanolamine phospholipid biosynthesis: the role of CTP:phosphoethanolamine cytidylyltransferase (Pcyt2). *Biochem Cell Biol*, *85*(3), 283-300. https://doi.org/10.1139/o07-006

Barry, R. M., Bitbol, A. F., Lorestani, A., Charles, E. J., Habrian, C. H., Hansen, J. M., . . . Gitai, Z. (2014). Large-scale filament formation inhibits the activity of CTP synthetase. *Elife*, *3*, e03638. https://doi.org/10.7554/eLife.03638

Bearne, S. L., Hekmat, O., & Macdonnell, J. E. (2001). Inhibition of *Escherichia coli* CTP synthase by glutamate gamma-semialdehyde and the role of the allosteric effector GTP in glutamine hydrolysis. *Biochem J*, *356*(Pt 1), 223-232. https://doi.org/10.1042/0264-6021:3560223

Beigel, J. H., Tomashek, K. M., Dodd, L. E., Mehta, A. K., Zingman, B. S., Kalil, A. C., . . . Members, A.-S. G. (2020). Remdesivir for the Treatment of Covid-19 - Final Report. *N Engl J Med*, *383*(19), 1813-1826. https://doi.org/10.1056/NEJMoa2007764

Bergmann, W., & Feeny, R. J. (1951). Contributions to the study of marine products; the nucleosides of sponges. *J. Org. Chem*, *16*, 981–987. https://doi.org/10.1021/jo01146a023

Bhatia, H. K., Singh, H., Grewal, N., & Natt, N. K. (2014). Sofosbuvir: A novel treatment option for chronic hepatitis C infection. *J Pharmacol Pharmacother*, *5*(4), 278-284. https://doi.org/10.4103/0976-500X.142464

Bierau, J., Van Gennip, A. H., Leen, R., Helleman, J., Caron, H. N., & Van Kuilenburg, A. B. (2003). Cyclopentenyl cytosine primes SK-N-BE(2)c neuroblastoma cells for cytarabine toxicity. *Int J Cancer*, *103*(3), 387-392. https://doi.org/10.1002/ijc.10858

Blaney, S. M., Grem, J. L., Balis, F. M., Cole, D. E., Adamson, P. C., & Poplack, D. G. (1993). Mechanism of resistance to cyclopentenyl cytosine (CPE-C) in Molt-4 lymphoblasts. *Biochem Pharmacol*, *45*(7), 1493-1501. https://doi.org/10.1016/0006-2952(93)90050-7

Bodenheimer, H. C., Lindsay, K. L., Davis, G. L., Lewis, J. H., Thung, S. N., & Seeff, L. B. (1997). Tolerance and efficacy of oral ribavirin treatment of chronic hepatitis C: a multicenter trial. *Hepatology*, *26*(2), 473-477. https://doi.org/10.1002/hep.510260231

Calise, S. J., Keppeke, G. D., Andrade, L. E., & Chan, E. K. (2015). Anti-rods/rings: a human model of drug-induced autoantibody generation. *Front Immunol*, *6*, 41. https://doi.org/10.3389/fimmu.2015.00041

Calise, S. J., Purich, D. L., Nguyen, T., Saleem, D. A., Krueger, C., Yin, J. D., & Chan, E. K. (2016). 'Rod and ring' formation from IMP dehydrogenase is regulated through the one-carbon metabolic pathway. *J Cell Sci*, *129*(15), 3042-3052. https://doi.org/10.1242/jcs.183400

Cao, B., Wang, Y., Wen, D., Liu, W., Wang, J., Fan, G., . . . Wang, C. (2020). A Trial of Lopinavir-Ritonavir in Adults Hospitalized with Severe Covid-19. *N Engl J Med*, *382*(19), 1787-1799. https://doi.org/10.1056/NEJMoa2001282

Carcamo, W. C., Calise, S. J., von Mühlen, C. A., Satoh, M., & Chan, E. K. (2014). Molecular cell biology and immunobiology of mammalian rod/ring structures. *Int Rev Cell Mol Biol*, *308*, 35-74. https://doi.org/10.1016/B978-0-12-800097-7.00002-6

Carcamo, W. C., Satoh, M., Kasahara, H., Terada, N., Hamazaki, T., Chan, J. Y., . . . Chan, E. K. (2011). Induction of cytoplasmic rods and rings structures by inhibition of the CTP and GTP synthetic pathway in mammalian cells. *PLoS One*, *6*(12), e29690. https://doi.org/10.1371/journal.pone.0029690

Ch'ien, L. T., Whitley, R. J., Alford, C. A., & Galasso, G. J. (1976). Adenine arabinoside for therapy of herpes zoster in immunosuppressed patients: preliminary results of a collaborative study. *J Infect Dis*, *133 Suppl*, A184-191. https://doi.org/10.1093/infdis/133.supplement_2.a184

Chang, C. C., Jeng, Y. M., Peng, M., Keppeke, G. D., Sung, L. Y., & Liu, J. L. (2017). CTP synthase forms the cytoophidium in human hepatocellular carcinoma. *Exp Cell Res*, *361*(2), 292-299. https://doi.org/10.1016/j.yexcr.2017.10.030

Chang, C. C., Lin, W. C., Pai, L. M., Lee, H. S., Wu, S. C., Ding, S. T., . . . Sung, L. Y. (2015). Cytoophidium assembly reflects upregulation of IMPDH activity. *J Cell Sci*, *128*(19), 3550-3555. https://doi.org/10.1242/jcs.175265

Chang, Y. F., & Carman, G. M. (2008). CTP synthetase and its role in phospholipid synthesis in the yeast *Saccharomyces cerevisiae. Prog Lipid Res*, *47*(5), 333-339. https://doi.org/10.1016/j.plipres.2008.03.004

Chien, M., Anderson, T. K., Jockusch, S., Tao, C., Li, X., Kumar, S., . . . Ju, J. (2020). Nucleotide Analogues as Inhibitors of SARS-CoV-2 Polymerase, a Key Drug Target for COVID-19. *J Proteome Res*, *19*(11), 4690-4697. https://doi.org/10.1021/acs.jproteome.0c00392

Clark, J. L., Hollecker, L., Mason, J. C., Stuyver, L. J., Tharnish, P. M., Lostia, S., . . . Pankiewicz, K. W. (2005). Design, synthesis, and antiviral activity of 2'-deoxy-2'-fluoro-2'-C-methylcytidine, a potent inhibitor of hepatitis C virus replication. *J Med Chem*, *48*(17), 5504-5508. https://doi.org/10.1021/jm0502788

Cluzel, N., Lambert, A., Maday, Y., Turinici, G., & Danchin, A. (2020). [Biochemical and statistical lessons from the evolution of the SARS-CoV-2 virus: paths for

novel antiviral warfare]. *C R Biol*, *343*(2), 177-209. https://doi.org/10.5802/crbiol.16

Cochran, J. C., Sontag, C. A., Maliga, Z., Kapoor, T. M., Correia, J. J., & Gilbert, S. P. (2004). Mechanistic analysis of the mitotic kinesin Eg5. *J Biol Chem*, *279*(37), 38861-38870. https://doi.org/10.1074/jbc.M404203200

Contreras-Sanz, A., Scott-Ward, T. S., Gill, H. S., Jacoby, J. C., Birch, R. E., Malone-Lee, J., . . . Wildman, S. S. (2012). Simultaneous quantification of 12 different nucleotides and nucleosides released from renal epithelium and in human urine samples using ion-pair reversed-phase HPLC. *Purinergic Signal*, *8*(4), 741-751. https://doi.org/10.1007/s11302-012-9321-8

Cornell, R. B., & Ridgway, N. D. (2015). CTP:phosphocholine cytidylyltransferase: Function, regulation, and structure of an amphitropic enzyme required for membrane biogenesis. *Prog Lipid Res*, *59*, 147-171. https://doi.org/10.1016/j.plipres.2015.07.001

Cox, R. M., Wolf, J. D., & Plemper, R. K. (2021). Therapeutically administered ribonucleoside analogue MK-4482/EIDD-2801 blocks SARS-CoV-2 transmission in ferrets. *Nat Microbiol*, *6*(1), 11-18. https://doi.org/10.1038/s41564-020-00835-2

Danchin, A., & Marlière, P. (2020). Cytosine drives evolution of SARS-CoV-2. *Environ Microbiol*, *22*(6), 1977-1985. https://doi.org/10.1111/1462-2920.15025

De Clercq, E. (1993). Antiviral agents: characteristic activity spectrum depending on the molecular target with which they interact. *Adv Virus Res*, *42*, 1-55. https://doi.org/10.1016/s0065-3527(08)60082-2

Decaro, N., Mari, V., Elia, G., Addie, D. D., Camero, M., Lucente, M. S., . . . Buonavoglia, C. (2010). Recombinant canine coronaviruses in dogs, Europe. *Emerg Infect Dis*, *16*(1), 41-47. https://doi.org/10.3201/eid1601.090726

Dereuddre-Bosquet, N., Roy, B., Routledge, K., Clayette, P., Foucault, G., & Lepoivre, M. (2004). Inhibitors of CTP biosynthesis potentiate the anti-human immunodeficiency virus type 1 activity of 3TC in activated peripheral blood mononuclear cells. *Antiviral Res*, *61*(1), 67-70. https://doi.org/10.1016/j.antiviral.2003.08.002

Di Bisceglie, A. M., Conjeevaram, H. S., Fried, M. W., Sallie, R., Park, Y., Yurdaydin, C., . . . Hoofnagle, J. H. (1995). Ribavirin as therapy for chronic hepatitis C. A randomized, double-blind, placebo-controlled trial. *Ann Intern Med*, *123*(12), 897-903. https://doi.org/10.7326/0003-4819-123-12-199512150-00001

Dominy, C. N., & Andrews, D. W. (2003). Site-directed mutagenesis by inverse PCR. *Methods Mol Biol*, *235*, 209-223. https://doi.org/10.1385/1-59259-409-3:209

Dusheiko, G., Main, J., Thomas, H., Reichard, O., Lee, C., Dhillon, A., . . . Weiland, O. (1996). Ribavirin treatment for patients with chronic hepatitis C: results of a placebo-controlled study. *J Hepatol*, *25*(5), 591-598. https://doi.org/10.1016/s0168-8278(96)80225-x

Elfiky, A. A. (2020a). Anti-HCV, nucleotide inhibitors, repurposing against COVID-19. *Life Sci*, *248*, 117477. https://doi.org/10.1016/j.lfs.2020.117477

Elfiky, A. A. (2020b). Ribavirin, Remdesivir, Sofosbuvir, Galidesivir, and Tenofovir against SARS-CoV-2 RNA dependent RNA polymerase (RdRp): A molecular docking study. *Life Sci*, *253*, 117592. https://doi.org/10.1016/j.lfs.2020.117592

Endrizzi, J. A., Kim, H., Anderson, P. M., & Baldwin, E. P. (2004). Crystal structure of Escherichia coli cytidine triphosphate synthetase, a nucleotide-regulated glutamine amidotransferase/ATP-dependent amidoligase fusion protein and homologue of anticancer and antiparasitic drug targets. *Biochemistry*, *43*(21), 6447-6463. https://doi.org/10.1021/bi0496945

Endrizzi, J. A., Kim, H., Anderson, P. M., & Baldwin, E. P. (2005). Mechanisms of product feedback regulation and drug resistance in cytidine triphosphate synthetases from the structure of a CTP-inhibited complex. *Biochemistry*, *44*(41), 13491-13499. https://doi.org/10.1021/bi051282o

Evans, D. R., & Guy, H. I. (2004). Mammalian pyrimidine biosynthesis: fresh insights into an ancient pathway. *J Biol Chem*, *279*(32), 33035-33038. https://doi.org/10.1074/jbc.R400007200

Falzarano, D., de Wit, E., Martellaro, C., Callison, J., Munster, V. J., & Feldmann, H. (2013). Inhibition of novel β coronavirus replication by a combination of interferon-α2b and ribavirin. *Sci Rep*, *3*, 1686. https://doi.org/10.1038/srep01686

Falzarano, D., de Wit, E., Rasmussen, A. L., Feldmann, F., Okumura, A., Scott, D. P., . . . Feldmann, H. (2013). Treatment with interferon-α2b and ribavirin improves outcome in MERS-CoV-infected *rhesus macaques*. *Nat Med*, *19*(10), 1313-1317. https://doi.org/10.1038/nm.3362

Gao, W. Y., Johns, D. G., & Mitsuya, H. (2000). Potentiation of the anti-HIV activity of zalcitabine and lamivudine by a CTP synthase inhibitor, 3-deazauridine. *Nucleosides Nucleotides Nucleic Acids*, *19*(1-2), 371-377. https://doi.org/10.1080/15257770008033015

Gasteiger, E., Gattiker, A., Hoogland, C., Ivanyi, I., Appel, R. D., & Bairoch, A. (2003). ExPASy: The proteomics server for in-depth protein knowledge and analysis. *Nucleic Acids Res*, *31*(13), 3784-3788. https://doi.org/10.1093/nar/gkg563

Gordon, C. J., Tchesnokov, E. P., Woolner, E., Perry, J. K., Feng, J. Y., Porter, D. P., & Götte, M. (2020). Remdesivir is a direct-acting antiviral that inhibits RNA-dependent RNA polymerase from severe acute respiratory syndrome coronavirus 2 with high potency. *J Biol Chem*, *295*(20), 6785-6797. https://doi.org/10.1074/jbc.RA120.013679

Goto, M., Omi, R., Hoseki, J., Nakagawa, N., Miyahara, I., & Hirotsu, K. (2003). Expression, purification and preliminary X-ray characterization of CTP synthetase from *Thermus thermophilus* HB8. *Acta Crystallogr D Biol Crystallogr*, *59*(Pt 3), 551-553. https://doi.org/10.1107/s0907444903000106

Goto, M., Omi, R., Nakagawa, N., Miyahara, I., & Hirotsu, K. (2004). Crystal structures of CTP synthetase reveal ATP, UTP, and glutamine binding sites. *Structure*, *12*(8), 1413-1423. https://doi.org/10.1016/j.str.2004.05.013

Graci, J. D., & Cameron, C. E. (2006). Mechanisms of action of ribavirin against distinct viruses. *Rev Med Virol*, *16*(1), 37-48. https://doi.org/10.1002/rmv.483

Grant, O. C., Montgomery, D., Ito, K., & Woods, R. J. (2020). Analysis of the SARS-CoV-2 spike protein glycan shield reveals implications for immune recognition. *Sci Rep*, *10*(1), 14991. https://doi.org/10.1038/s41598-020-71748-7

Greene, M. R., & Sambrook, J. (2012). Molecular Cloning: A Laboratory Manual. In (4 ed., Vol. 1, pp. 157-260): Cold Spring Harbor Laboratory Press.

Gritsenko, D., & Hughes, G. (2015). Ledipasvir/Sofosbuvir (harvoni): improving options for hepatitis C virus infection. *P T*, *40*(4), 256-276.
Habrian, C., Chandrasekhara, A., Shahrvini, B., Hua, B., Lee, J., Jesinghaus, R., . . . Baldwin, E. P. (2016). Inhibition of *Escherichia coli* CTP Synthetase by NADH and Other Nicotinamides and Their Mutual Interactions with CTP and GTP. *Biochemistry*, *55*(39), 5554-5565. https://doi.org/10.1021/acs.biochem.6b00383
Hager, P. W., Collart, F. R., Huberman, E., & Mitchell, B. S. (1995). Recombinant human inosine monophosphate dehydrogenase type I and type II proteins. Purification and characterization of inhibitor binding. *Biochem Pharmacol*, *49*(9), 1323-1329. https://doi.org/10.1016/0006-2952(95)00026-v
Han, G. S., Sreenivas, A., Choi, M. G., Chang, Y. F., Martin, S. S., Baldwin, E. P., & Carman, G. M. (2005). Expression of Human CTP synthetase in *Saccharomyces cerevisiae* reveals phosphorylation by protein kinase A. *J Biol Chem*, *280*(46), 38328-38336. https://doi.org/10.1074/jbc.M509622200
Heinemann, V., Schulz, L., Issels, R. D., & Plunkett, W. (1995). Gemcitabine: a modulator of intracellular nucleotide and deoxynucleotide metabolism. *Semin Oncol*, *22*(4 Suppl 11), 11-18.
Helmy, Y. A., Fawzy, M., Elaswad, A., Sobieh, A., Kenney, S. P., & Shehata, A. A. (2020). The COVID-19 Pandemic: A Comprehensive Review of Taxonomy, Genetics, Epidemiology, Diagnosis, Treatment, and Control. *J Clin Med*, *9*(4). https://doi.org/10.3390/jcm9041225
Hernandez-Santiago, B. I., Beltran, T., Stuyver, L., Chu, C. K., & Schinazi, R. F. (2004). Metabolism of the anti-hepatitis C virus nucleoside beta-D-N4-hydroxycytidine in different liver cells. *Antimicrob Agents Chemother*, *48*(12), 4636-4642. https://doi.org/10.1128/AAC.48.12.4636-4642.2004
Hiratsuka, T. (2003). Fluorescent and colored trinitrophenylated analogs of ATP and GTP. *Eur J Biochem*, *270*(17), 3479-3485. https://doi.org/10.1046/j.1432-1033.2003.03748.x
Hofer, A., Steverding, D., Chabes, A., Brun, R., & Thelander, L. (2001). *Trypanosoma brucei* CTP synthetase: a target for the treatment of African sleeping sickness. *Proc Natl Acad Sci U S A*, *98*(11), 6412-6416. https://doi.org/10.1073/pnas.111139498
Hung, I. F., Lung, K. C., Tso, E. Y., Liu, R., Chung, T. W., Chu, M. Y., . . . Yuen, K. Y. (2020). Triple combination of interferon beta-1b, lopinavir-ritonavir, and ribavirin in the treatment of patients admitted to hospital with COVID-19: an open-label, randomised, phase 2 trial. *Lancet*, *395*(10238), 1695-1704. https://doi.org/10.1016/S0140-6736(20)31042-4
Ianevski, A., Yao, R., Biza, S., Zusinaite, E., Mannik, A., Kivi, G., . . . Kainov, D. E. (2020). Identification and Tracking of Antiviral Drug Combinations. *Viruses*, *12*(10). https://doi.org/10.3390/v12101178
Ingerson-Mahar, M., Briegel, A., Werner, J. N., Jensen, G. J., & Gitai, Z. (2010). The metabolic enzyme CTP synthase forms cytoskeletal filaments. *Nat Cell Biol*, *12*(8), 739-746. https://doi.org/10.1038/ncb2087
Iyengar, A., & Bearne, S. L. (2003). Aspartate-107 and leucine-109 facilitate efficient coupling of glutamine hydrolysis to CTP synthesis by *Escherichia coli* CTP synthase. *Biochem J*, *369*(Pt 3), 497-507. https://doi.org/10.1042/BJ20021110

Ji, Y., Gu, J., Makhov, A. M., Griffith, J. D., & Mitchell, B. S. (2006). Regulation of the interaction of inosine monophosphate dehydrogenase with mycophenolic Acid by GTP. *J Biol Chem*, *281*(1), 206-212. https://doi.org/10.1074/jbc.M507056200

Jockusch, S., Tao, C., Li, X., Chien, M., Kumar, S., Morozova, I., . . . Ju, J. (2020). Sofosbuvir terminated RNA is more resistant to SARS-CoV-2 proofreader than RNA terminated by Remdesivir. *Sci Rep*, *10*(1), 16577. https://doi.org/10.1038/s41598-020-73641-9

Joshi, S., Parkar, J., Ansari, A., Vora, A., Talwar, D., Tiwaskar, M., . . . Barkate, H. (2020). Role of favipiravir in the treatment of COVID-19. *Int J Infect Dis*. https://doi.org/10.1016/j.ijid.2020.10.069

Ju, J., Li, X., Kumar, S., Jockusch, S., Chien, M., Tao, C., . . . Russo, J. J. (2020). Nucleotide analogues as inhibitors of SARS-CoV Polymerase. *Pharmacol Res Perspect*, *8*(6), e00674. https://doi.org/10.1002/prp2.674

Jácome, R., Campillo-Balderas, J. A., Ponce de León, S., Becerra, A., & Lazcano, A. (2020). Sofosbuvir as a potential alternative to treat the SARS-CoV-2 epidemic. *Sci Rep*, *10*(1), 9294. https://doi.org/10.1038/s41598-020-66440-9

Jørgensen, C. M., Hammer, K., & Martinussen, J. (2003). CTP limitation increases expression of CTP synthase in *Lactococcus lactis*. *J Bacteriol*, *185*(22), 6562-6574. https://doi.org/10.1128/jb.185.22.6562-6574.2003

Kang, G. J., Cooney, D. A., Moyer, J. D., Kelley, J. A., Kim, H. Y., Marquez, V. E., & Johns, D. G. (1989). Cyclopentenylcytosine triphosphate. Formation and inhibition of CTP synthetase. *J Biol Chem*, *264*(2), 713-718.

Keppeke, G. D., Calise, S. J., Chan, E. K., & Andrade, L. E. (2015). Assembly of IMPDH2-based, CTPS-based, and mixed rod/ring structures is dependent on cell type and conditions of induction. *J Genet Genomics*, *42*(6), 287-299. https://doi.org/10.1016/j.jgg.2015.04.002

Khalili, J. S., Zhu, H., Mak, N. S. A., Yan, Y., & Zhu, Y. (2020). Novel coronavirus treatment with ribavirin: Groundwork for an evaluation concerning COVID-19. *J Med Virol*, *92*(7), 740-746. https://doi.org/10.1002/jmv.25798

Kirchdoerfer, R. N., & Ward, A. B. (2019). Structure of the SARS-CoV nsp12 polymerase bound to nsp7 and nsp8 co-factors. *Nat Commun*, *10*(1), 2342. https://doi.org/10.1038/s41467-019-10280-3

Kizaki, H., Ohsaka, F., & Sakurada, T. (1985). CTP synthetase from *Ehrlich ascites* tumor cells. Subunit stoichiometry and regulation of activity. *Biochim Biophys Acta*, *829*(1), 34-43. https://doi.org/10.1016/0167-4838(85)90065-2

Kizaki, H., Williams, J. C., Morris, H. P., & Weber, G. (1980). Increased cytidine 5'-triphosphate synthetase activity in rat and human tumors. *Cancer Res*, *40*(11), 3921-3927.

Koshland, D. E., & Levitzki, A. (1974). 16. CTP Synthetase and Related Enzymes. In (Vol. 10, pp. 539-559): The Enzymes.

Kursula, P., Flodin, S., Ehn, M., Hammarström, M., Schüler, H., Nordlund, P., & Stenmark, P. (2006). Structure of the synthetase domain of human CTP synthetase, a target for anticancer therapy. *Acta Crystallogr Sect F Struct Biol Cryst Commun*, *62*(Pt 7), 613-617. https://doi.org/10.1107/S1744309106018136

Lauritsen, I., Willemoës, M., Jensen, K. F., Johansson, E., & Harris, P. (2011). Structure of the dimeric form of CTP synthase from *Sulfolobus solfataricus*. *Acta*

Crystallogr Sect F Struct Biol Cryst Commun, *67*(Pt 2), 201-208. https://doi.org/10.1107/S1744309110052334
Lee, W. W., Benitez , A., Goodman, L., & Baker, B. R. (1960). Potential anticancer agents; Synthesis of the β-anomer of 9-(D-arabinofuranosyl)-adenine. *J. Am. Chem. Soc.*, *82*, 2648–2649. https://doi.org/10.1021/ja01495a070
Levitzki, A., & Koshland, D. E. (1971). Cytidine triphosphate synthetase. Covalent intermediates and mechanisms of action. *Biochemistry*, *10*(18), 3365-3371. https://doi.org/10.1021/bi00794a008
Levitzki, A., & Koshland, D. E. (1972a). Ligand-induced dimer-to-tetramer transformation in cytosine triphosphate synthetase. *Biochemistry*, *11*(2), 247-253. https://doi.org/10.1021/bi00752a016
Levitzki, A., & Koshland, D. E. (1972b). Role of an allosteric effector. Guanosine triphosphate activation in cytosine triphosphate synthetase. *Biochemistry*, *11*(2), 241-246. https://doi.org/10.1021/bi00752a015
Lewis, D. A., & Villafranca, J. J. (1989). Investigation of the mechanism of CTP synthetase using rapid quench and isotope partitioning methods. *Biochemistry*, *28*(21), 8454-8459. https://doi.org/10.1021/bi00447a027
Li, H., Xiong, N., Li, C., Gong, Y., Liu, L., Yang, H., . . . Yin, X. (2021). Efficacy of ribavirin and interferon-α therapy for hospitalized patients with COVID-19: A multicenter, retrospective cohort study. *Int J Infect Dis*, *104*, 641-648. https://doi.org/10.1016/j.ijid.2021.01.055
Li, J. Y., You, Z., Wang, Q., Zhou, Z. J., Qiu, Y., Luo, R., & Ge, X. Y. (2020). The epidemic of 2019-novel-coronavirus (2019-nCoV) pneumonia and insights for emerging infectious diseases in the future. *Microbes Infect*, *22*(2), 80-85. https://doi.org/10.1016/j.micinf.2020.02.002
Lieberman, I. (1956). Enzymatic amination of uridine triphosphate to cytidine triphosphate. *J Biol Chem*, *222*(2), 765-775.
Lizano, E., Scheibe, M., Rammelt, C., Betat, H., & Mörl, M. (2008). A comparative analysis of CCA-adding enzymes from human and *E. coli*: differences in CCA addition and tRNA 3'-end repair. *Biochimie*, *90*(5), 762-772. https://doi.org/10.1016/j.biochi.2007.12.007
Long, C. W., & Pardee, A. B. (1967). Cytidine triphosphate synthetase of *Escherichia coli* B. I. Purification and kinetics. *J Biol Chem*, *242*(20), 4715-4721.
Lucas-Hourani, M., Dauzonne, D., Jorda, P., Cousin, G., Lupan, A., Helynck, O., . . . Vidalain, P. O. (2013). Inhibition of pyrimidine biosynthesis pathway suppresses viral growth through innate immunity. *PLoS Pathog*, *9*(10), e1003678. https://doi.org/10.1371/journal.ppat.1003678
Lunn, F. A., & Bearne, S. L. (2004). Alternative substrates for wild-type and L109A E. coli CTP synthases: kinetic evidence for a constricted ammonia tunnel. *Eur J Biochem*, *271*(21), 4204-4212. https://doi.org/10.1111/j.1432-1033.2004.04360.x
Lunn, F. A., MacDonnell, J. E., & Bearne, S. L. (2008). Structural requirements for the activation of *Escherichia coli* CTP synthase by the allosteric effector GTP are stringent, but requirements for inhibition are lax. *J Biol Chem*, *283*(4), 2010-2020. https://doi.org/10.1074/jbc.M707803200
Lynch, E. M., DiMattia, M. A., Albanese, S., van Zundert, G. C. P., Hansen, J. M., Quispe, J. D., . . . Kollman, J. M. (2021). Structural basis for isoform-specific

inhibition of human CTPS1. *Proc Natl Acad Sci U S A*, *118*(40). https://doi.org/10.1073/pnas.2107968118

Lynch, E. M., Hicks, D. R., Shepherd, M., Endrizzi, J. A., Maker, A., Hansen, J. M., . . . Kollman, J. M. (2017). Human CTP synthase filament structure reveals the active enzyme conformation. *Nat Struct Mol Biol*, *24*(6), 507-514. https://doi.org/10.1038/nsmb.3407

Lynch, E. M., & Kollman, J. M. (2020). Coupled structural transitions enable highly cooperative regulation of human CTPS2 filaments. *Nat Struct Mol Biol*, *27*(1), 42-48. https://doi.org/10.1038/s41594-019-0352-5

MacDonnell, J. E., Lunn, F. A., & Bearne, S. L. (2004). Inhibition of *E. coli* CTP synthase by the "positive" allosteric effector GTP. *Biochim Biophys Acta*, *1699*(1-2), 213-220. https://doi.org/10.1016/j.bbapap.2004.03.002

MacLeod, T. J., Lunn, F. A., & Bearne, S. L. (2006). The role of lysine residues 297 and 306 in nucleoside triphosphate regulation of *E. coli* CTP synthase: inactivation by 2',3'-dialdehyde ATP and mutational analyses. *Biochim Biophys Acta*, *1764*(2), 199-210. https://doi.org/10.1016/j.bbapap.2005.11.021

Markland, W., McQuaid, T. J., Jain, J., & Kwong, A. D. (2000). Broad-spectrum antiviral activity of the IMP dehydrogenase inhibitor VX-497: a comparison with ribavirin and demonstration of antiviral additivity with alpha interferon. *Antimicrob Agents Chemother*, *44*(4), 859-866. https://doi.org/10.1128/AAC.44.4.859-866.2000

Martin, E., Palmic, N., Sanquer, S., Lenoir, C., Hauck, F., Mongellaz, C., . . . Latour, S. (2014). CTP synthase 1 deficiency in humans reveals its central role in lymphocyte proliferation. *Nature*, *510*(7504), 288-292. https://doi.org/10.1038/nature13386

McCluskey, G. D., & Bearne, S. L. (2018a). Biophysical Analysis of Bacterial CTP Synthase Filaments Formed in the Presence of the Chemotherapeutic Metabolite Gemcitabine-5'-triphosphate. *J Mol Biol*, *430*(8), 1201-1217. https://doi.org/10.1016/j.jmb.2018.02.019

McCluskey, G. D., & Bearne, S. L. (2018b). "Pinching" the ammonia tunnel of CTP synthase unveils coordinated catalytic and allosteric-dependent control of ammonia passage. *Biochim Biophys Acta Gen Subj*, *1862*(12), 2714-2727. https://doi.org/10.1016/j.bbagen.2018.08.008

McCluskey, G. D., Mohamady, S., Taylor, S. D., & Bearne, S. L. (2016). Exploring the Potent Inhibition of CTP Synthase by Gemcitabine-5'-Triphosphate. *Chembiochem*, *17*(23), 2240-2249. https://doi.org/10.1002/cbic.201600405

McHutchison, J. G., Gordon, S. C., Schiff, E. R., Shiffman, M. L., Lee, W. M., Rustgi, V. K., . . . Albrecht, J. K. (1998). Interferon alfa-2b alone or in combination with ribavirin as initial treatment for chronic hepatitis C. Hepatitis Interventional Therapy Group. *N Engl J Med*, *339*(21), 1485-1492. https://doi.org/10.1056/NEJM199811193392101

Micheli, V., Camici, M., Tozzi, M. G., Ipata, P. L., Sestini, S., Bertelli, M., & Pompucci, G. (2011). Neurological disorders of purine and pyrimidine metabolism. *Curr Top Med Chem*, *11*(8), 923-947. https://doi.org/10.2174/156802611795347645

Min, J. S., Kim, G. W., Kwon, S., & Jin, Y. H. (2020). A Cell-Based Reporter Assay for Screening Inhibitors of MERS Coronavirus RNA-Dependent RNA Polymerase Activity. *J Clin Med*, *9*(8). https://doi.org/10.3390/jcm9082399

Mongia, A., Saha, S. K., Chouzenoux, E., & Majumdar, A. (2021). A computational approach to aid clinicians in selecting anti-viral drugs for COVID-19 trials. *Sci Rep*, *11*(1), 9047. https://doi.org/10.1038/s41598-021-88153-3

Mori, G., Chiarelli, L. R., Esposito, M., Makarov, V., Bellinzoni, M., Hartkoorn, R. C., . . . Pasca, M. R. (2015). Thiophenecarboxamide Derivatives Activated by EthA Kill *Mycobacterium tuberculosis* by Inhibiting the CTP Synthetase PyrG. *Chem Biol*, *22*(7), 917-927. https://doi.org/10.1016/j.chembiol.2015.05.016

Muller, M. P., Dresser, L., Raboud, J., McGeer, A., Rea, E., Richardson, S. E., . . . Network, C. S. R. (2007). Adverse events associated with high-dose ribavirin: evidence from the Toronto outbreak of severe acute respiratory syndrome. *Pharmacotherapy*, *27*(4), 494-503. https://doi.org/10.1592/phco.27.4.494

Müller, W. E., Maidhof, A., Taschner, H., & Zahn, R. K. (1977). Virazole (1-beta-D-ribofuranosyl-1,2,4-triazole-3-carboxamide; a cytostatic agent. *Biochem Pharmacol*, *26*(11), 1071-1075. https://doi.org/10.1016/0006-2952(77)90246-5

Narvaez-Ortiz, H. Y., Lopez, A. J., Gupta, N., & Zimmermann, B. H. (2018). A CTP Synthase Undergoing Stage-Specific Spatial Expression Is Essential for the Survival of the Intracellular Parasite. *Front Cell Infect Microbiol*, *8*, 83. https://doi.org/10.3389/fcimb.2018.00083

Negishi, K., Harada, C., Ohara, Y., Oohara, K., Nitta, N., & Hayatsu, H. (1983). N4-aminocytidine, a nucleoside analog that has an exceptionally high mutagenic activity. *Nucleic Acids Res*, *11*(15), 5223-5233. https://doi.org/10.1093/nar/11.15.5223

Novagen. (1997). *pET System Manual* (7 ed.).

Nyhan, W. L. (2005). Disorders of purine and pyrimidine metabolism. *Mol Genet Metab*, *86*(1-2), 25-33. https://doi.org/10.1016/j.ymgme.2005.07.027

Ostrander, D. B., O'Brien, D. J., Gorman, J. A., & Carman, G. M. (1998). Effect of CTP synthetase regulation by CTP on phospholipid synthesis in *Saccharomyces cerevisiae*. *J Biol Chem*, *273*(30), 18992-19001. https://doi.org/10.1074/jbc.273.30.18992

Ou, Z., Ouzounis, C., Wang, D., Sun, W., Li, J., Chen, W., . . . Danchin, A. (2020). A Path toward SARS-CoV-2 Attenuation: Metabolic Pressure on CTP Synthesis Rules the Virus Evolution. *Genome Biol Evol*, *12*(12), 2467-2485. https://doi.org/10.1093/gbe/evaa229

Page, T., & Connor, J. D. (1990). The metabolism of ribavirin in erythrocytes and nucleated cells. *Int J Biochem*, *22*(4), 379-383. https://doi.org/10.1016/0020-711x(90)90140-x

Painter, G. R., Bowen, R. A., Bluemling, G. R., DeBergh, J., Edpuganti, V., Gruddanti, P. R., . . . Kolykhalov, A. A. (2019). The prophylactic and therapeutic activity of a broadly active ribonucleoside analog in a murine model of intranasal venezuelan equine encephalitis virus infection. *Antiviral Res*, *171*, 104597. https://doi.org/10.1016/j.antiviral.2019.104597

Painter, G. R., Guthrie, D. B., Bluemling, G. R., & Natchus, M. G. (2016). *N4-Hydroxycytidine and Derivatives and Anti-viral Uses Related Thereto*.

Pappas, A., Park, T. S., & Carman, G. M. (1999). Characterization of a novel dUTP-dependent activity of CTP synthetase from *Saccharomyces cerevisiae*. *Biochemistry*, *38*(50), 16671-16677. https://doi.org/10.1021/bi9920127

Park, C. K., & Horton, N. C. (2019). Structures, functions, and mechanisms of filament forming enzymes: a renaissance of enzyme filamentation. *Biophys Rev*, *11*(6), 927-994. https://doi.org/10.1007/s12551-019-00602-6

Peck, M. L., & Herschlag, D. (2003). Adenosine 5'-O-(3-thio)triphosphate (ATPgammaS) is a substrate for the nucleotide hydrolysis and RNA unwinding activities of eukaryotic translation initiation factor eIF4A. *RNA*, *9*(10), 1180-1187. https://doi.org/10.1261/rna.2103703

Pinkus, L. M. (1977). Glutamine binding sites. *Methods Enzymol*, *46*, 414-427. https://doi.org/10.1016/s0076-6879(77)46049-x

Prajapat, M., Shekhar, N., Sarma, P., Avti, P., Singh, S., Kaur, H., . . . Medhi, B. (2020). Virtual screening and molecular dynamics study of approved drugs as inhibitors of spike protein S1 domain and ACE2 interaction in SARS-CoV-2. *J Mol Graph Model*, *101*, 107716. https://doi.org/10.1016/j.jmgm.2020.107716

Privat de Garilhe, M., & De Rudder, J. (1964). Effect of 2 arabinose nucleosides on the multiplication of herpes virus and vaccine in cell culture. *C R Hebd Seances Acad Sci*, *259*, 2725-2728.

Prusiner, P., & Sundaralingam, M. (1973). A new class of synthetic nucleoside analogues with broad-spectrum antiviral properties. *Nat New Biol*, *244*(134), 116-118. https://doi.org/10.1038/newbio244116a0

Prussia, A. J., & Chennamadhavuni, S. (2021). Biostructural Models for the Binding of Nucleoside Analogs to SARS-CoV-2 RNA-Dependent RNA Polymerase. *J Chem Inf Model*, *61*(3), 1402-1411. https://doi.org/10.1021/acs.jcim.0c01277

Reeve, R. M. (1958). A specific hydroxylamine-ferric chloride reaction for histochemical localization of pectin. In.

Rivera-Serrano, E. E., Gizzi, A. S., Arnold, J. J., Grove, T. L., Almo, S. C., & Cameron, C. E. (2020). Viperin Reveals Its True Function. *Annu Rev Virol*, *7*(1), 421-446. https://doi.org/10.1146/annurev-virology-011720-095930

Robertson, J. G., & Villafranca, J. J. (1993). Characterization of metal ion activation and inhibition of CTP synthetase. *Biochemistry*, *32*(14), 3769-3777. https://doi.org/10.1021/bi00065a032

Romano, M., Ruggiero, A., Squeglia, F., Maga, G., & Berisio, R. (2020). A Structural View of SARS-CoV-2 RNA Replication Machinery: RNA Synthesis, Proofreading and Final Capping. *Cells*, *9*(5). https://doi.org/10.3390/cells9051267

Sadeghi, A., Ali Asgari, A., Norouzi, A., Kheiri, Z., Anushirvani, A., Montazeri, M., . . . Merat, S. (2020). Sofosbuvir and daclatasvir compared with standard of care in the treatment of patients admitted to hospital with moderate or severe coronavirus infection (COVID-19): a randomized controlled trial. *J Antimicrob Chemother*, *75*(11), 3379-3385. https://doi.org/10.1093/jac/dkaa334

Sandalli, C., Saral, A., Ülker, S., Karaoglu, H., Belduz, A. O., & Çopur Çiek, A. (2013). Cloning, expression, and characterization of a novel CTP synthase gene from *Anoxybacillus gonensis* G2. *Turkish Journal of Biology*, *38*, 111-117. https://doi.org/10.3906/biy-1304-76

Savage, C. R., & Weinfeld, H. (1970). Purification and properties of mammalian liver cytidine triphosphate synthetase. *J Biol Chem*, *245*(10), 2529-2535.

Schabel, F. M. (1968). The antiviral activity of 9-beta-D-arabinofuranosyladenine (ARA-A). *Chemotherapia (Basel)*, *13*(6), 321-338. https://doi.org/10.1159/000220567

Scheit, K. H., & Linke, H. J. (1982). Substrate specificity of CTP synthetase from *Escherichia coli*. *Eur J Biochem*, *126*(1), 57-60. https://doi.org/10.1111/j.1432-1033.1982.tb06745.x

Schimmel, K. J., Gelderblom, H., & Guchelaar, H. J. (2007). Cyclopentenyl cytosine (CPEC): an overview of its in vitro and in vivo activity. *Curr Cancer Drug Targets*, *7*(5), 504-509. https://doi.org/10.2174/156800907781386579

Segel, I. H. (1975). *Enzyme Kinetics*. John Wiley and Sons.

Sheahan, T. P., Sims, A. C., Zhou, S., Graham, R. L., Pruijssers, A. J., Agostini, M. L., . . . Baric, R. S. (2020). An orally bioavailable broad-spectrum antiviral inhibits SARS-CoV-2 in human airway epithelial cell cultures and multiple coronaviruses in mice. *Sci Transl Med*, *12*(541). https://doi.org/10.1126/scitranslmed.abb5883

Shi, L. E., Ying, G. Q., Tang, Z. X., Yi, Y., Shan, J. F., & Liu, H. Z. (2008). Separation of cytidine 5'-triphosphate biosynthesized from cytidine 5'-monophosphate on ion-exchange resin and HPLC analysis of cytidine compounds. *Appl Biochem Biotechnol*, *144*(1), 1-14. https://doi.org/10.1007/s12010-007-8015-0

Shridas, P., & Waechter, C. J. (2006). Human dolichol kinase, a polytopic endoplasmic reticulum membrane protein with a cytoplasmically oriented CTP-binding site. *J Biol Chem*, *281*(42), 31696-31704. https://doi.org/10.1074/jbc.M604087200

Sidwell, R. W., Huffman, J. H., Khare, G. P., Allen, L. B., Witkowski, J. T., & Robins, R. K. (1972). Broad-spectrum antiviral activity of Virazole: 1-beta-D-ribofuranosyl-1,2,4-triazole-3-carboxamide. *Science*, *177*(4050), 705-706. https://doi.org/10.1126/science.177.4050.705

Siegel, D., Hui, H. C., Doerffler, E., Clarke, M. O., Chun, K., Zhang, L., . . . Mackman, R. L. (2017). Discovery and Synthesis of a Phosphoramidate Prodrug of a Pyrrolo[2,1-f][triazin-4-amino] Adenine C-Nucleoside (GS-5734) for the Treatment of Ebola and Emerging Viruses. *J Med Chem*, *60*(5), 1648-1661. https://doi.org/10.1021/acs.jmedchem.6b01594

Simard, D., Hewitt, K. A., Lunn, F., Iyengar, A., & Bearne, S. L. (2003). Limited proteolysis of *Escherichia coli* cytidine 5'-triphosphate synthase. Identification of residues required for CTP formation and GTP-dependent activation of glutamine hydrolysis. *Eur J Biochem*, *270*(10), 2195-2206. https://doi.org/10.1046/j.1432-1033.2003.03588.x

Singh, T. U., Parida, S., Lingaraju, M. C., Kesavan, M., Kumar, D., & Singh, R. K. (2020). Drug repurposing approach to fight COVID-19. *Pharmacol Rep*, *72*(6), 1479-1508. https://doi.org/10.1007/s43440-020-00155-6

Smith, E. C., Blanc, H., Surdel, M. C., Vignuzzi, M., & Denison, M. R. (2013). Coronaviruses lacking exoribonuclease activity are susceptible to lethal mutagenesis: evidence for proofreading and potential therapeutics. *PLoS Pathog*, *9*(8), e1003565. https://doi.org/10.1371/journal.ppat.1003565

Sofia, M. J., Bao, D., Chang, W., Du, J., Nagarathnam, D., Rachakonda, S., . . . Furman, P. A. (2010). Discovery of a β-d-2'-deoxy-2'-α-fluoro-2'-β-C-methyluridine nucleotide prodrug (PSI-7977) for the treatment of hepatitis C virus. *J Med Chem*, *53*(19), 7202-7218. https://doi.org/10.1021/jm100863x

Strochlic, T. I., Stavrides, K. P., Thomas, S. V., Nicolas, E., O'Reilly, A. M., & Peterson, J. R. (2014). Ack kinase regulates CTP synthase filaments during Drosophila

oogenesis. *EMBO Rep*, *15*(11), 1184-1191. https://doi.org/10.15252/embr.201438688
Strzelecka, D., Chmielinski, S., Bednarek, S., Jemielity, J., & Kowalska, J. (2017). Analysis of mononucleotides by tandem mass spectrometry: investigation of fragmentation pathways for phosphate- and ribose-modified nucleotide analogues. *Sci Rep*, *7*(1), 8931. https://doi.org/10.1038/s41598-017-09416-6
Stuyver, L. J., McBrayer, T. R., Tharnish, P. M., Clark, J., Hollecker, L., Lostia, S., . . . Otto, M. J. (2006). Inhibition of hepatitis C replicon RNA synthesis by beta-D-2'-deoxy-2'-fluoro-2'-C-methylcytidine: a specific inhibitor of hepatitis C virus replication. *Antivir Chem Chemother*, *17*(2), 79-87. https://doi.org/10.1177/095632020601700203
Stuyver, L. J., Whitaker, T., McBrayer, T. R., Hernandez-Santiago, B. I., Lostia, S., Tharnish, P. M., . . . Schinazi, R. F. (2003). Ribonucleoside analogue that blocks replication of bovine viral diarrhea and hepatitis C viruses in culture. *Antimicrob Agents Chemother*, *47*(1), 244-254. https://doi.org/10.1128/AAC.47.1.244-254.2003
Sun, Z., & Liu, J. L. (2019). Forming cytoophidia prolongs the half-life of CTP synthase. *Cell Discov*, *5*, 32. https://doi.org/10.1038/s41421-019-0098-6
Tam, R. C., Lau, J. Y., & Hong, Z. (2001). Mechanisms of action of ribavirin in antiviral therapies. *Antivir Chem Chemother*, *12*(5), 261-272. https://doi.org/10.1177/095632020101200501
Tao, T., & Lamkin, M. (1981). Excitation energy transfer studies on the proximity between SH1 and the adenosinetriphosphatase site in myosin subfragment 1. *Biochemistry*, *20*(17), 5051-5055. https://doi.org/10.1021/bi00520a035
Tatusov, R. L., Natale, D. A., Garkavtsev, I. V., Tatusova, T. A., Shankavaram, U. T., Rao, B. S., . . . Koonin, E. V. (2001). The COG database: new developments in phylogenetic classification of proteins from complete genomes. *Nucleic Acids Res*, *29*(1), 22-28. https://doi.org/10.1093/nar/29.1.22
Taylor, S. D., Lunn, F. A., & Bearne, S. L. (2008). Ground state, intermediate, and multivalent nucleotide analogue inhibitors of cytidine 5'-triphosphate synthase. *ChemMedChem*, *3*(12), 1853-1857. https://doi.org/10.1002/cmdc.200800236
Tong, S., Su, Y., Yu, Y., Wu, C., Chen, J., Wang, S., & Jiang, J. (2020). Ribavirin therapy for severe COVID-19: a retrospective cohort study. *Int J Antimicrob Agents*, *56*(3), 106114. https://doi.org/10.1016/j.ijantimicag.2020.106114
Toschi, L., Finocchiaro, G., Bartolini, S., Gioia, V., & Cappuzzo, F. (2005). Role of gemcitabine in cancer therapy. *Future Oncol*, *1*(1), 7-17. https://doi.org/10.1517/14796694.1.1.7
Traut, T. W. (1994). Physiological concentrations of purines and pyrimidines. *Mol Cell Biochem*, *140*(1), 1-22. https://doi.org/10.1007/BF00928361
Trudel, M., Van Genechten, T., & Meuth, M. (1984). Biochemical characterization of the hamster thy mutator gene and its revertants. *J Biol Chem*, *259*(4), 2355-2359.
Urakova, N., Kuznetsova, V., Crossman, D. K., Sokratian, A., Guthrie, D. B., Kolykhalov, A. A., . . . Frolov, I. (2018). β-d-N 4-Hydroxycytidine Is a Potent Anti-alphavirus Compound That Induces a High Level of Mutations in the Viral Genome. *J Virol*, *92*(3). https://doi.org/10.1128/JVI.01965-17

van Moorsel, C. J., Bergman, A. M., Veerman, G., Voorn, D. A., Ruiz van Haperen, V. W., Kroep, J. R., . . . Peters, G. J. (2000). Differential effects of gemcitabine on ribonucleotide pools of twenty-one solid tumour and leukaemia cell lines. *Biochim Biophys Acta*, *1474*(1), 5-12. https://doi.org/10.1016/s0304-4165(99)00209-3

Verschuur, A. C., Van Gennip, A. H., Leen, R., & Van Kuilenburg, A. B. (2004). Increased cytotoxicity of 2',2'-difluoro-2'-deoxycytidine in human leukemic cell-lines after a preincubation with cyclopentenyl cytosine. *Nucleosides Nucleotides Nucleic Acids*, *23*(8-9), 1517-1521. https://doi.org/10.1081/NCN-200027733

Verschuur, A. C., Van Gennip, A. H., Leen, R., Voûte, P. A., Brinkman, J., & Van Kuilenburg, A. B. (2002). Cyclopentenyl cytosine increases the phosphorylation and incorporation into DNA of 1-beta-D-arabinofuranosyl cytosine in a human T-lymphoblastic cell line. *Int J Cancer*, *98*(4), 616-623. https://doi.org/10.1002/ijc.10211

von der Saal, W., Anderson, P. M., & Villafranca, J. J. (1985). Mechanistic investigations of *Escherichia coli* cytidine-5'-triphosphate synthetase. Detection of an intermediate by positional isotope exchange experiments. *J Biol Chem*, *260*(28), 14993-14997.

Wahl, A., Gralinski, L. E., Johnson, C. E., Yao, W., Kovarova, M., Dinnon, K. H., . . . Garcia, J. V. (2021). SARS-CoV-2 infection is effectively treated and prevented by EIDD-2801. *Nature*, *591*(7850), 451-457. https://doi.org/10.1038/s41586-021-03312-w

Wang, M., Cao, R., Zhang, L., Yang, X., Liu, J., Xu, M., . . . Xiao, G. (2020). Remdesivir and chloroquine effectively inhibit the recently emerged novel coronavirus (2019-nCoV) in vitro. *Cell Res*, *30*(3), 269-271. https://doi.org/10.1038/s41422-020-0282-0

Weinfeld, H., Savage, C. R., & McPartland, R. P. (1978). CTP synthetase of bovine calf liver. *Methods Enzymol*, *51*, 84-90. https://doi.org/10.1016/s0076-6879(78)51015-x

Wellner, K., Betat, H., & Mörl, M. (2018). A tRNA's fate is decided at its 3' end: Collaborative actions of CCA-adding enzyme and RNases involved in tRNA processing and degradation. *Biochim Biophys Acta Gene Regul Mech*, *1861*(4), 433-441. https://doi.org/10.1016/j.bbagrm.2018.01.012

Weng, M. L., & Zalkin, H. (1987). Structural role for a conserved region in the CTP synthetase glutamine amide transfer domain. *J Bacteriol*, *169*(7), 3023-3028. https://doi.org/10.1128/jb.169.7.3023-3028.1987

Whelan, J., Smith, T., Phear, G., Rohatiner, A., Lister, A., & Meuth, M. (1994). Resistance to cytosine arabinoside in acute leukemia: the significance of mutations in CTP synthetase. *Leukemia*, *8*(2), 264-265.

Willemoës, M., Mølgaard, A., Johansson, E., & Martinussen, J. (2005). Lid L11 of the glutamine amidotransferase domain of CTP synthase mediates allosteric GTP activation of glutaminase activity. *FEBS J*, *272*(3), 856-864. https://doi.org/10.1111/j.1742-4658.2004.04525.x

Willemoës, M., & Sigurskjold, B. W. (2002). Steady-state kinetics of the glutaminase reaction of CTP synthase from *Lactococcus lactis*. The role of the allosteric

activator GTP incoupling between glutamine hydrolysis and CTP synthesis. *Eur J Biochem*, *269*(19), 4772-4779. https://doi.org/10.1046/j.1432-1033.2002.03175.x
Williams, J. C., Kizaki, H., Weber, G., & Morris, H. P. (1978). Increased CTP synthetase activity in cancer cells. *Nature*, *271*(5640), 71-73. https://doi.org/10.1038/271071a0
Wishart, D. S., Knox, C., Guo, A. C., Eisner, R., Young, N., Gautam, B., . . . Forsythe, I. (2009). HMDB: a knowledgebase for the human metabolome. *Nucleic Acids Res*, *37*(Database issue), D603-610. https://doi.org/10.1093/nar/gkn810
Wylie, J. L., Berry, J. D., & McClarty, G. (1996). *Chlamydia trachomatis* CTP synthetase: molecular characterization and developmental regulation of expression. *Mol Microbiol*, *22*(4), 631-642. https://doi.org/10.1046/j.1365-2958.1996.d01-1717.x
Wylie, J. L., Wang, L. L., Tipples, G., & McClarty, G. (1996). A single point mutation in CTP synthetase of *Chlamydia trachomatis* confers resistance to cyclopentenyl cytosine. *J Biol Chem*, *271*(26), 15393-15400. https://doi.org/10.1074/jbc.271.26.15393
Yamauchi, M., Yamauchi, N., & Meuth, M. (1990). Molecular cloning of the human CTP synthetase gene by functional complementation with purified human metaphase chromosomes. *EMBO J*, *9*(7), 2095-2099.
Yang, W. L., McDonough, V. M., Ozier-Kalogeropoulos, O., Adeline, M. T., Flocco, M. T., & Carman, G. M. (1994). Purification and characterization of CTP synthetase, the product of the URA7 gene in *Saccharomyces cerevisiae*. *Biochemistry*, *33*(35), 10785-10793. https://doi.org/10.1021/bi00201a028
Yates, D. W., & Duance, V. C. (1976). The binding of nucleotides and bivalent cations to the calcium-and-magnesium ion-dependent adenosine triphosphatase from rabbit muscle sarcoplasmic reticulum. *Biochem J*, *159*(3), 719-728. https://doi.org/10.1042/bj1590719
Yount, R. G. (1975). ATP analogs. *Adv Enzymol Relat Areas Mol Biol*, *43*, 1-56. https://doi.org/10.1002/9780470122884.ch1
Yuan, P., Hendriks, E. F., Fernandez, H. R., O'Sullivan, W. J., & Stewart, T. S. (2005). Functional expression of the gene encoding cytidine triphosphate synthetase from *Plasmodium falciparum* which contains two novel sequences that are potential antimalarial targets. *Mol Biochem Parasitol*, *143*(2), 200-208. https://doi.org/10.1016/j.molbiopara.2005.06.004
Zandi, K., Amblard, F., Musall, K., Downs-Bowen, J., Kleinbard, R., Oo, A., . . . Schinazi, R. F. (2020). Repurposing Nucleoside Analogs for Human Coronaviruses. *Antimicrob Agents Chemother*, *65*(1). https://doi.org/10.1128/AAC.01652-20
Zhang, H., Cooney, D. A., Zhang, M. H., Ahluwalia, G., Ford, H., & Johns, D. G. (1993). Resistance to cyclopentenylcytosine in murine leukemia L1210 cells. *Cancer Res*, *53*(23), 5714-5720.
Zhang, H., Saravanan, K. M., Yang, Y., Hossain, M. T., Li, J., Ren, X., . . . Wei, Y. (2020). Deep Learning Based Drug Screening for Novel Coronavirus 2019-nCov. *Interdiscip Sci*, *12*(3), 368-376. https://doi.org/10.1007/s12539-020-00376-6
Zhou, S., Hill, C. S., Sarkar, S., Tse, L. V., Woodburn, B. M. D., Schinazi, R. F., . . . Swanstrom, R. (2021). β-D-N 4-hydroxycytidine (NHC) Inhibits SARS-CoV-2

Through Lethal Mutagenesis But Is Also Mutagenic To Mammalian Cells. *J Infect Dis*. https://doi.org/10.1093/infdis/jiab247

Zhou, X., Guo, C. J., Chang, C. C., Zhong, J., Hu, H. H., Lu, G. M., & Liu, J. L. (2021). Structural basis for ligand binding modes of CTP synthase. *Proc Natl Acad Sci U S A*, *118*(30). https://doi.org/10.1073/pnas.2026621118

Zhou, X., Guo, C. J., Hu, H. H., Zhong, J., Sun, Q., Liu, D., . . . Liu, J. L. (2019). Drosophila CTP synthase can form distinct substrate- and product-bound filaments. *J Genet Genomics*, *46*(11), 537-545. https://doi.org/10.1016/j.jgg.2019.11.006

Zimmerman, T. P., & Deeprose, R. D. (1978). Metabolism of 5-amino-1-beta-D-ribofuranosylimidazole-4-carboxamide and related five-membered heterocycles to 5'-triphosphates in human blood and L5178Y cells. *Biochem Pharmacol*, *27*(5), 709-716. https://doi.org/10.1016/0006-2952(78)90508-7